MINOS:
Do it yourself

- Introducing MINOS
- Introducing NuMI

} ◆Bird's view ◆Highlights

- MINOS detectors

  ("Building a ship in a bottle")
  - "technological" issues
  - work "fronts"
- Lessons learned (hopefully)

"Anyone who has never made a mistake has never tried anything new."

Albert Einstein

MINOS

Main **I**njector **N**eutrino **O**scillation **S***tudies*

Strategy for precision measurements:

- Two-detector measurement
  - ⇨ long baseline (735km)
  - ⇨ underground (CR shielding + physics)
- High intensity beam from 120 GeV Main Injector
  - ⇨ (up to) 4×10^{13} protons/pulse (0.4 MW beam)
    (potential for ~4×10^{20} protons/year)
  - ⇨ single turn extraction (8.67 μs)
- Flexible & well-controlled beam
  - ⇨ two parabolic magnetic horns
  - ⇨ movable target (→energy spectrum)

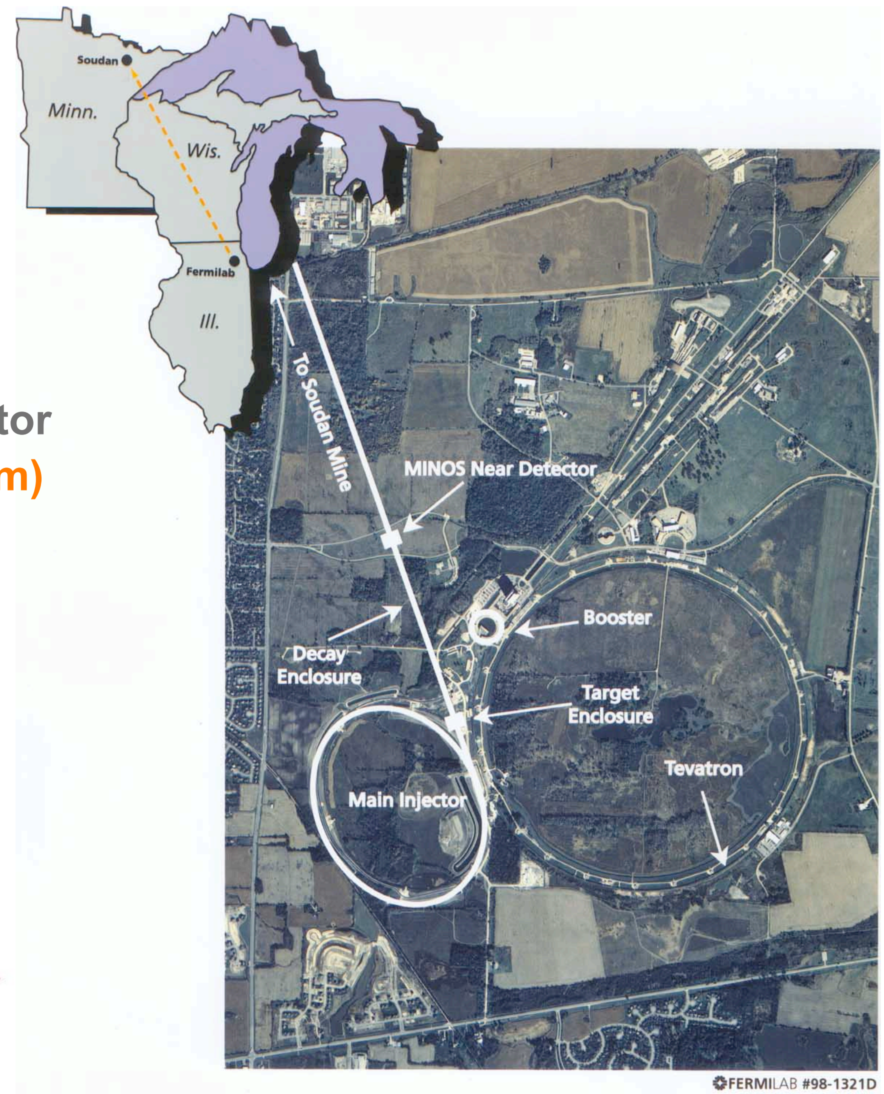

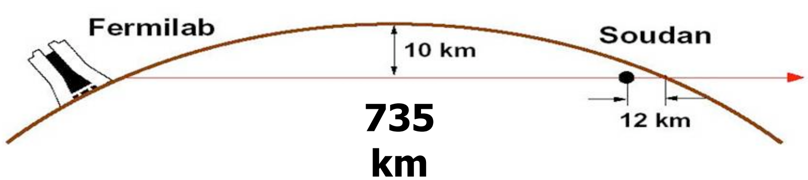

MINOS Physics Program

Main goals:

- Decisive low-systematics observation of disappearance ($\nu_\mu \rightarrow \nu_x$)
- Determine $|\Delta m_{32}^2|$ and $\sin^2 2\theta_{23}$ with < 10% accuracy
- Measure (or improve limits) on $\nu_\mu \rightarrow \nu_e$ / $\nu_\mu \rightarrow \nu_{sterile}$ / "exotic" transitions
- Test **CPT** in atmospheric CC_μ charge-separated interactions

The method:

$$P(\nu_\mu \rightarrow \nu_\mu) = 1 - \sin^2 2\theta \bullet \sin^2(1.267 \Delta m^2 L / E)$$

1 2

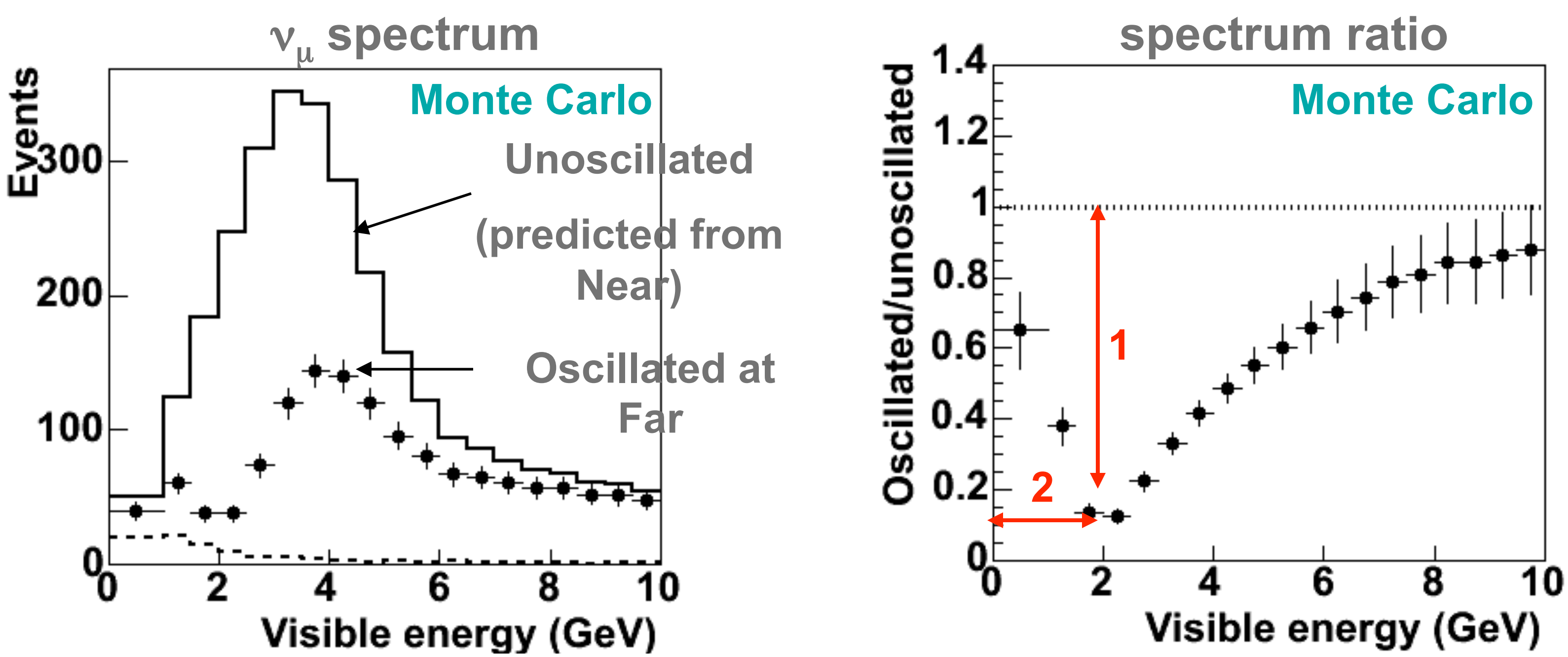

Monte Carlo plots for $\Delta m^2 = 0.003$ eV^2 and 7.4×10^{20} pot

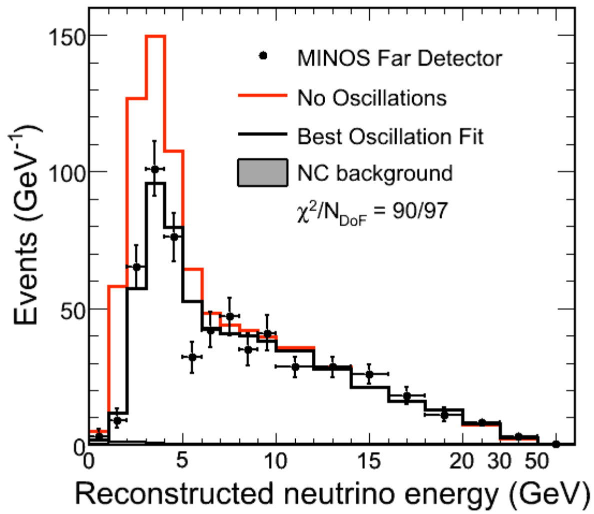

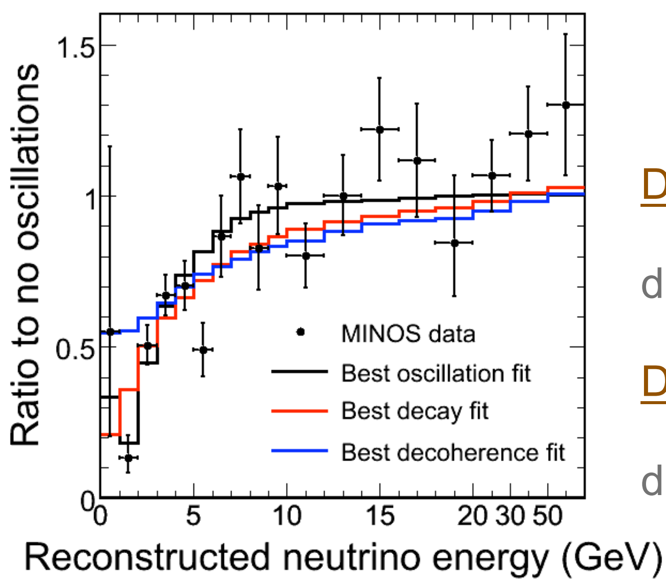

Constrained ($\sin^2(2\theta)=1.$) fit

$|\Delta m|^2 = (2.43 \pm 0.13) \times 10^{-3}$ eV^2

$\sin^2(2\theta) > 0.95$ [χ^2/ndof = 90/97, 68% C.L.]

Unconstrained fit:

$|\Delta m|^2 = 2.33 \times 10^{-3}$ eV^2

$\sin^2(2\theta)=1.07$

[$\Delta\chi^2$=-0.6]

Decay

χ^2 = 104/97

disfavored at 3.7σ

Decoherence

χ^2 = 123/97

disfavored at 5.7σ

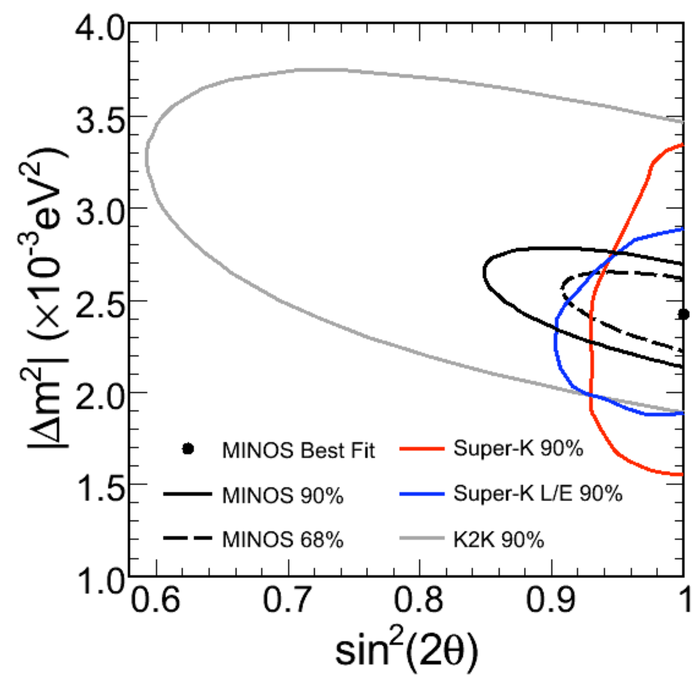

P. Adamson *et al.*, Phys. Rev. Lett. **101**,131802 (2008)

Beam: a how to

(Main Injector = MI)

- MI is fed 1.56 μs batches from 8 GeV Booster
  (MI ramp time ~1.5sec)
- NuMI designed for
  - ➔ 8.67 μsec single turn extraction
  - ➔ 4×10^{13}ppp @ 120 GeV
  - ➔ 1.9 second cycle time
  - ➔ beam power ~400kW
- Typical performance to date:
  - ➔ 3.2×10^{13} ppp @ 120 GeV
  - ➔ 2.2 second cycle time
- Achieved records:
  - ➔ 3.7×10^{13} ppp @ 120 GeV
  - ➔ 2.0 second cycle time
  - ➔ 320 kW

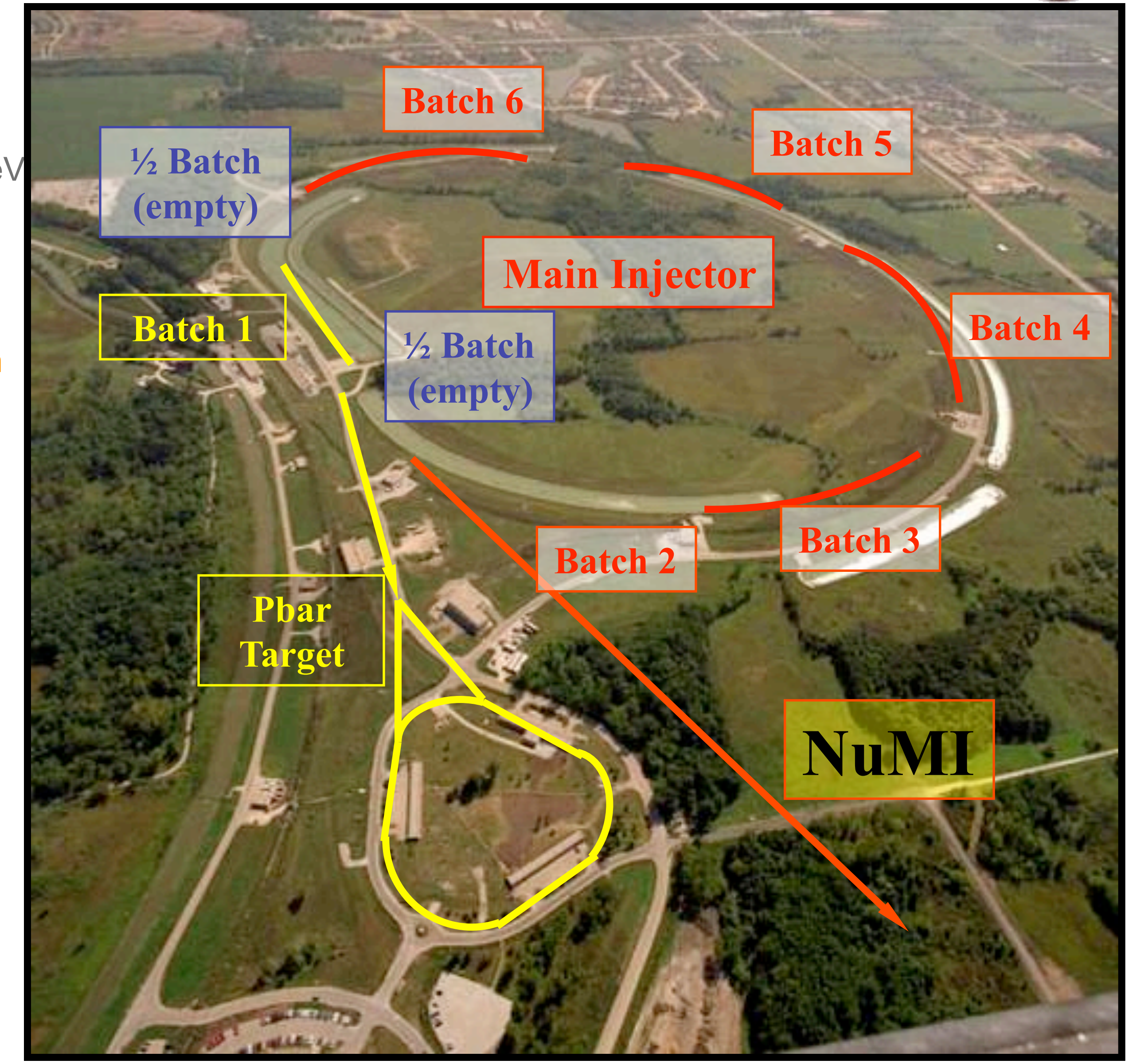

Experimental setup: NuMI beam

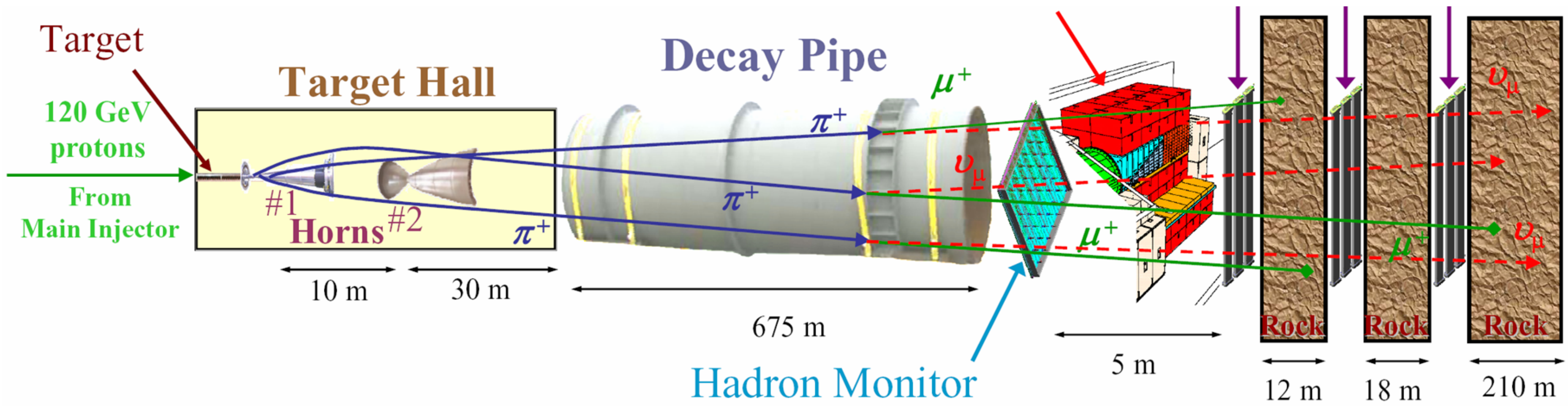

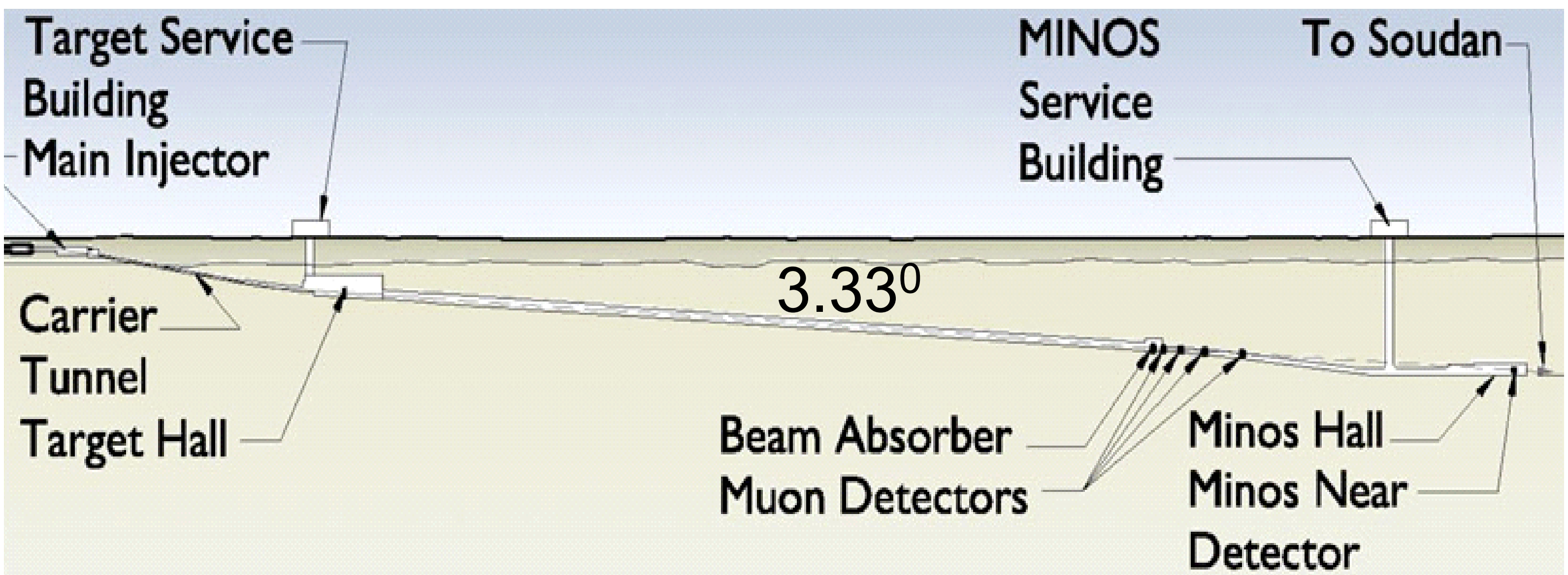

Intense beam

- As of now, we have replaced the target twice and both horns!

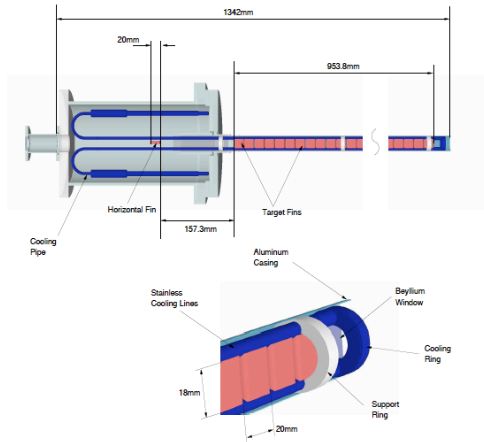

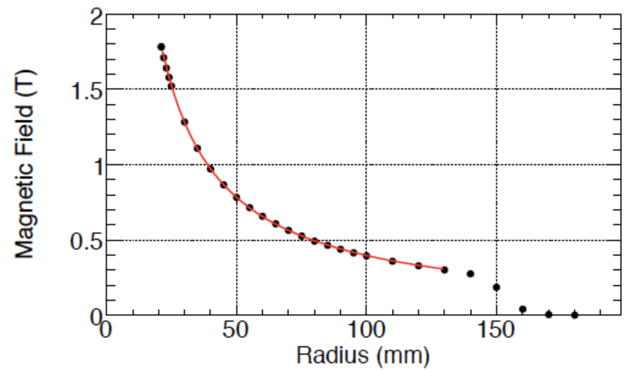

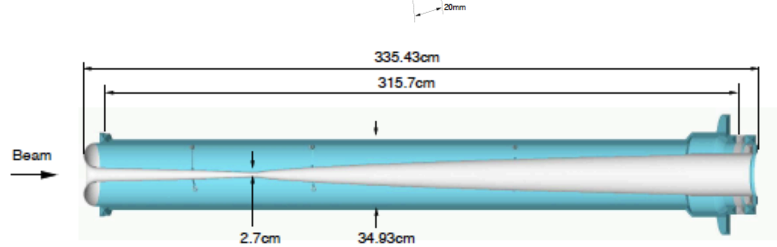

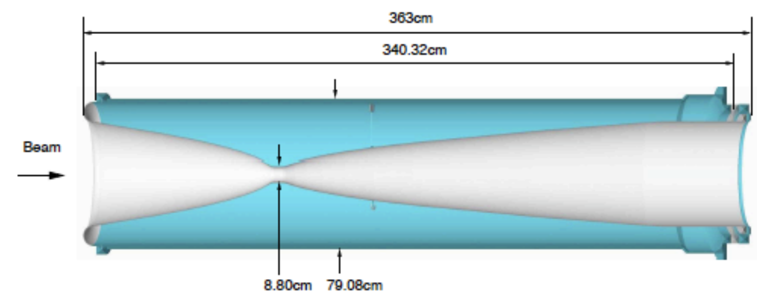

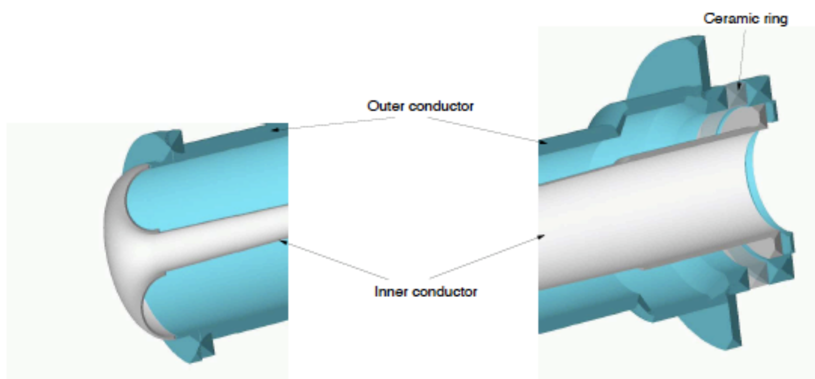

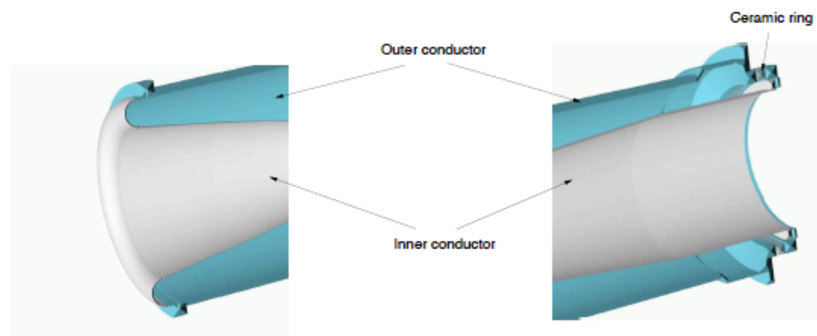

NuMI – multi-beam

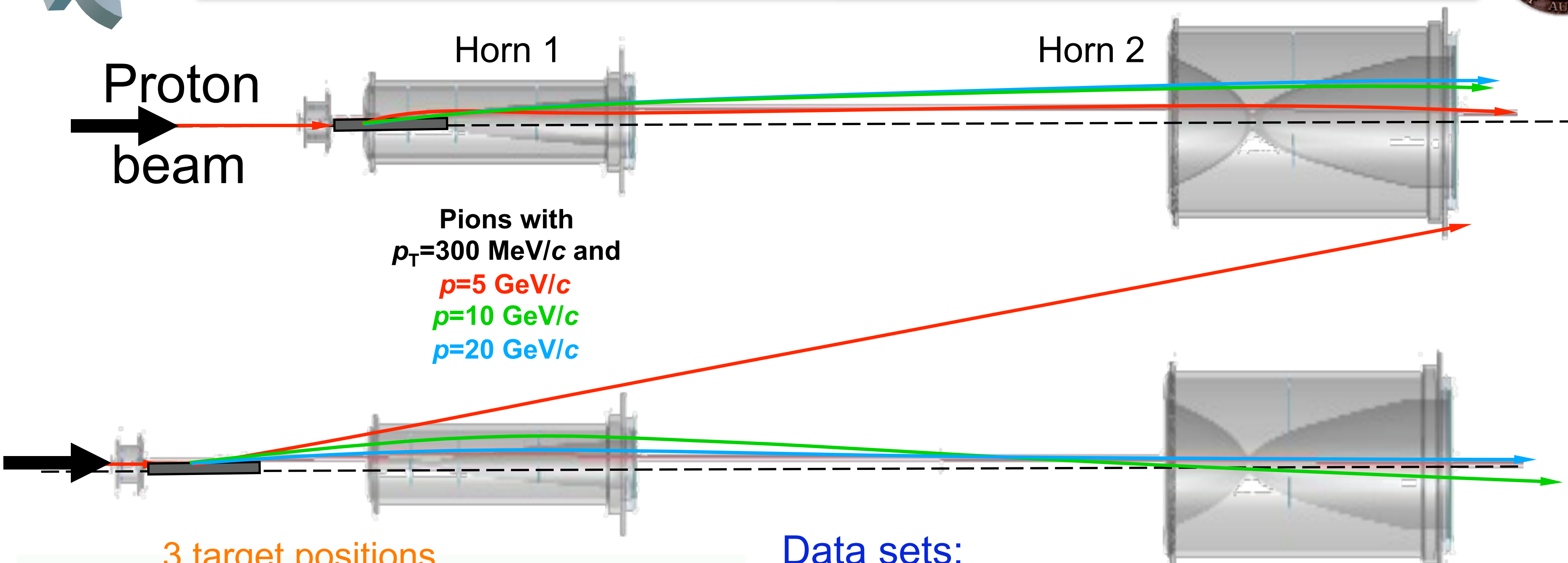

3 target positions

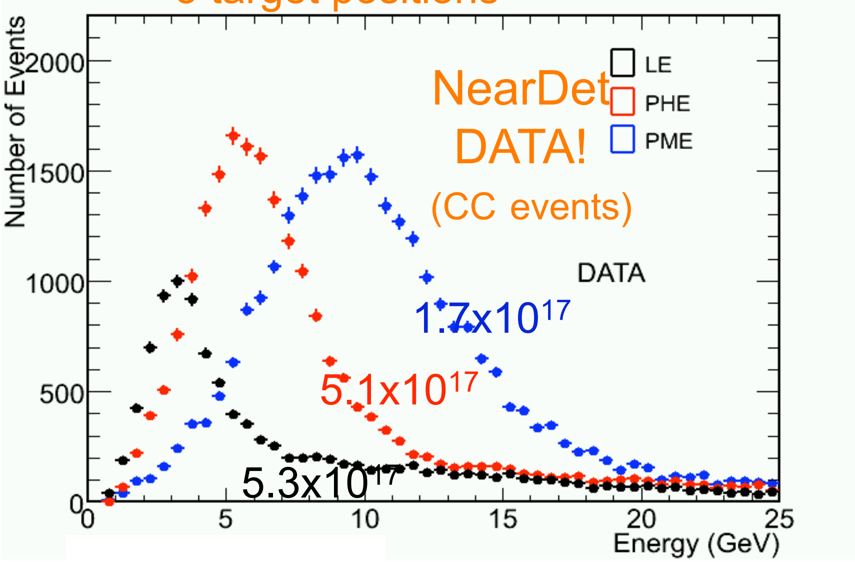

Data sets:

Beam	Target z position (cm)	FD Events per $1x10^{20}$ pot	Horn Current (kA)
LE-10	-10	390	0,170, 185 ,200
pME	-100	970	200
pHE	-250	1340	200

95% data

LE-10: Far Det: 1 event / ~4hrs

Flavor composition: 92.9% ν_μ
5.8% anti- ν_μ,
1.2% ν_e, 0.1%anti- ν_e

Focusing

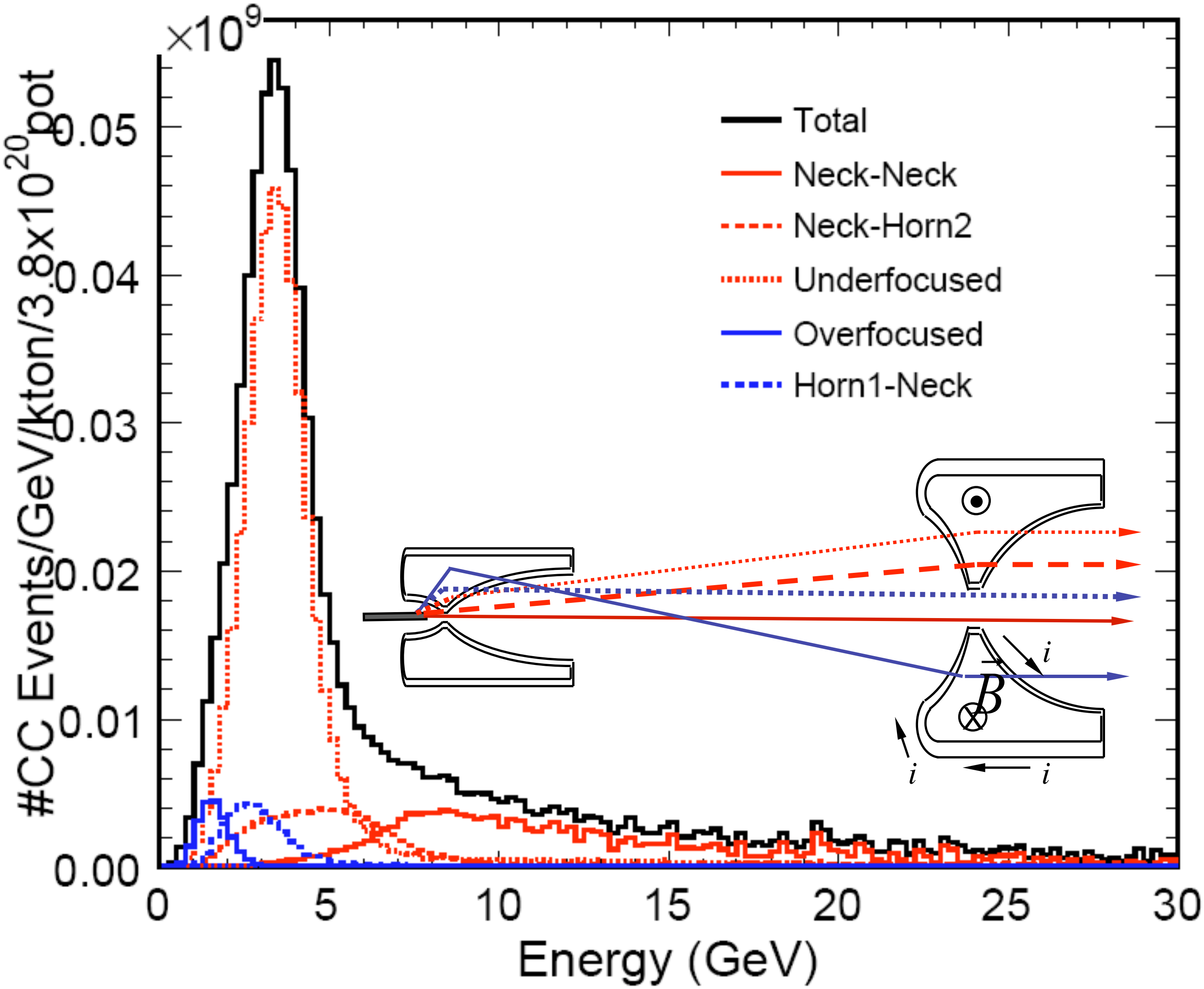

×10^9
#CC Events/GeV/kton/3.8x10^20 pot
0.00
0.01
0.02
0.03
0.04
0.05
0
5
10
15
20
25
30
Energy (GeV)
Total
Neck-Neck
Neck-Horn2
Underfocused
Overfocused
Horn1-Neck
i
B
i
i

MINOS Target Hall

Hall probe

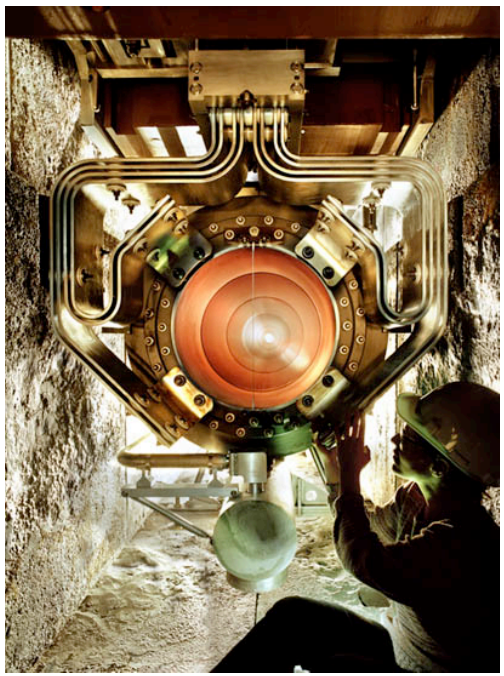

Horn 2 suspended from shielding module being lowered into shielding pit

Muon Monitors to Study ν Beam

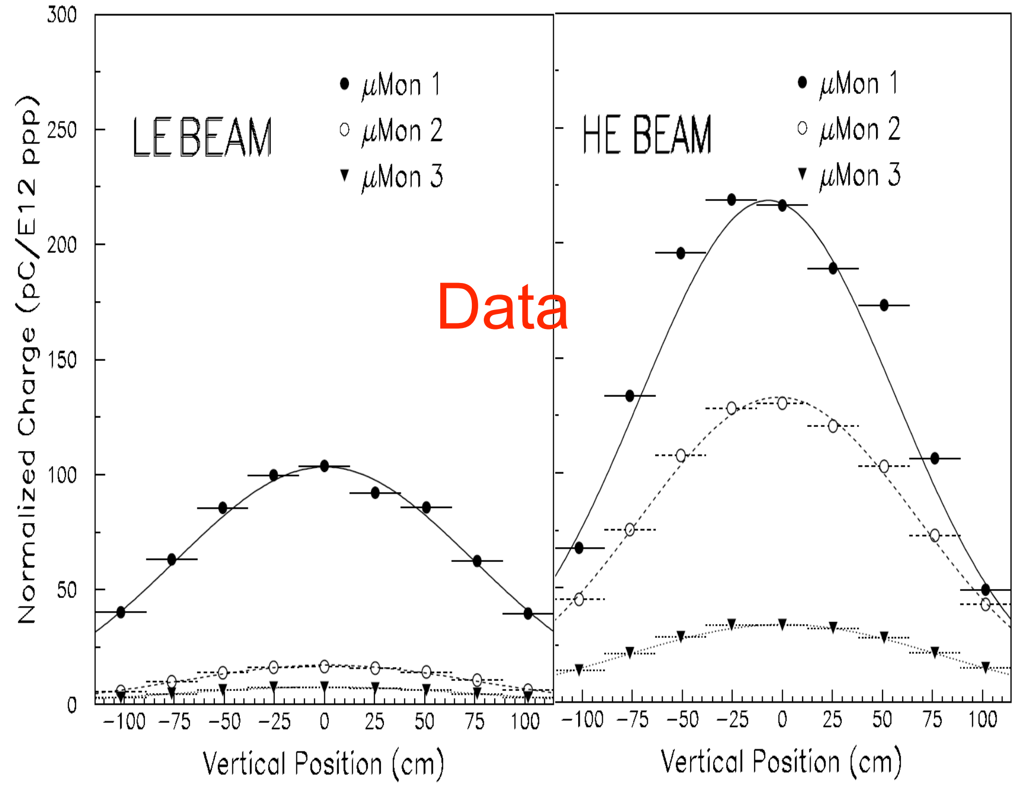

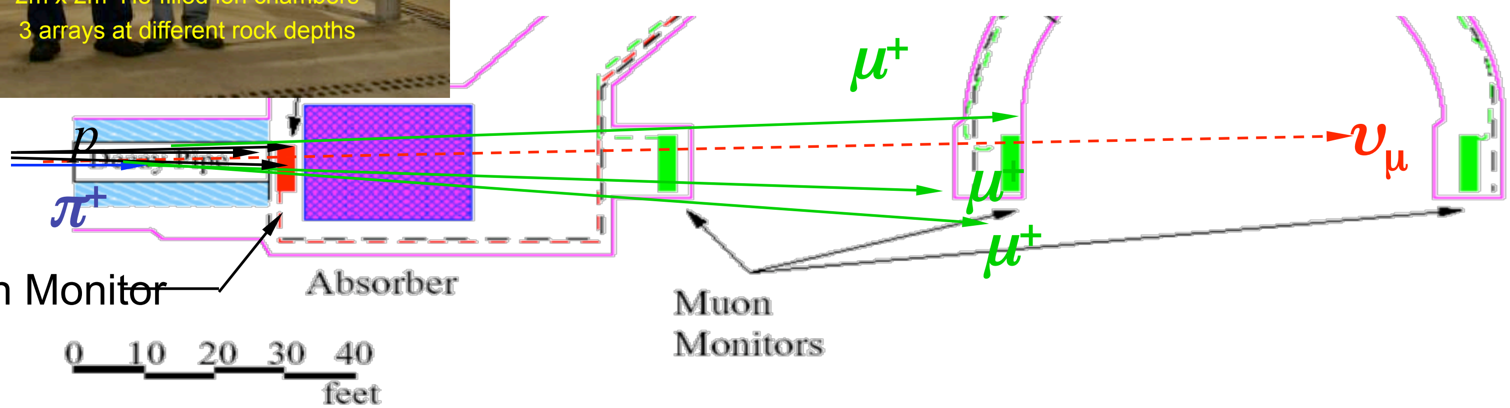

Accumulated Beam Data

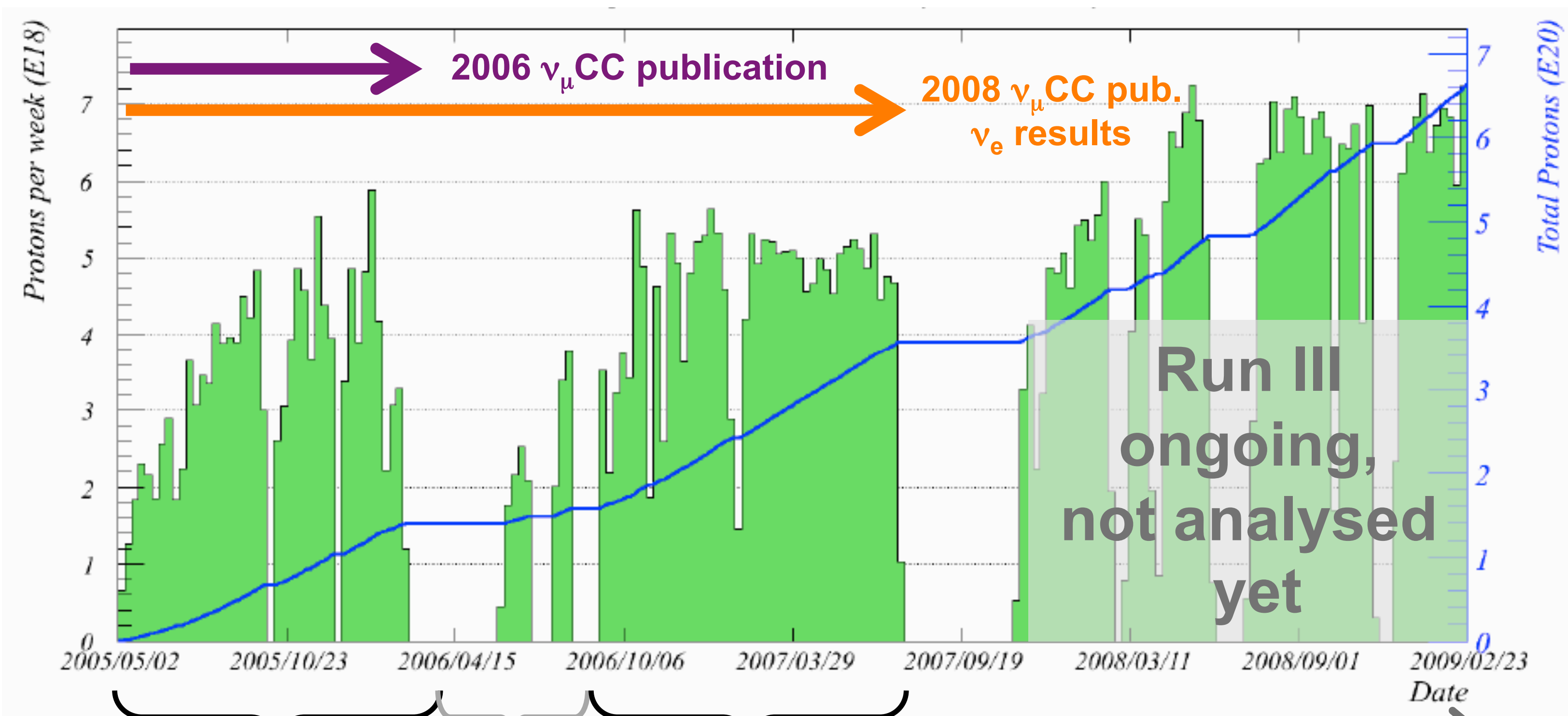

RUN I	Higher energy beam	RUN II	RUN III
1.27×10^{20} POT	0.15×10^{20} POT	1.87×10^{20} POT	$>3\times10^{20}$ POT

Nuclear Instruments and Methods in Physics Research A 596 (2008) 190–228

ELSEVIER

Contents lists available at ScienceDirect

Nuclear Instruments and Methods in Physics Research A

journal homepage: www.elsevier.com/locate/nima

The magnetized steel and scintillator calorimeters of the MINOS experiment

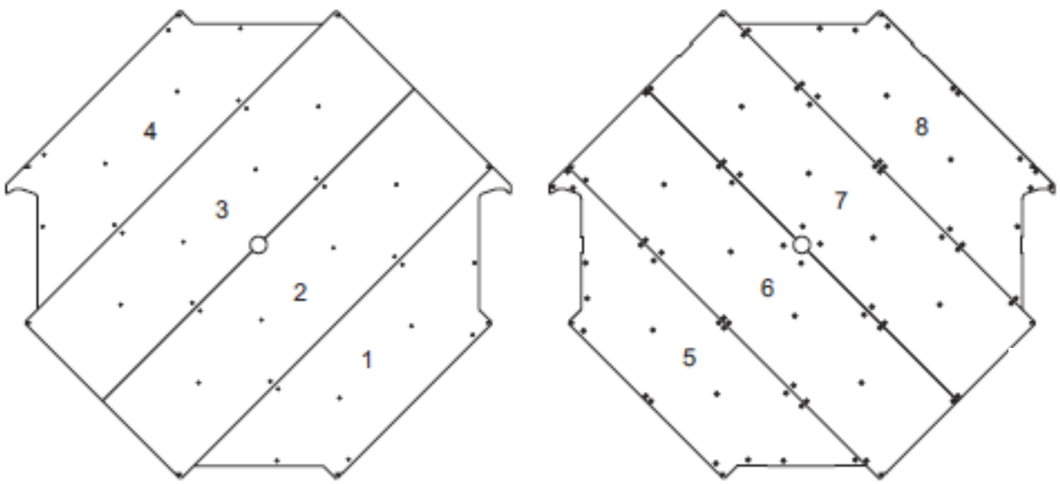

It's like
building a ship in a bottle

Octagonal steel plates
made out of 8 welded
together long plates
which fit through the shaft

Soudan Mine
(MN)

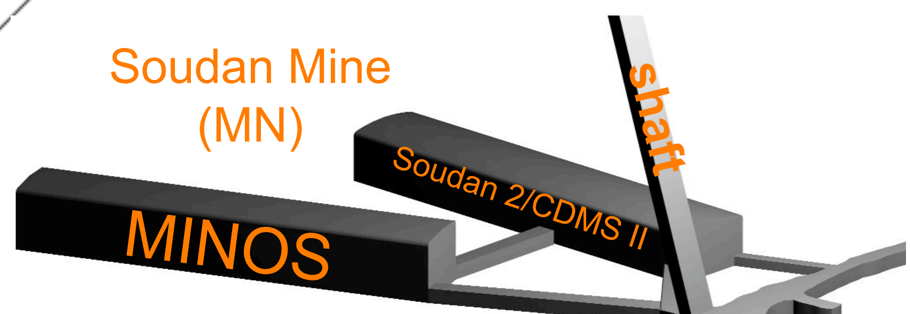

Depth=2,070mwe

Nuclear Instruments and Methods in Physics Research A 596 (2008) 190–228

Contents lists available at ScienceDirect

Nuclear Instruments and Methods in Physics Research A

journal homepage: www.elsevier.com/locate/nima

The magnetized steel and scintillator calorimeters of the MINOS experiment

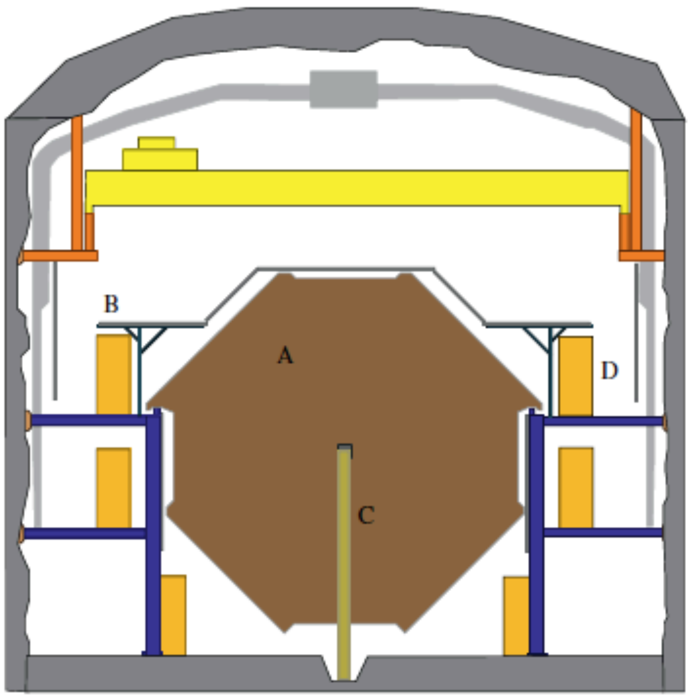

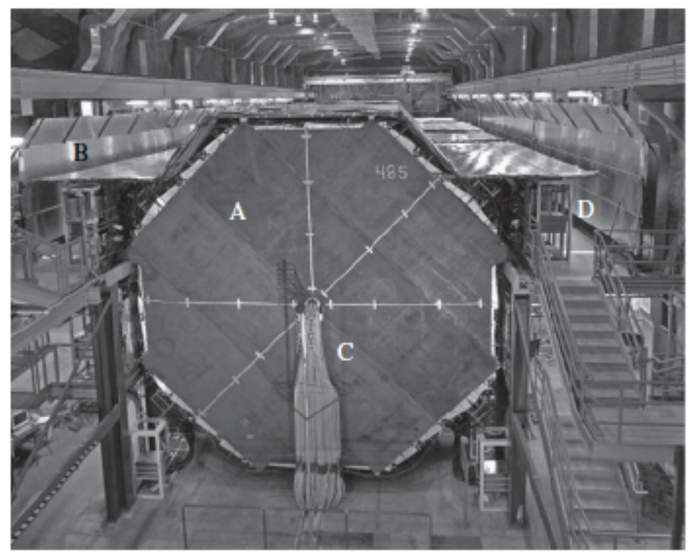

Fig. 1. End views of the second far detector supermodule, looking toward Fermilab. The drawing (left) identifies detector elements shown in the photograph (right): "A" is the furthest downstream steel plane, "B" is the cosmic ray veto shield, "C" is the end of the magnet coil and "D" is an electronics rack on one of the elevated walkways alongside the detector. The horizontal structure above the detector is the overhead crane bridge.

Near Detector at Fermilab
100 m underground

D.G. Michael et al. / Nuclear Instruments and Methods in Physics Research A 596 (2008) 190–228 193

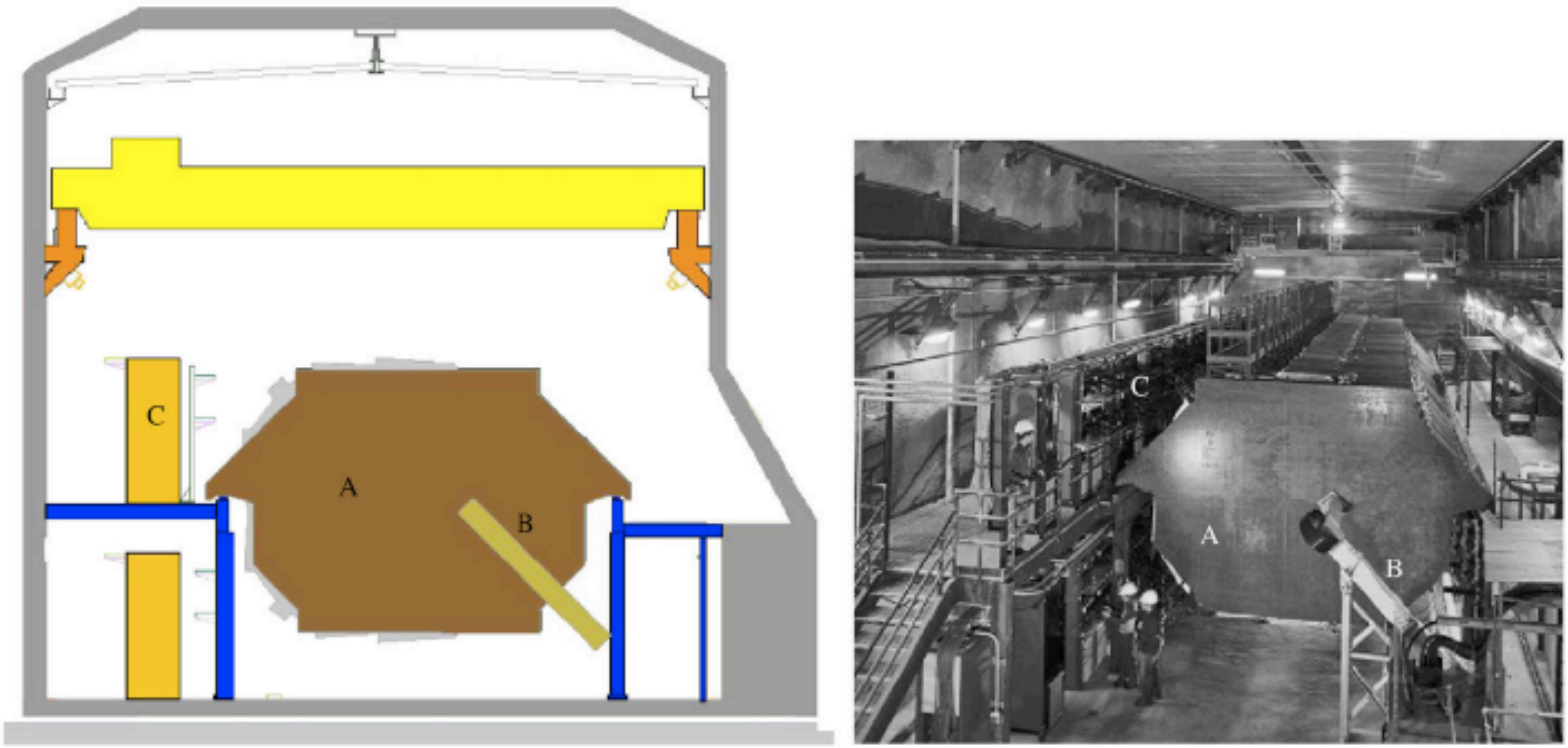

Fig. 2. End view of the near detector, looking toward Soudan. The drawing (left) identifies detector elements shown in the photograph (right): "A" is the furthest upstream steel plane, "B" is the magnet coil, and "C" is an electronics rack on the elevated walkway. Above the detector is the overhead crane bridge. The NuMI beam intersects the near detector near the "A" label.

Near Detector – 1,040 m from the target at Fermilab

- veto - target - μ spectrometer
- mass = 1 kT
- 153 scintillator planes
- QIE-based front-end
- 3.8 x 4.8 "squeezed" octagon
- 12,300 scint.strips
- 1-end readout
- no-multiplexing
- 220 M64s
- 282 steel planes
- 65 km WLS fiber
- 51 km clear fiber

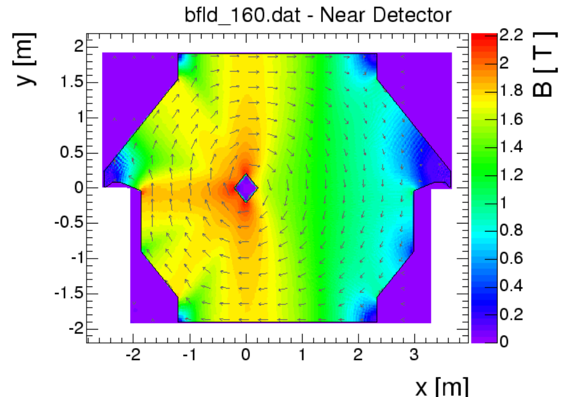

103 m underground

ν target region

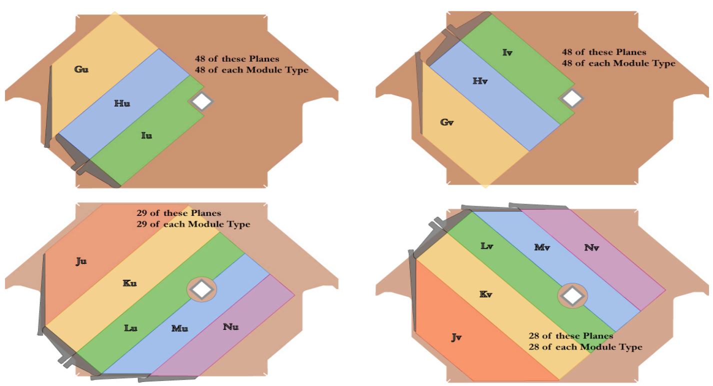

μ spectrometer region

Far Detector – 735.3 km away
(Soudan Mine, Mn)

Running since July 2003

- 2 Supermodules
- 5.4 kT
- 484 scint. planes
- CR veto shield (2,070mwe)
- B ~ 1.5T (R=2m)
- 93,120 strips (4.1 x 1.0 cm)
- 8-fold MUXed 2-ended readout
- 1551 M16s
- 722 km of WLS fiber
- 794 km of clear fiber
- HAD = 56% / E $^{1/2}$
- EM = 23% / E ^{½}

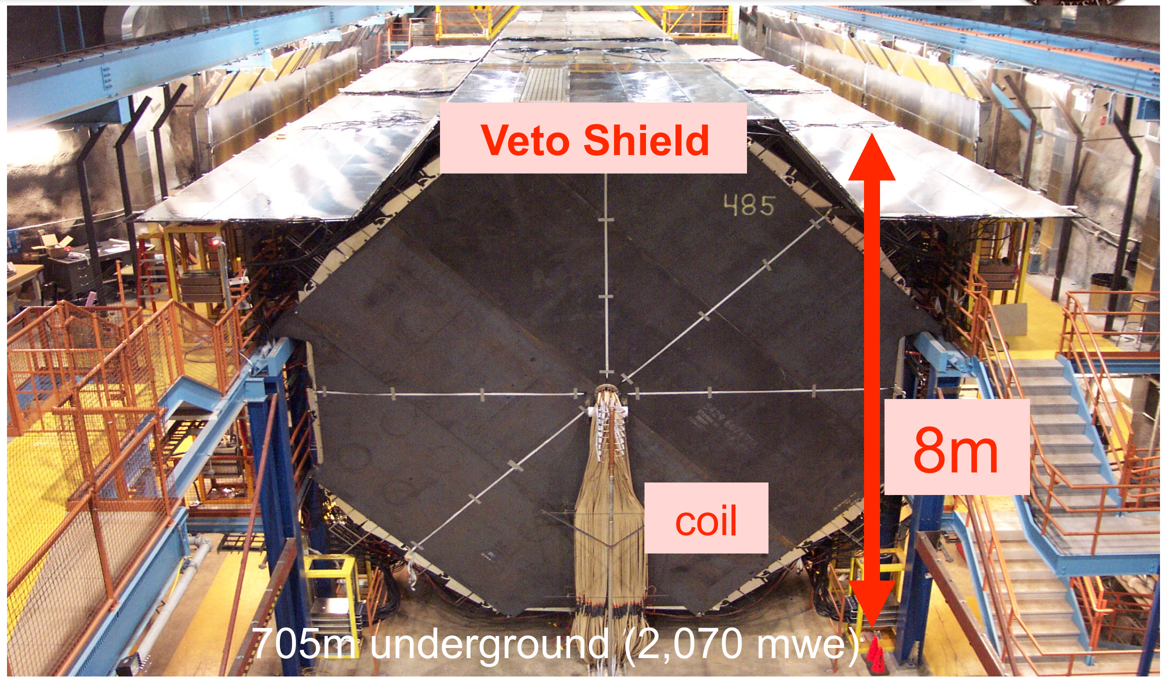

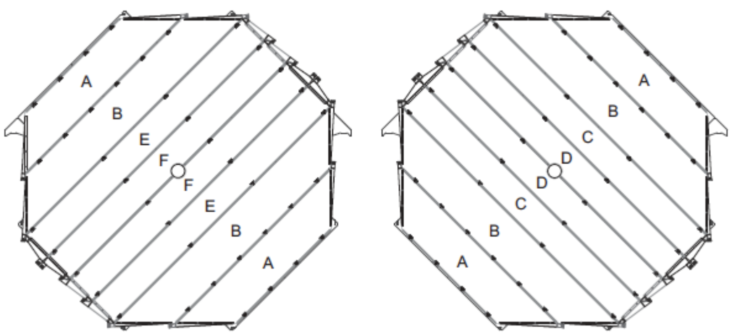

Scintillator Plane
(8 modules, 192 strips)

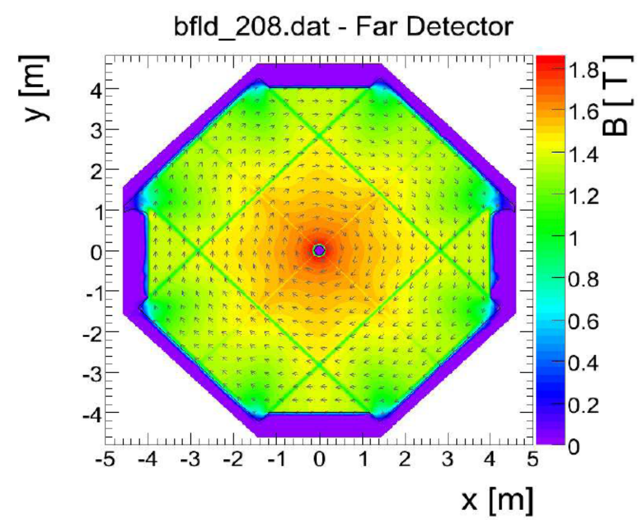

“MINOS technology”

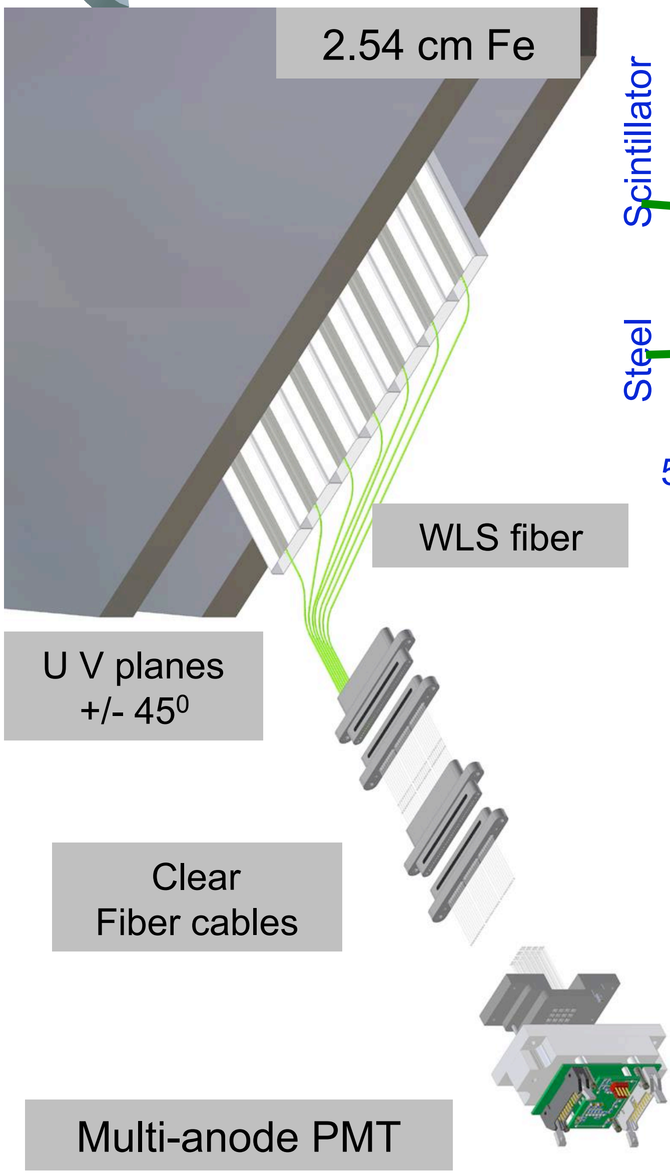

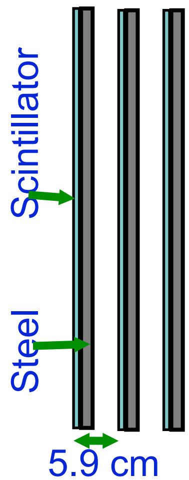

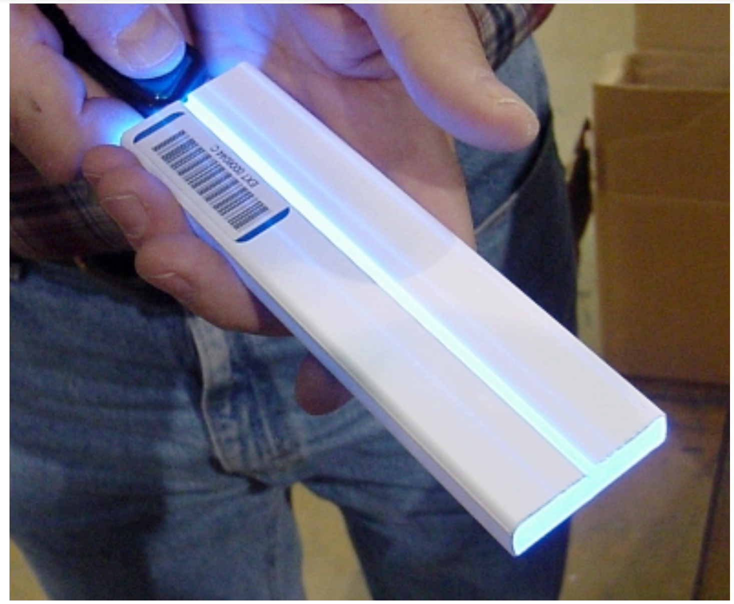

Extruded
PS scint.
4.1 x 1 cm

Far Det

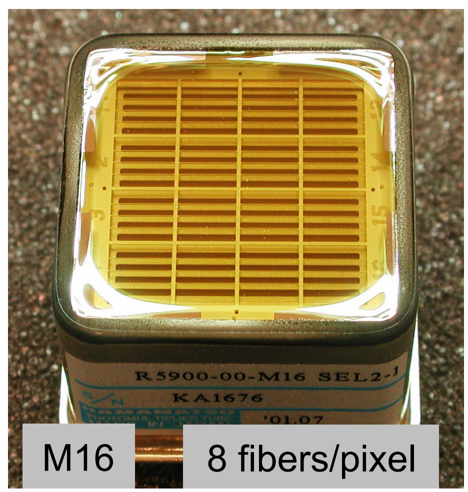

Near Det

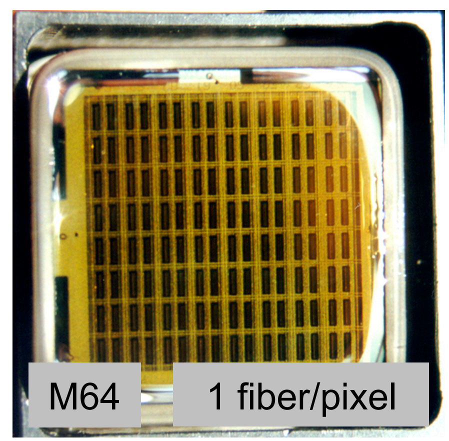

EXTRUDED SCINTILLATORS

Co-extruded scintillator strip + reflector use wavelength shifting (WLS) fibers as readout.

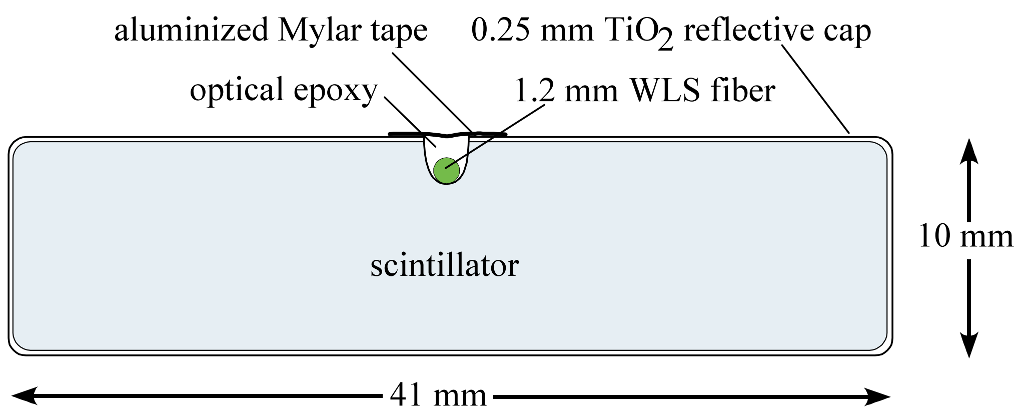

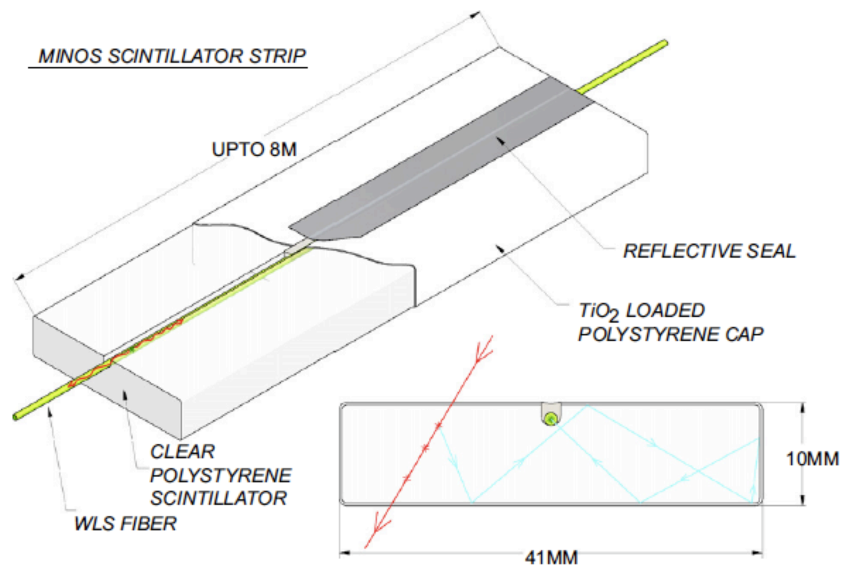

SELECTION OF RAW MATERIALS

BLUE SCINTILLATOR CORE

- **Polystyrene: Dow Styron 663 W**
- **Dopants: 1% PPO + 0.03% POPOP**

WHITE CAPSTOCKING

- **Polystyrene with 12% TiO_2 – 0.25 mm thick**

GREEN FIBER

- **K-27 fiber – 1.2 mm diameter**

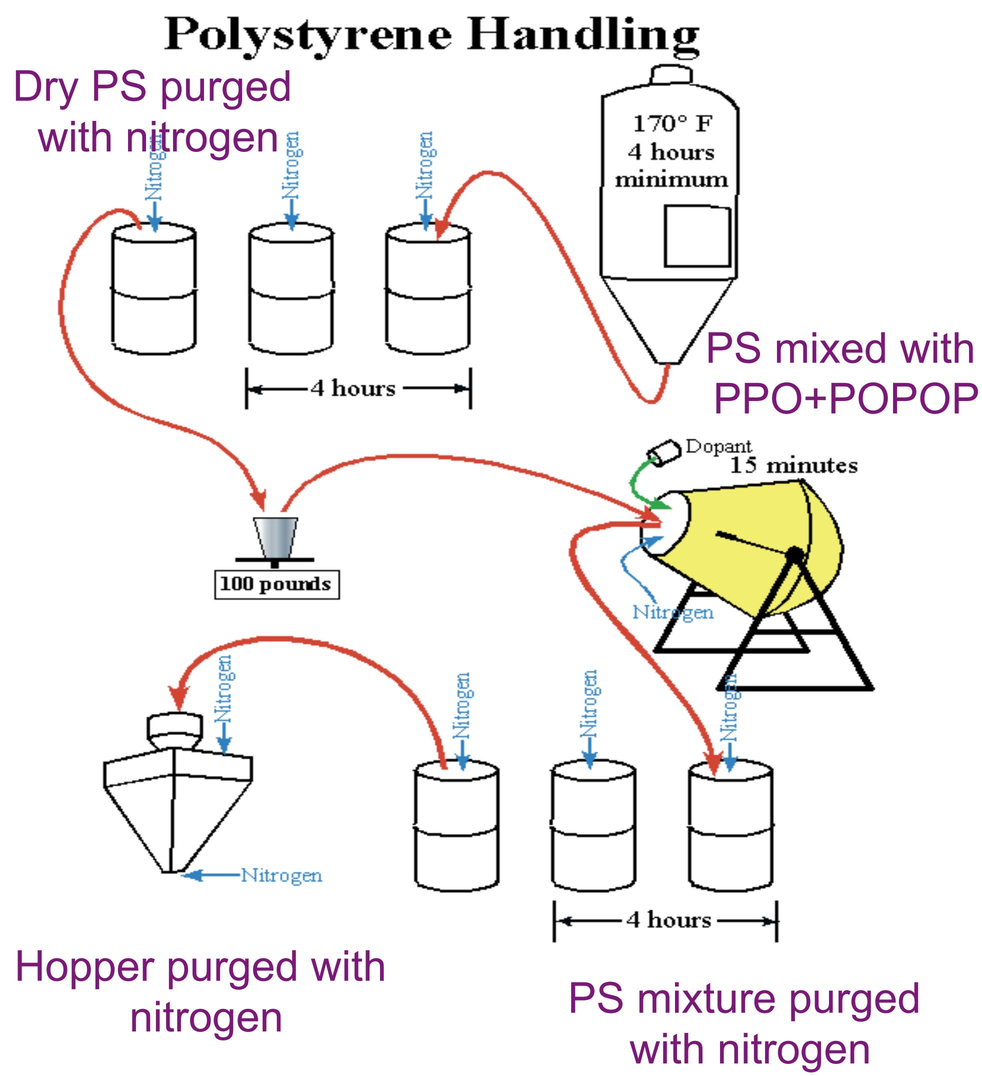

EXTRUSION AT ITASCA PLASTICS

EXTRUSION AT ITASCA PLASTICS

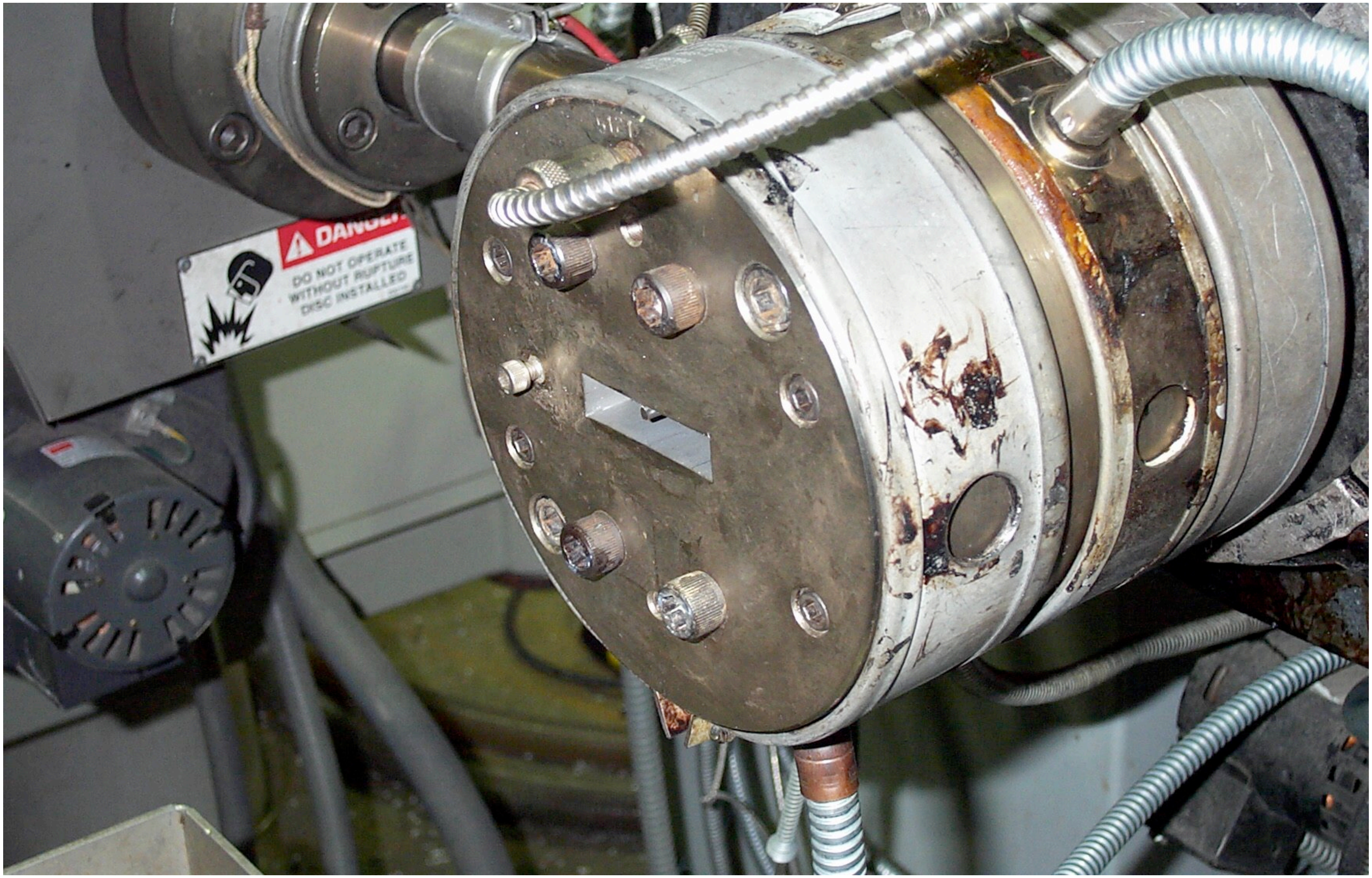

EXTRUSION AT ITASCA PLASTICS

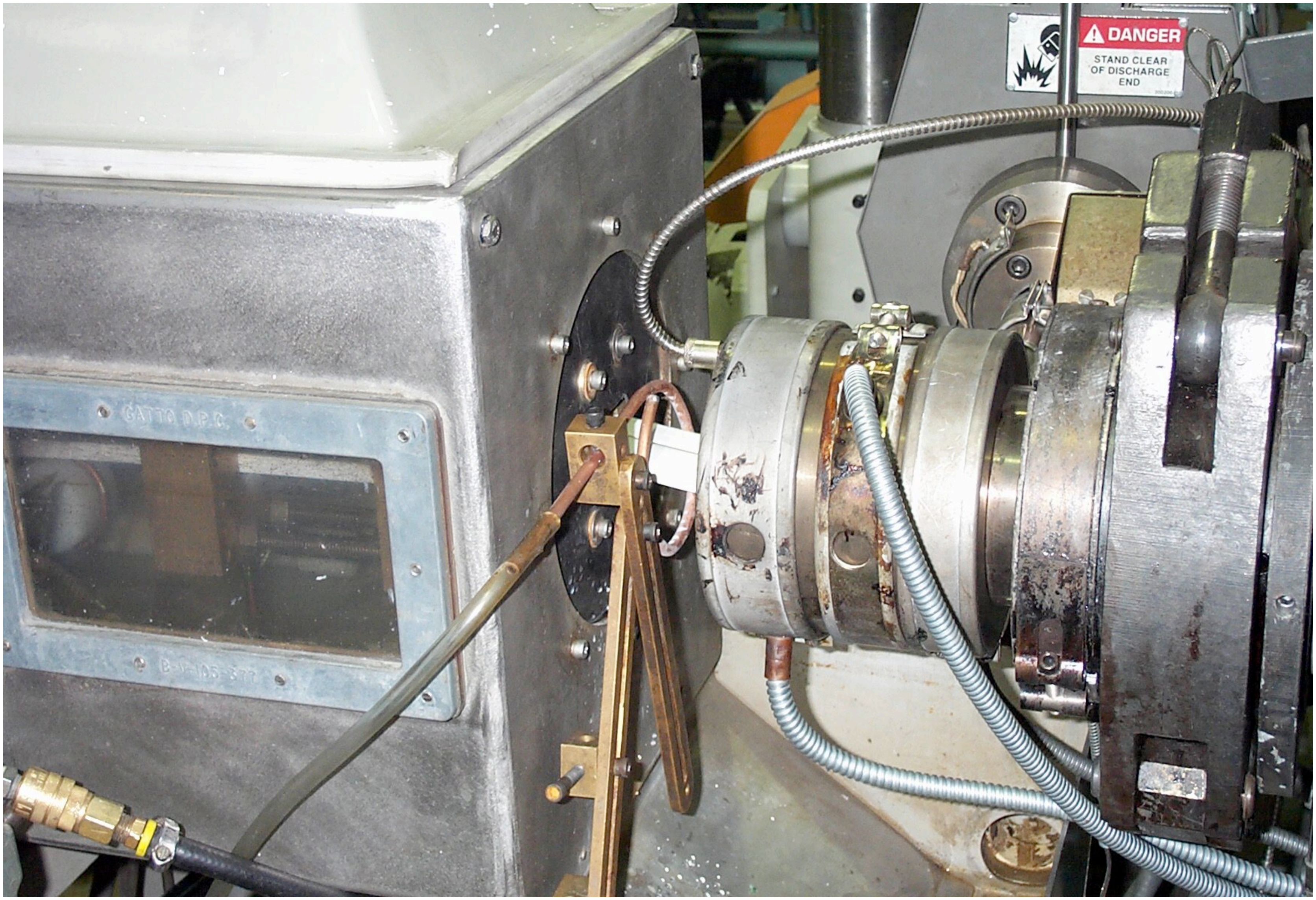

EXTRUDED SCINTILLATOR STRIPS

QC: LIGHT YIELD

QC SETUP AT THE FACTORY

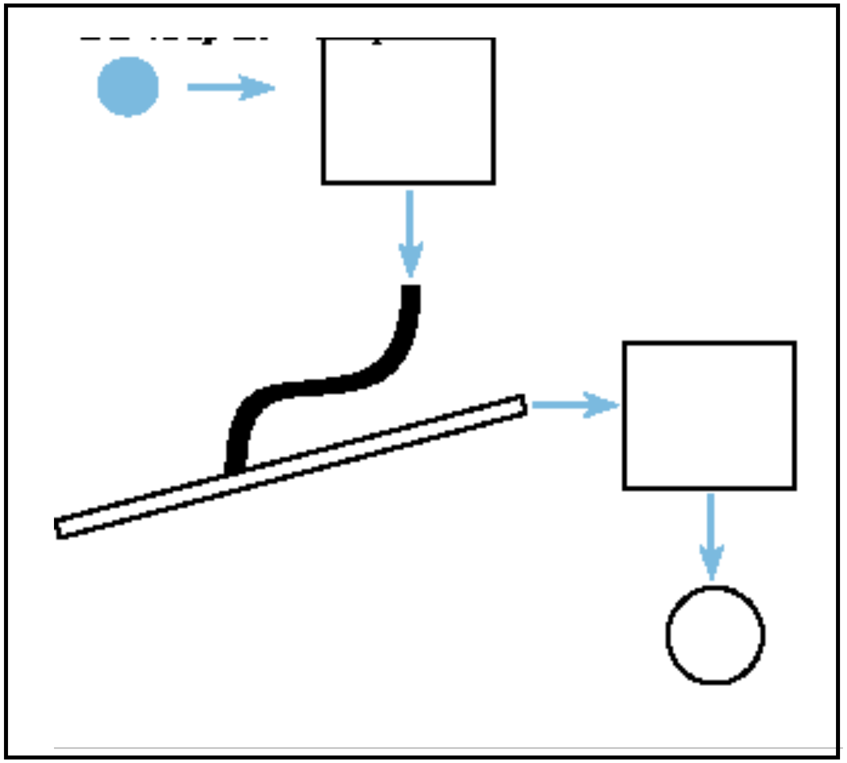

COMPARISON OF MEASUREMENTS

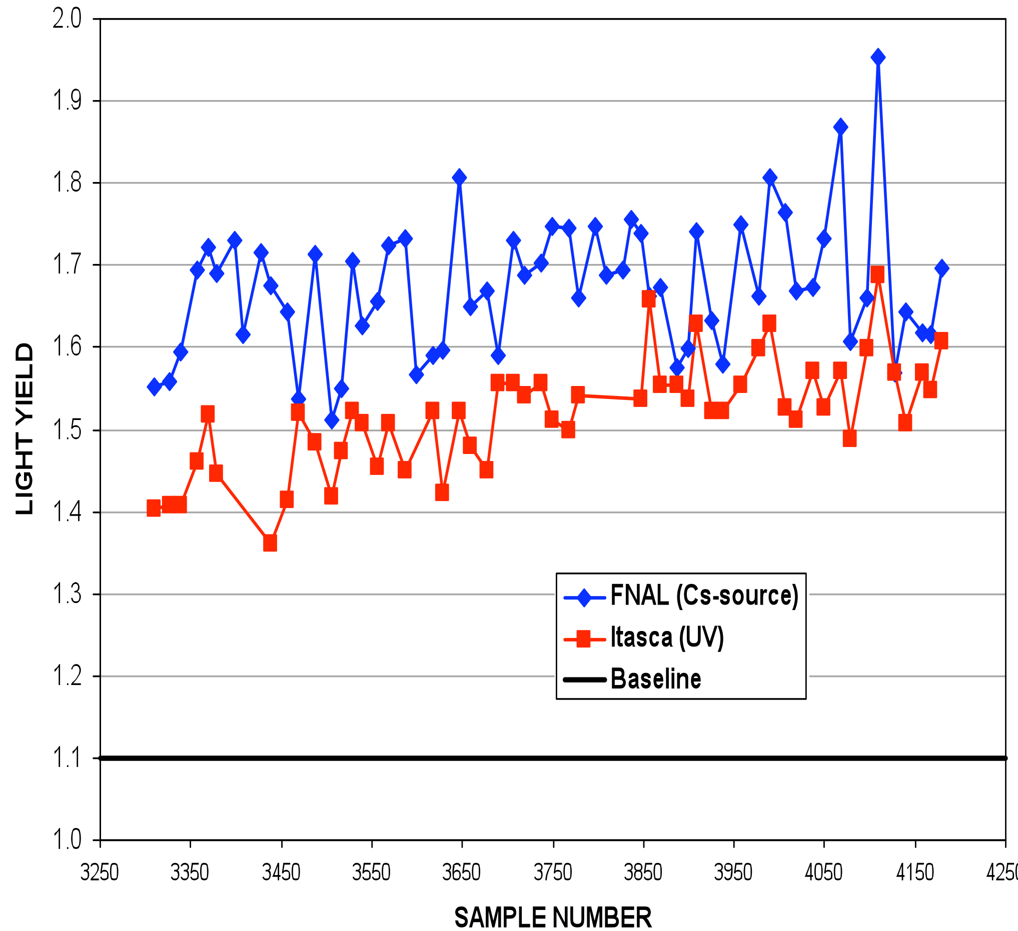

Module Assembly II

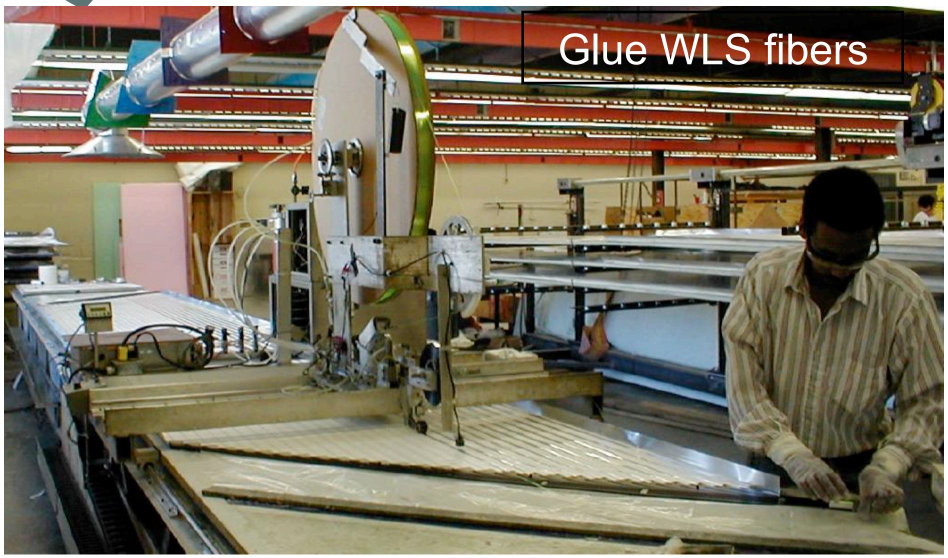

Scenes from Minnesota Module Factory

45 Degree End Manifold

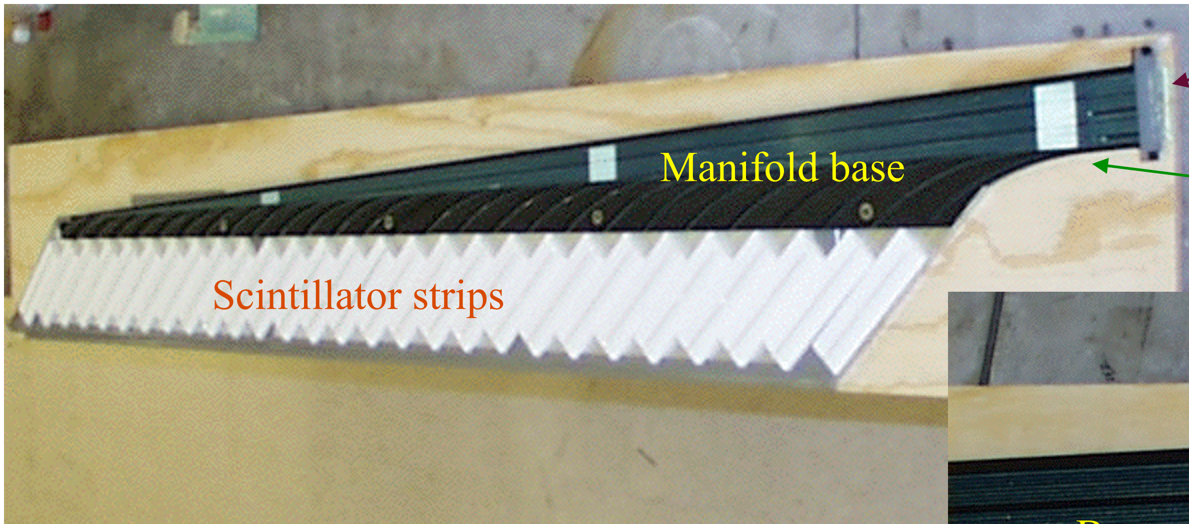

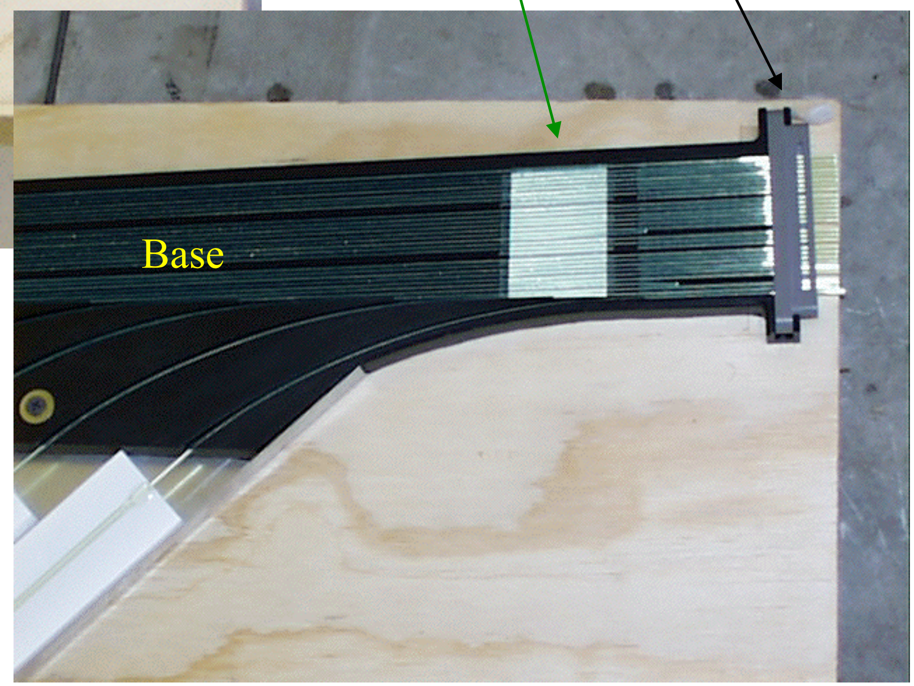

- Identical construction (modulo a mirror image) for all 45^o modules.
- The longest manifold part but with relatively easy fiber routing constraints.

Module Assembly

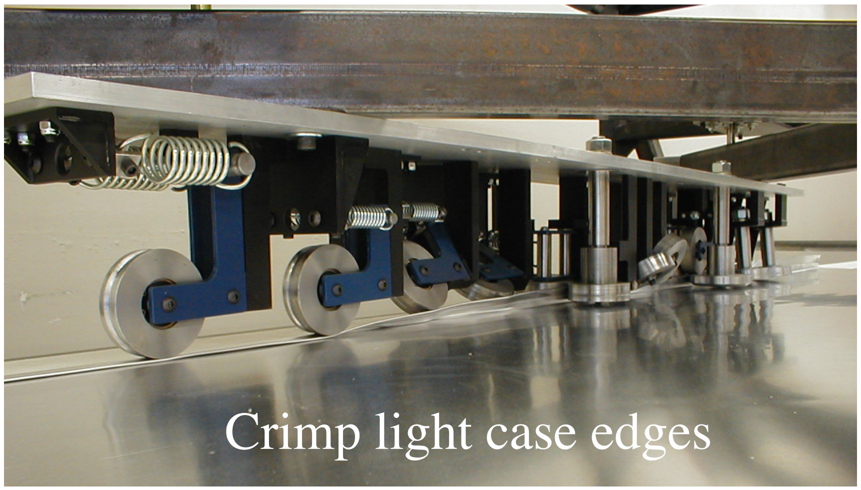
Crimp light case edges

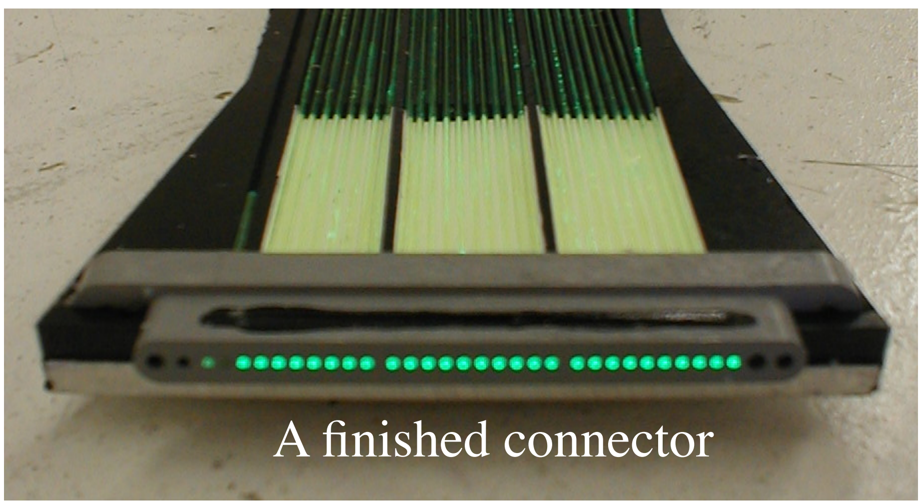
A finished connector


Flycut optical connector

Scenes from Minnesota Module Factory

NearDet construction (finished in Dec'2004)

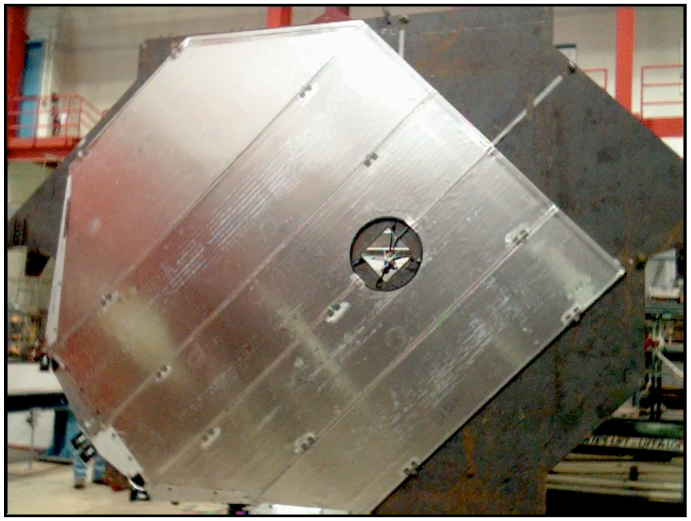

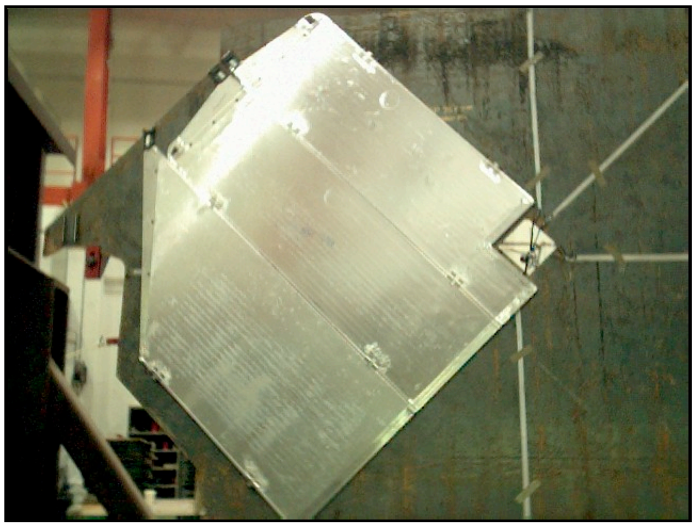

Radioactive source mapping

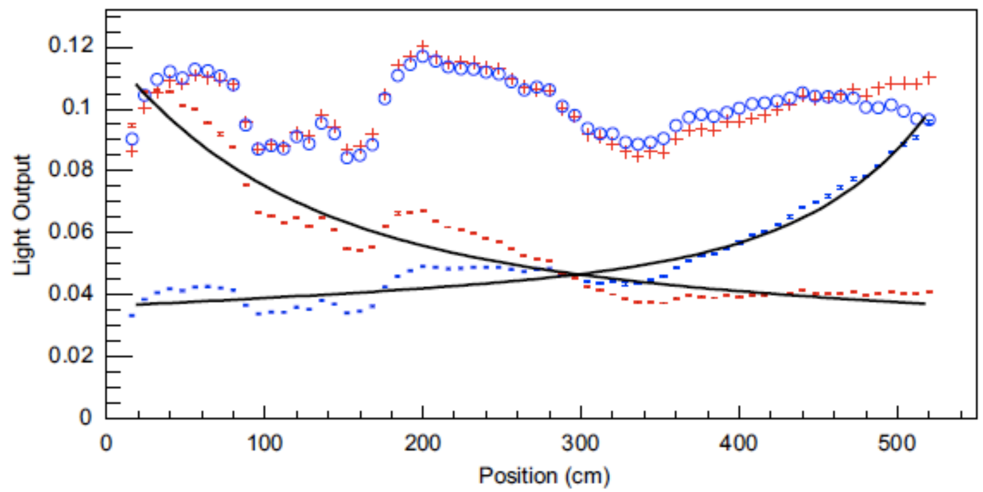

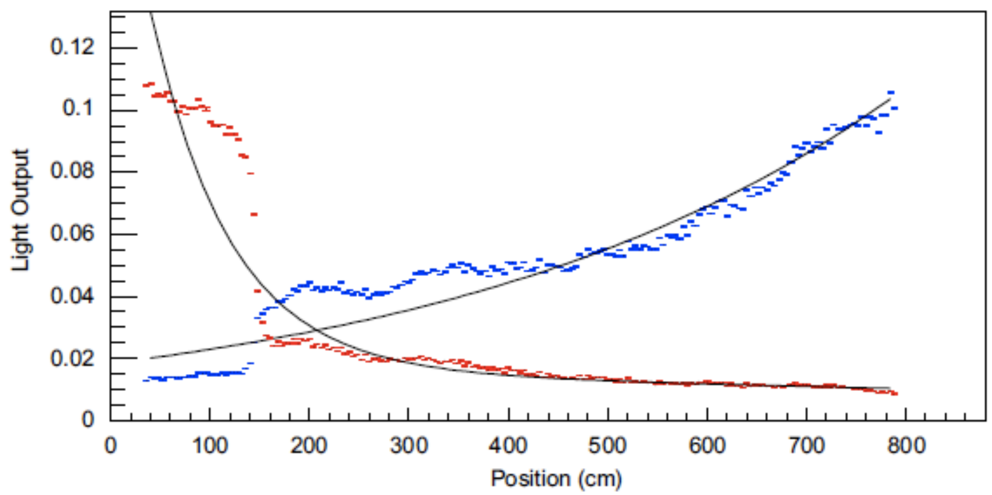

Plane assembly

Steel Welded and modules placed.

Plane lifted to vertical

Crane carries plane down the hall for installation

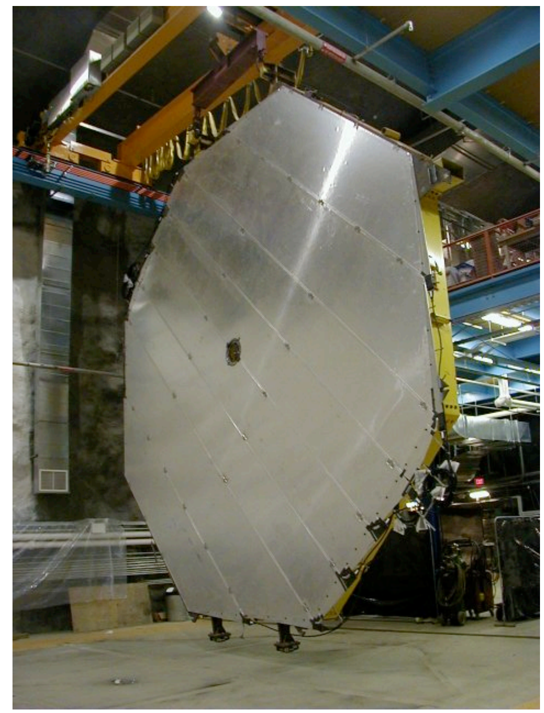

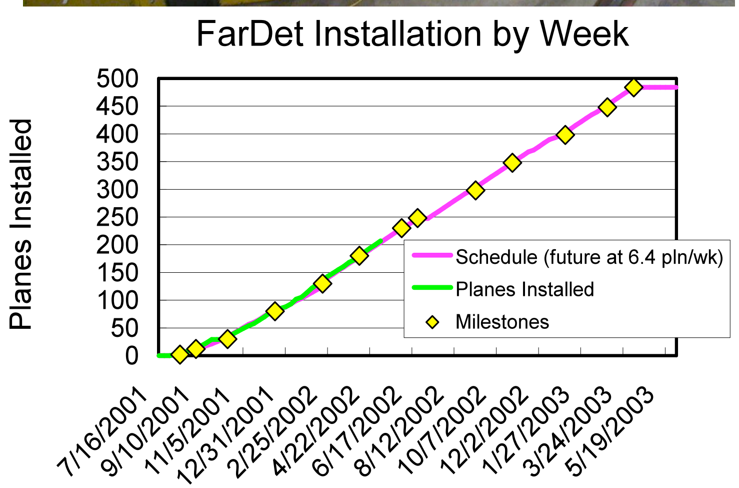

6-8 Planes per week

4-Plane Prototype

Built ‘99 Summer at Fermilab

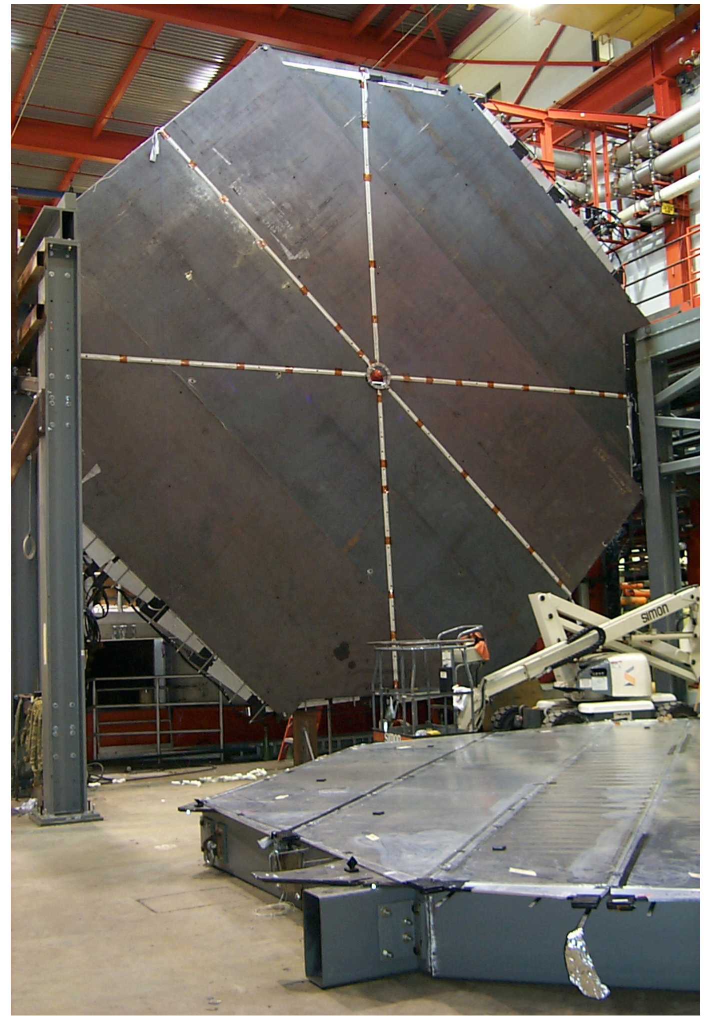

FarDet: Done (summer 2003)

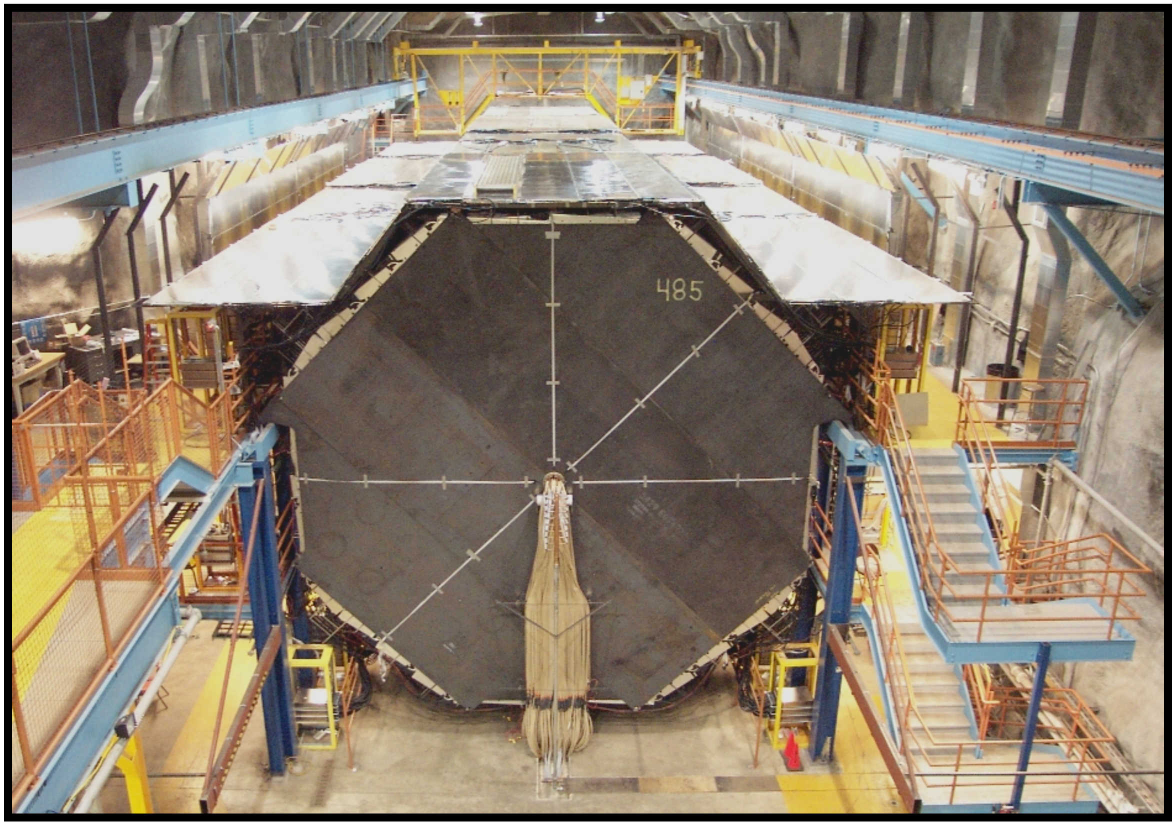

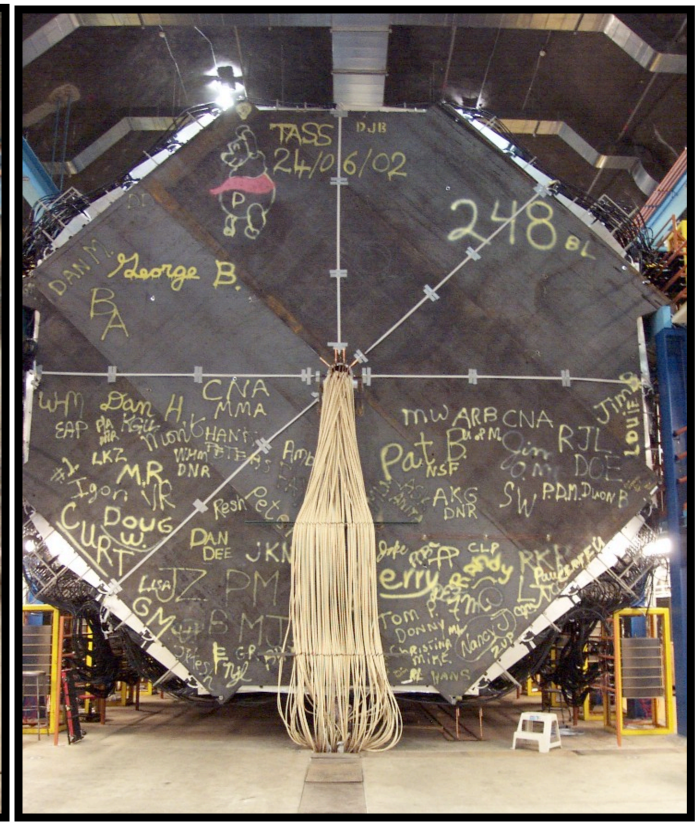

SM 1 + SM2 (248 + 237 = 485planes)

WLS Fiber Test Apparatus

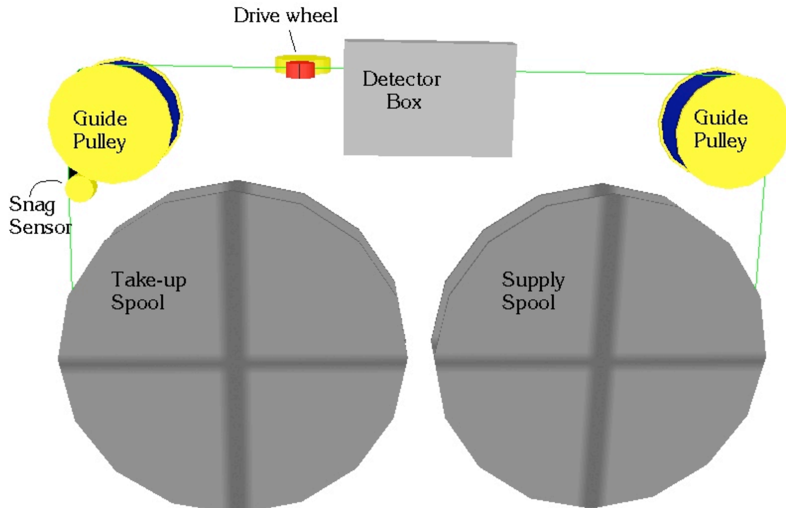

Spool Testing Device and performance

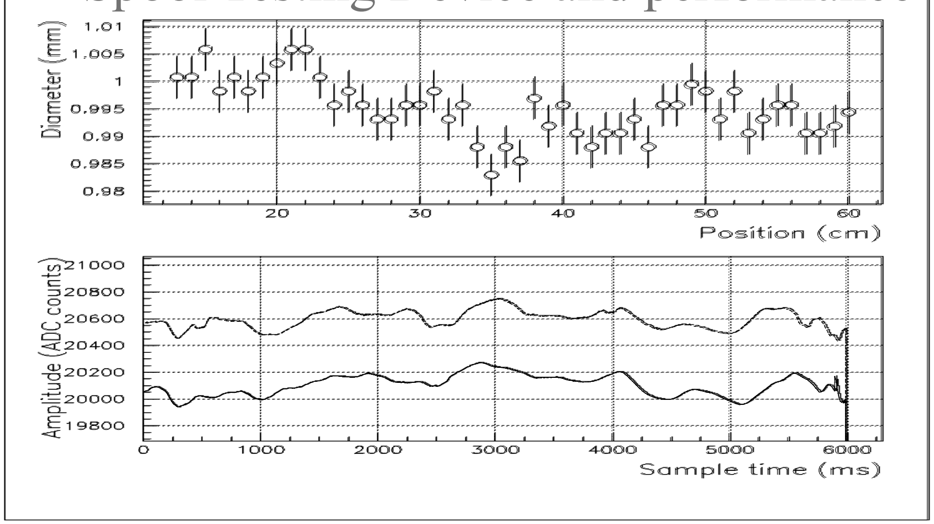

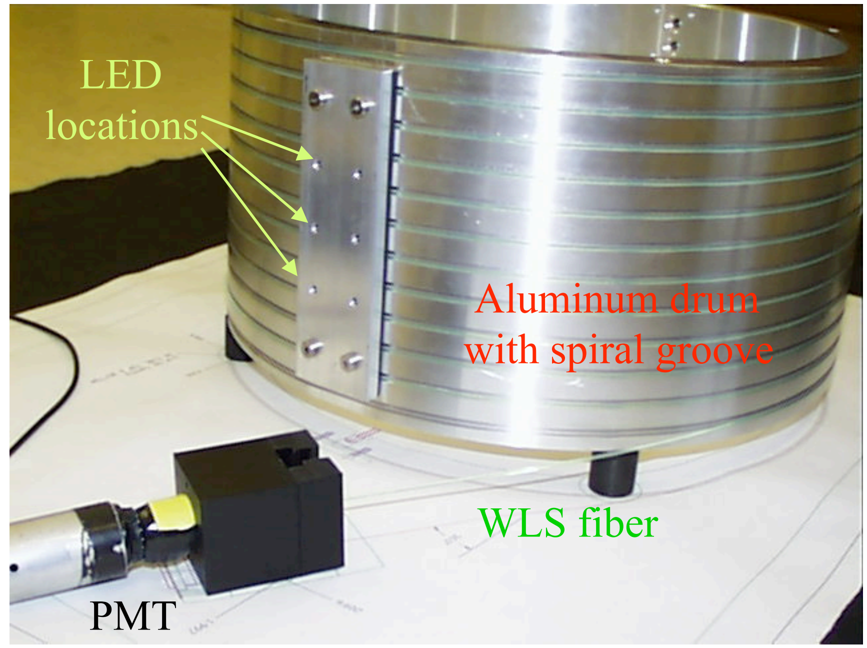

Sample fiber attenuation length measuring device.

Measurement of diameter variations in a spool.

Light yield in MINOS modules
Far Detector

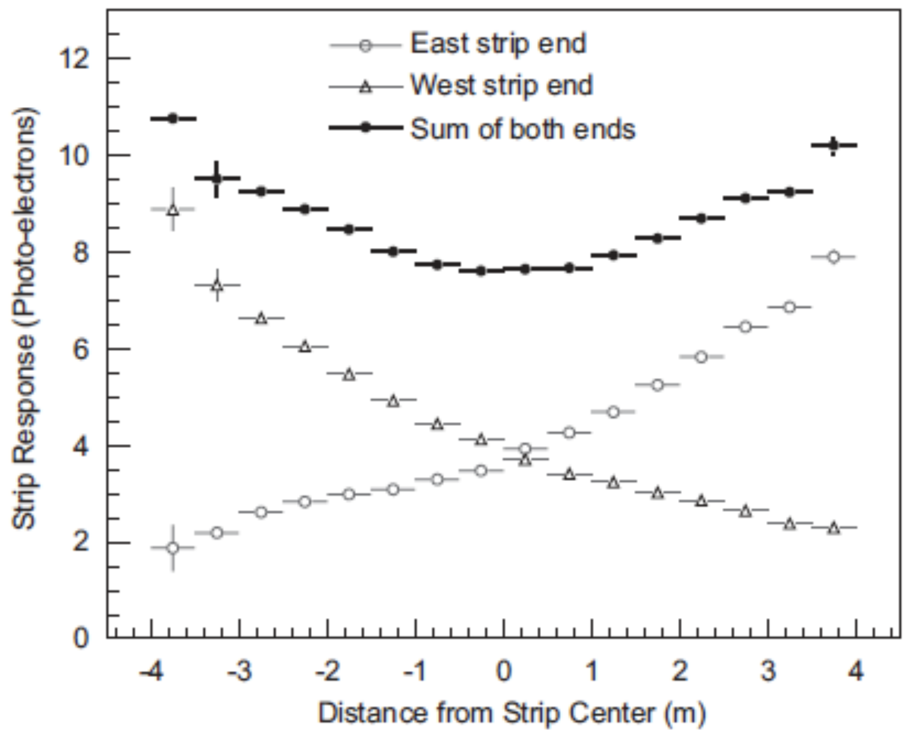

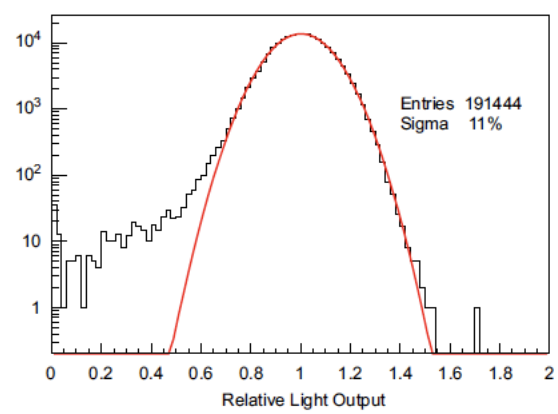

Drift (down) of light yield

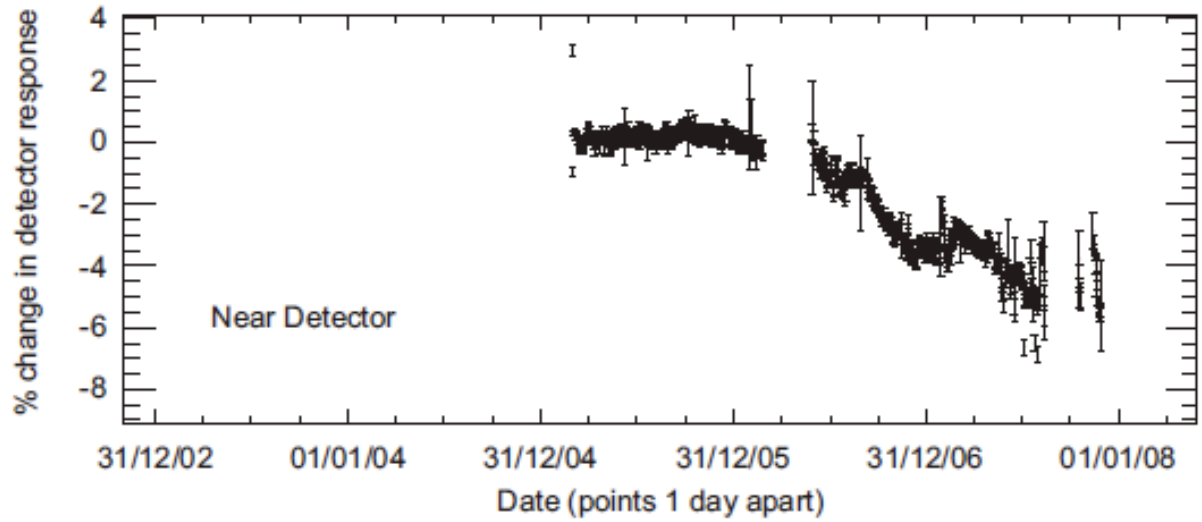

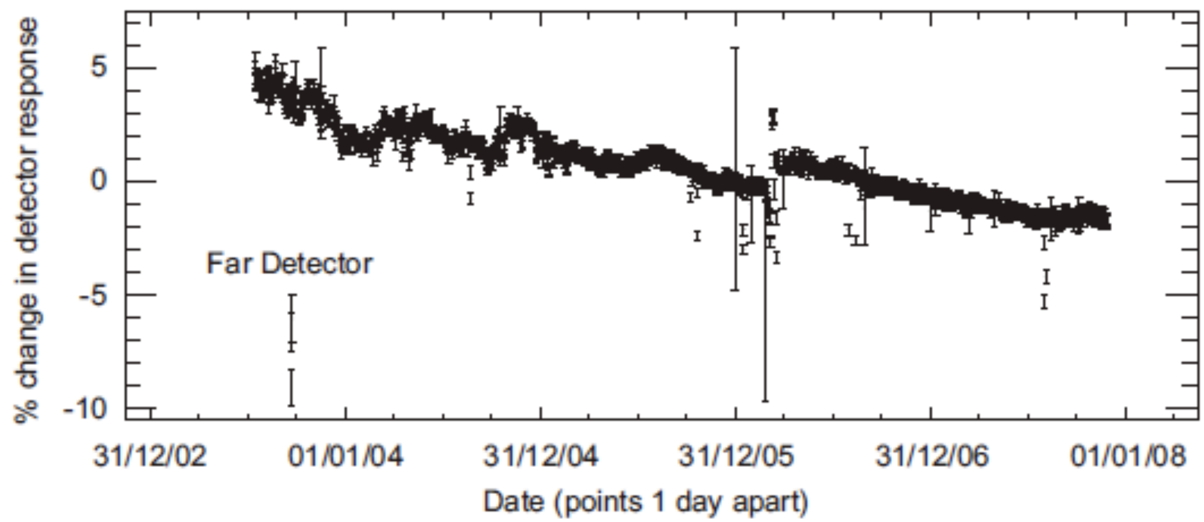

Available online at www.sciencedirect.com
SCIENCE DIRECT®
ELSEVIER
Nuclear Instruments and Methods in Physics Research A 545 (2005) 852–871
NUCLEAR INSTRUMENTS & METHODS IN PHYSICS RESEARCH Section A
www.elsevier.com/locate/nima

Characterization of 1600 Hamamatsu 16-anode photomultipliers for the MINOS Far detector

K. Lang[a,*], J. Day[a], S. Eilerts[a], S. Fuqua[a], A. Guillen[a], M. Kordosky[a], M. Lang[a], J. Liu[a], W. Opaska[a], M. Proga[a], P. Vahle[a], A. Winbow[a], G. Drake[b], J. Thomas[c], C. Andreopoulos[d], N. Saoulidou[d], P. Stamoulis[d], G. Tzanakos[d], M. Zois[d], A. Weber[e], D. Michael[f]

FAR Detector

Hamamatsu's R-5900

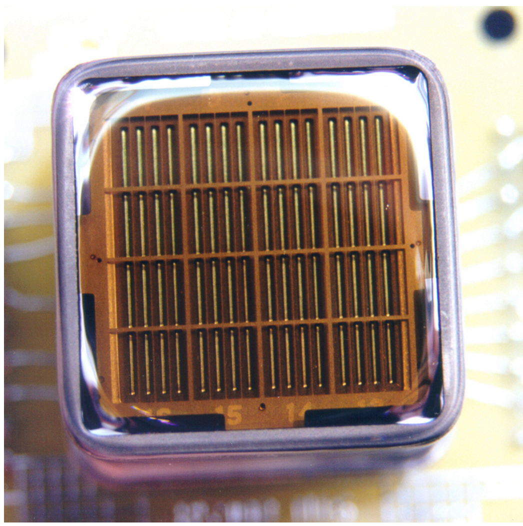

NEAR Detector

Hamamatsu's R-5900

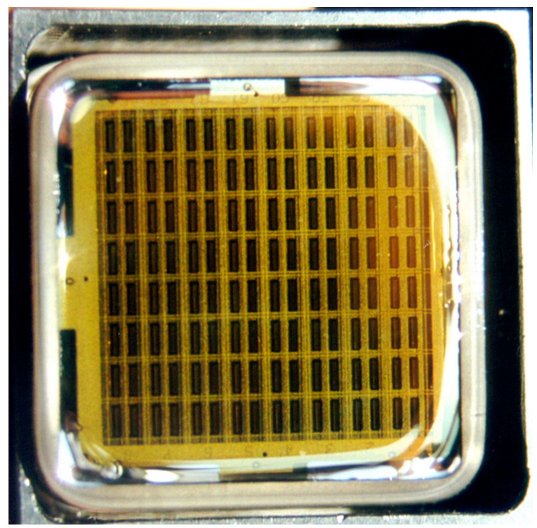

"The Eyes of MINOS"

Multi-anode PMTs + fibers

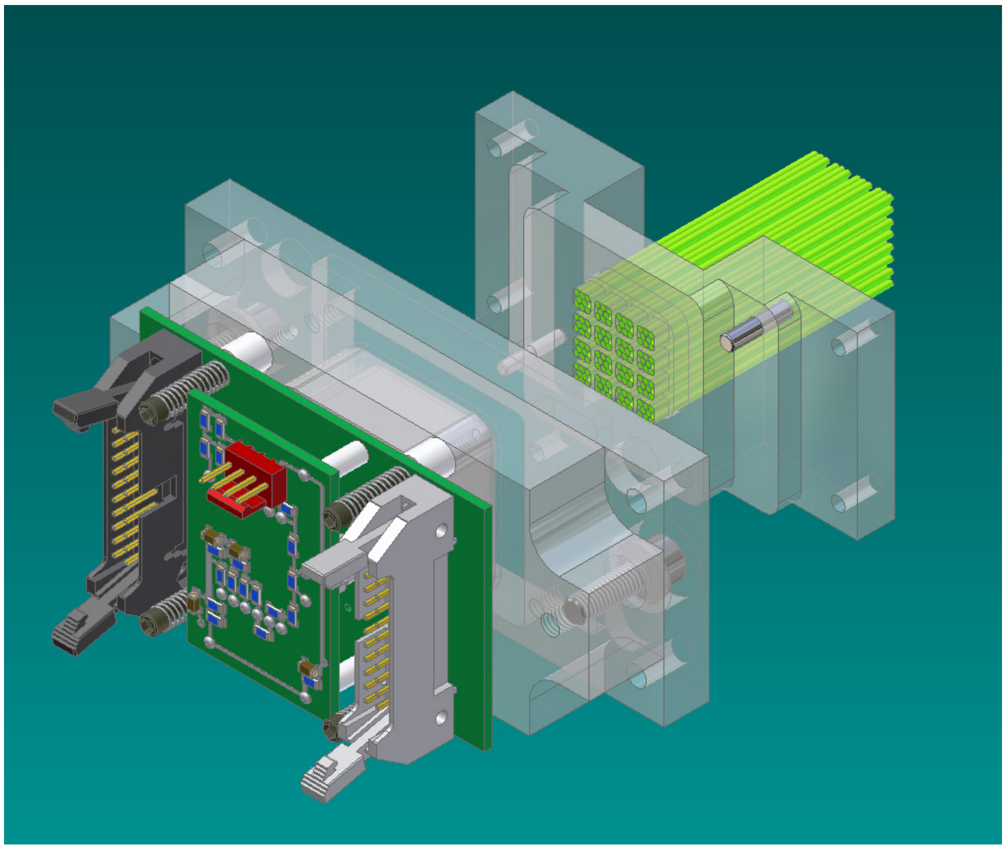

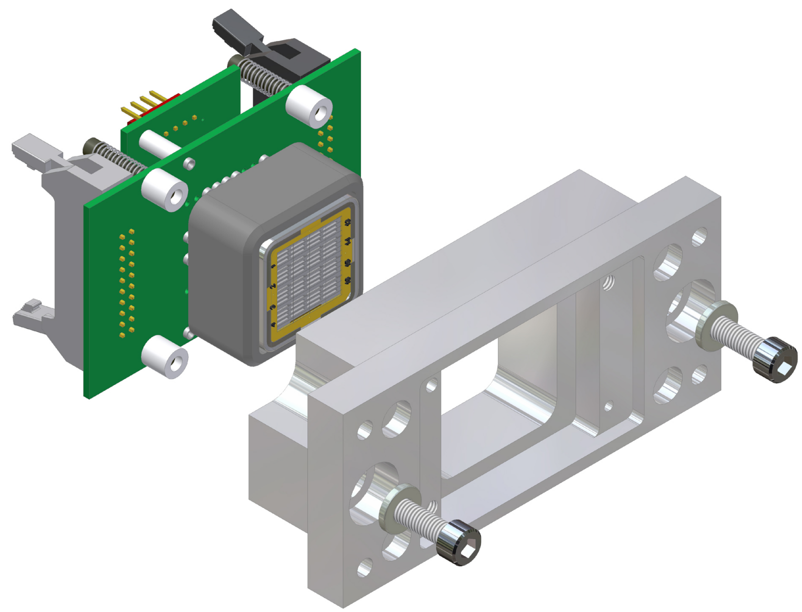

PMT Base and Mounting

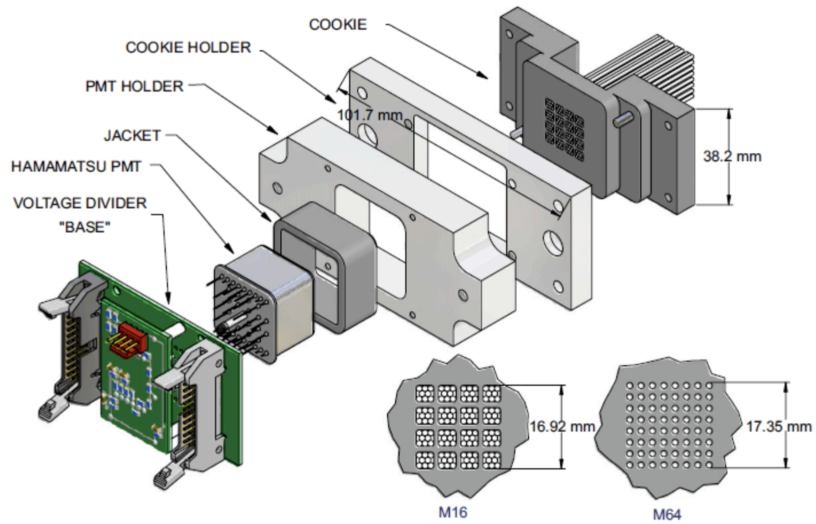

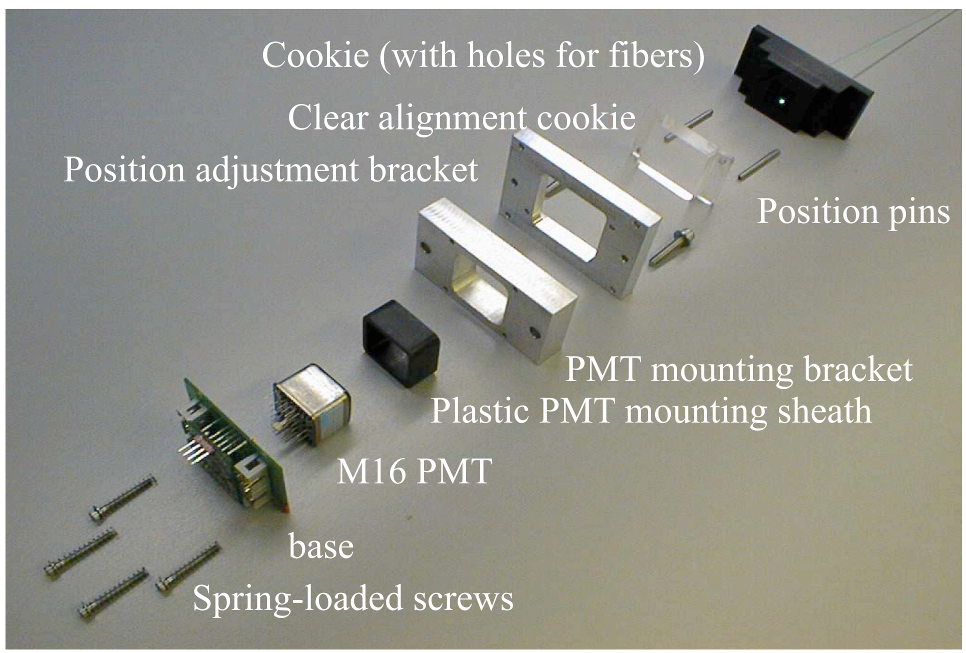

M16 Photodetectors
Read out 128 fibers

- Many new measurements of PMT response have been made in the last several months.
  - ⇨ Tubes are scanned with 1.2 mm WLS fibers excited by blue LEDs.
  - ⇨ The results from the positions of "final installed fibers" are tabulated.
- The measurements and other studies have confirmed the baseline plan for the far detector is optimal.
- We are still comparing M64 and M16 in the near detector due to no multiplexing.

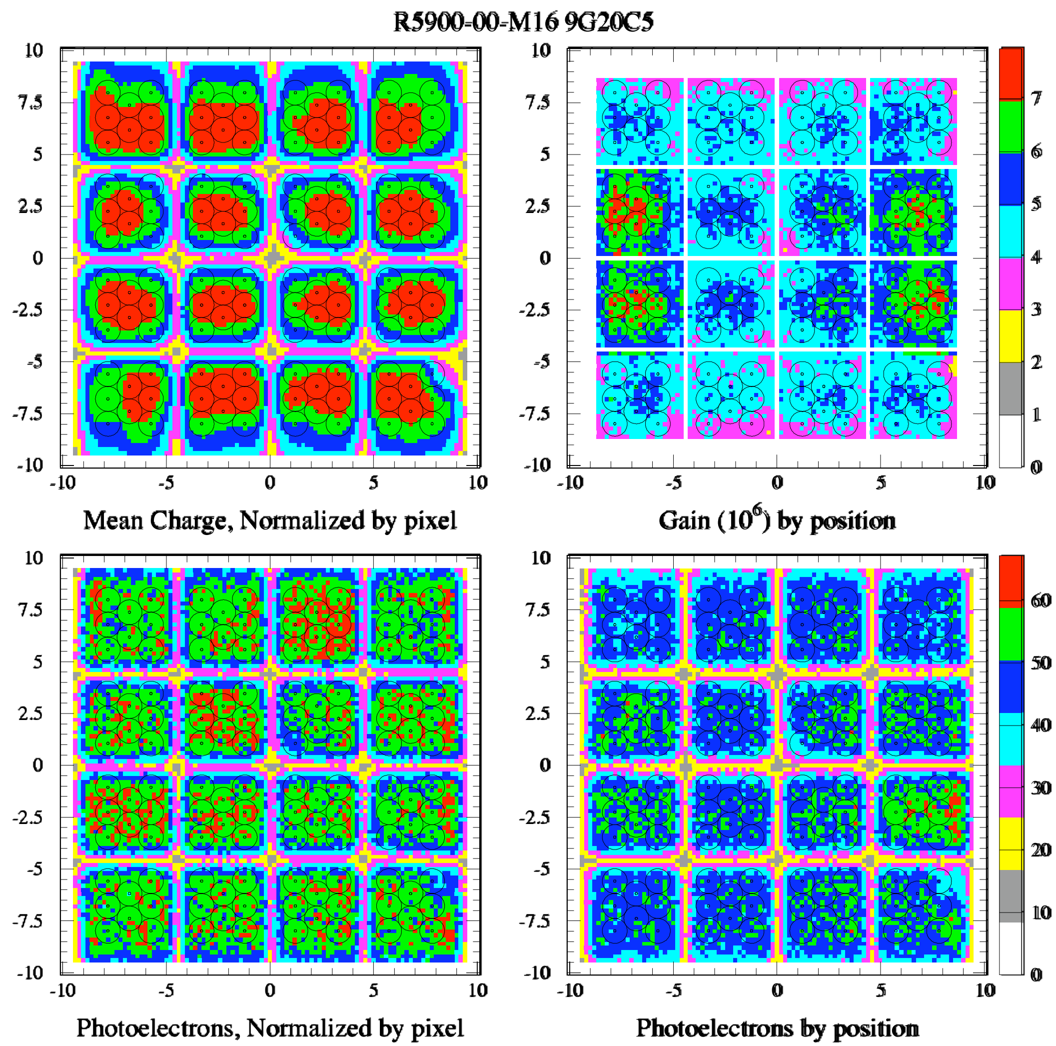

M16 test stand
1536 fibers into 128 "plugs"

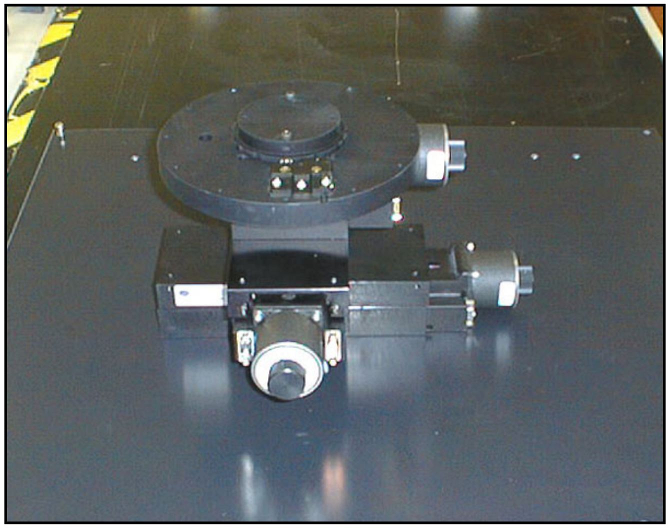

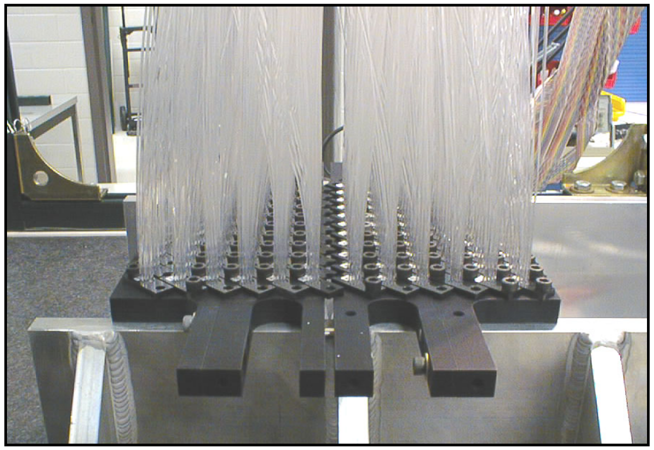

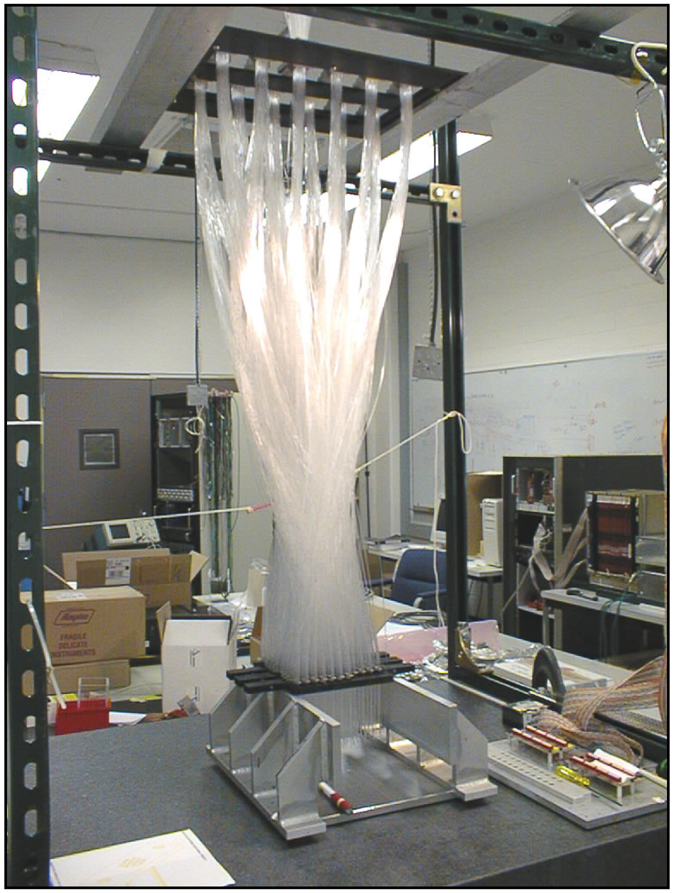

M16 alignment

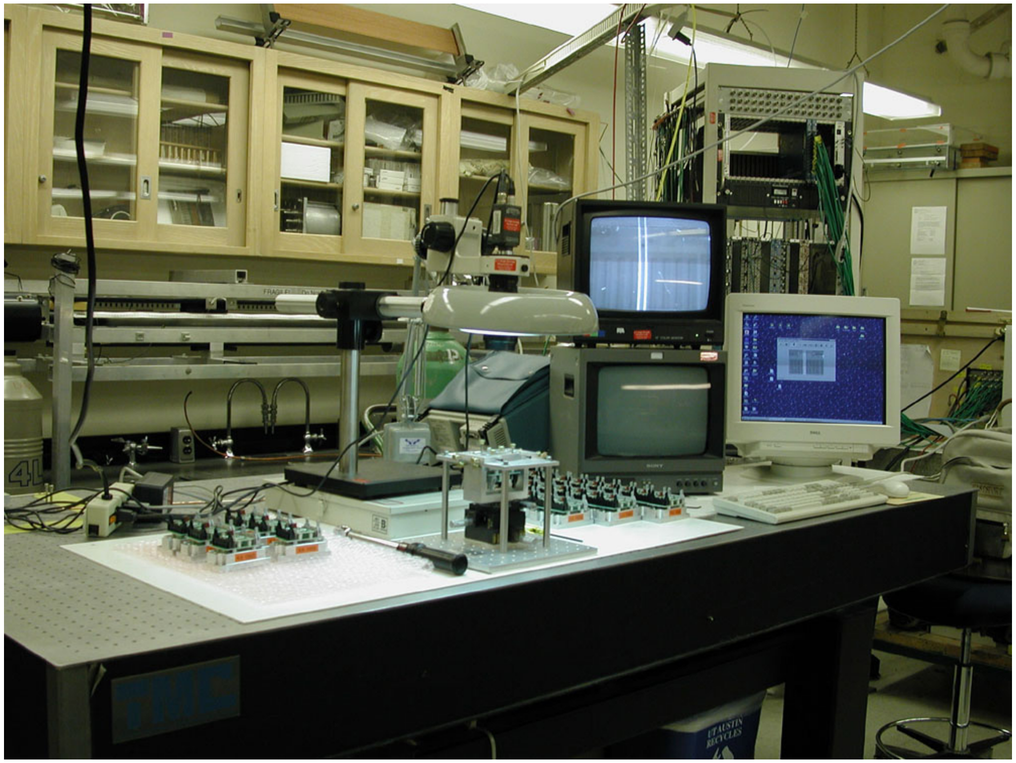

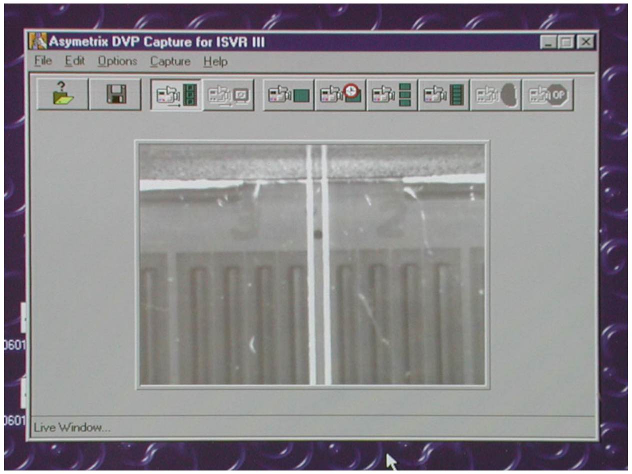

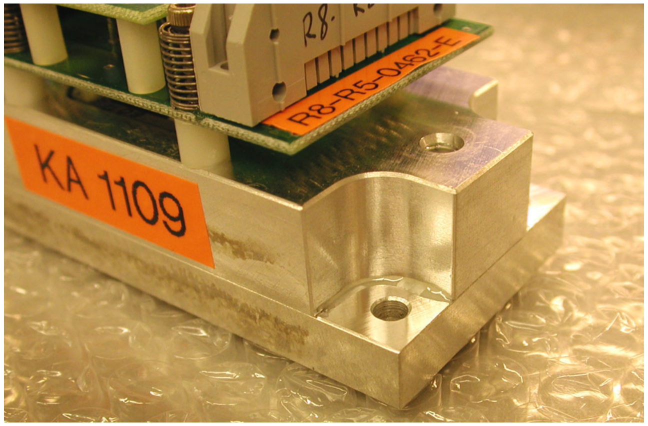

A PMT "certificate"

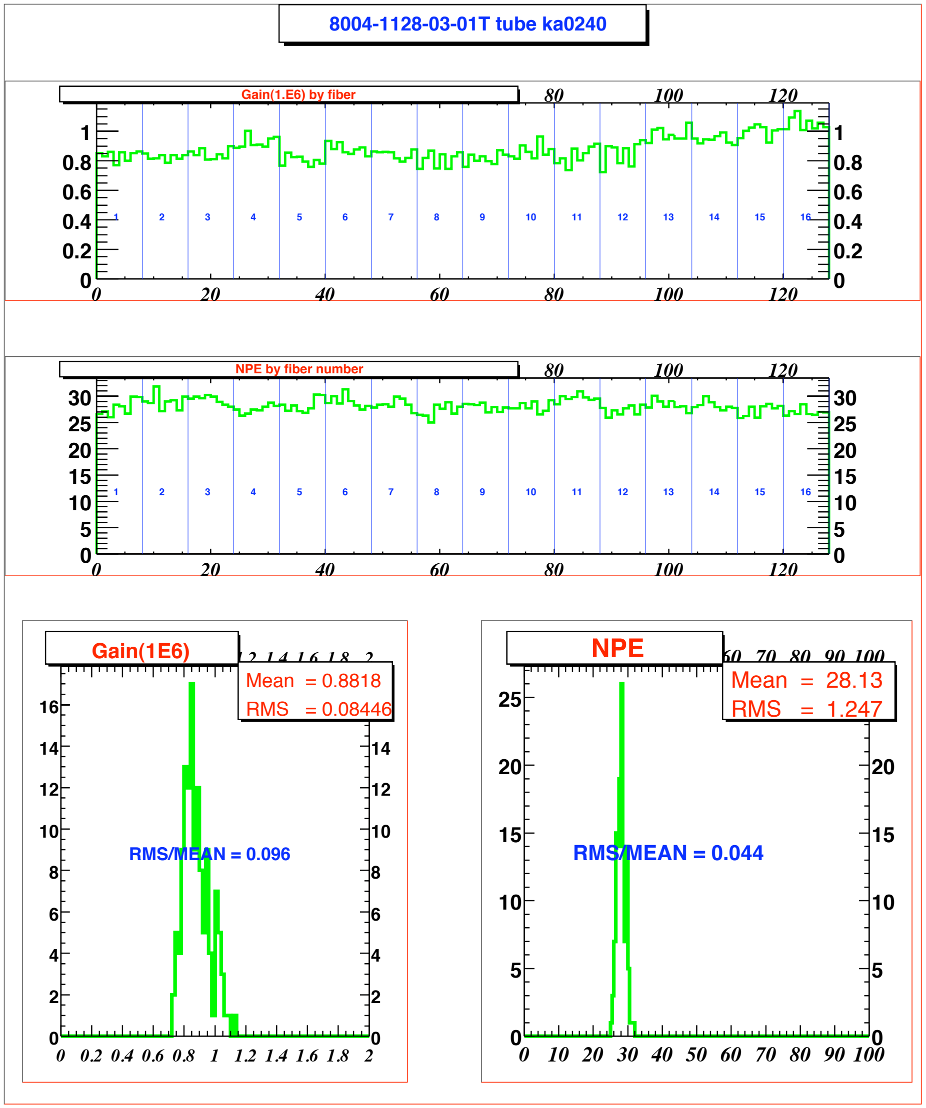

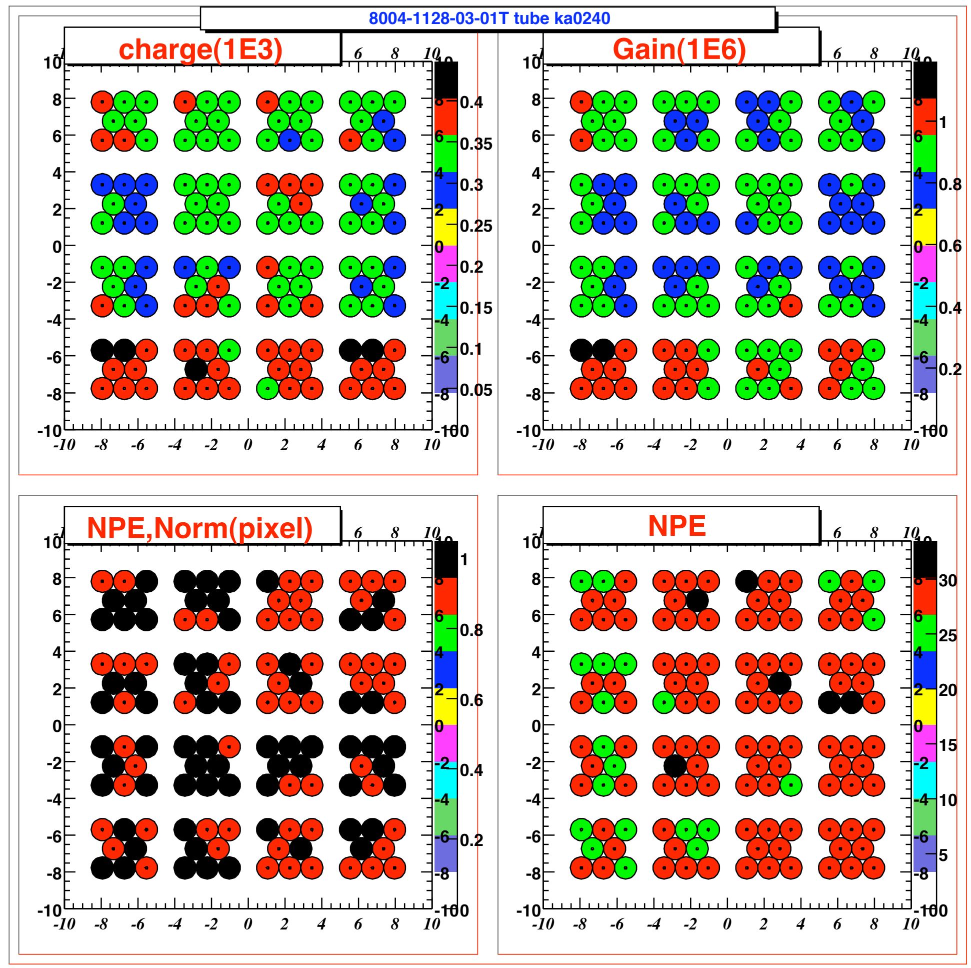

M16 cross talk

866 K. Lang et al. / Nuclear Instruments and Methods in Physics Research A 545 (2005) 852–871

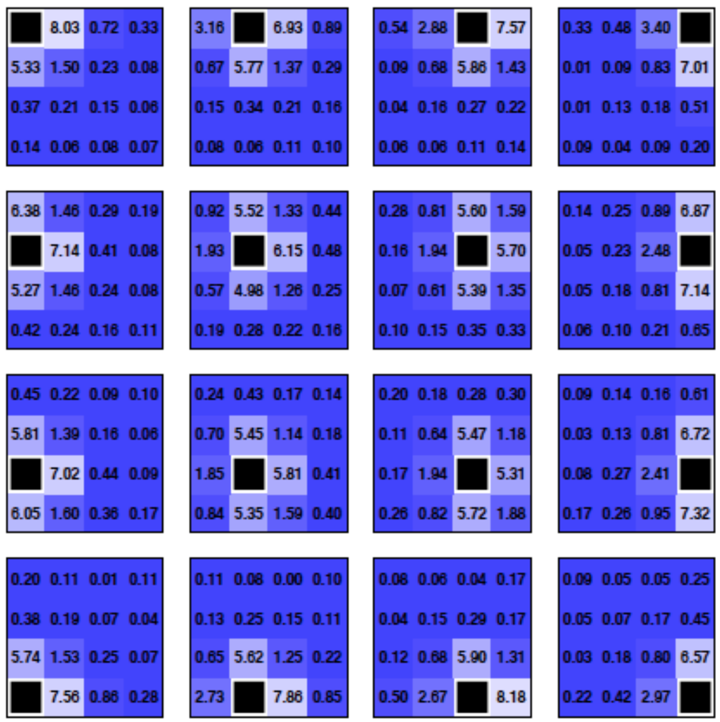

Fig. 11. The fraction of charge detected in a pixel due to optical cross-talk. The black square indicates the illuminate fiber #4 was illuminated. Results are in units of 10^{-3}.

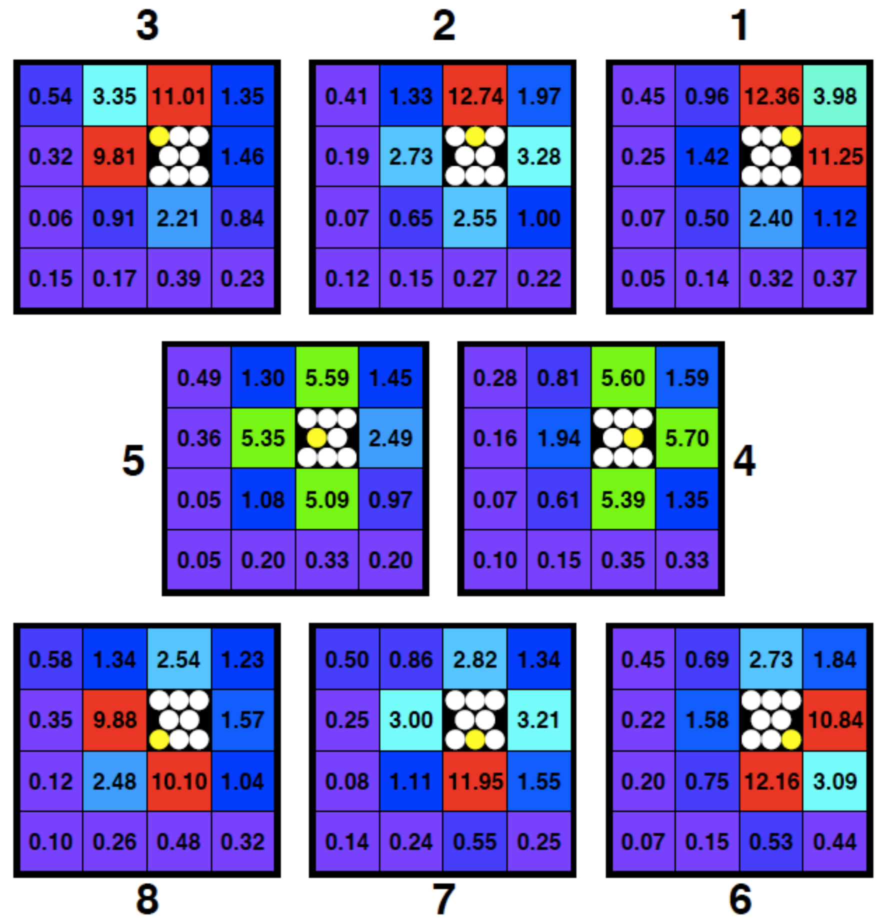

Event display

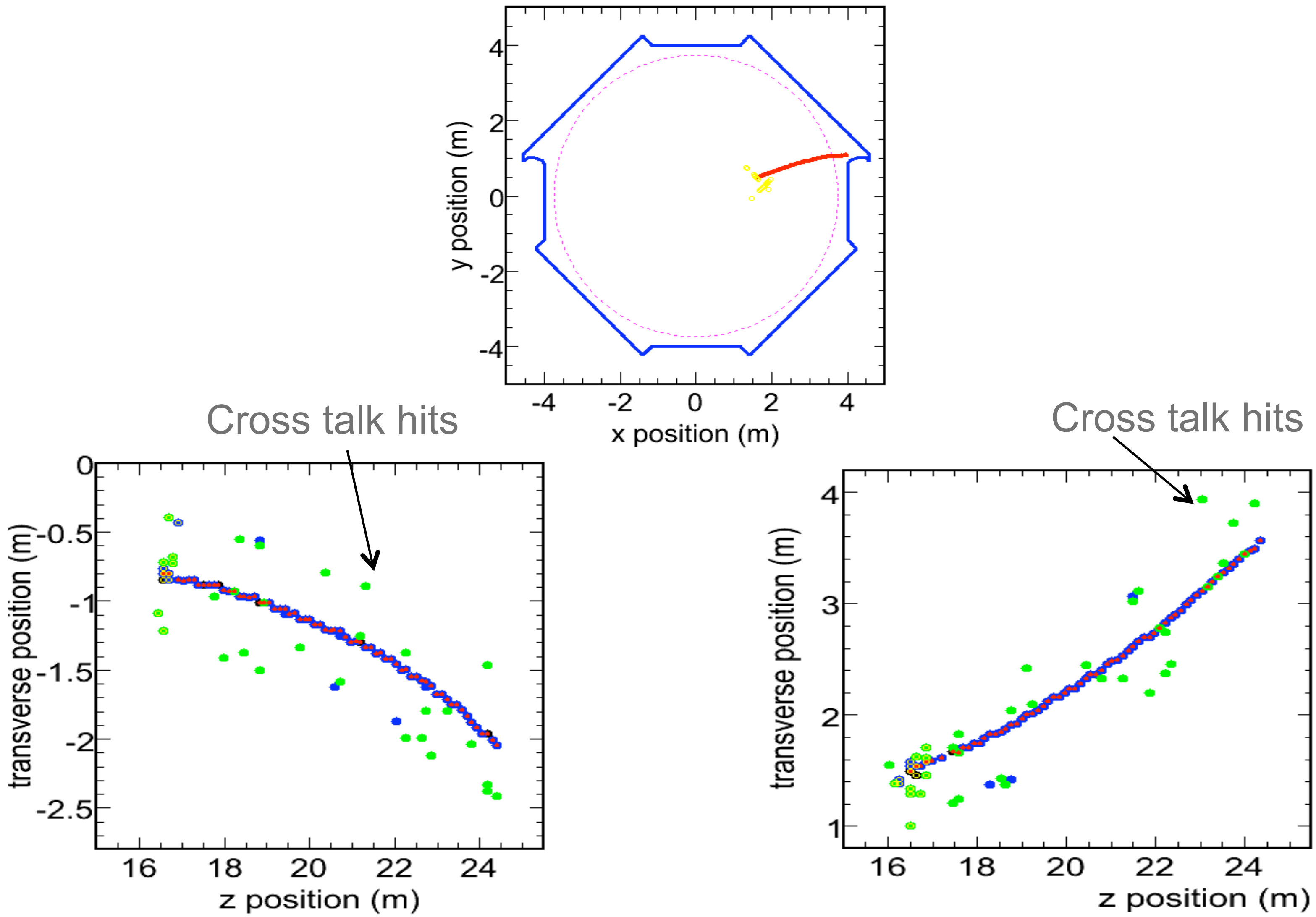

M16 uniformity

862 K. Lang et al. / Nuclear Instruments and Methods in Physics Research A 545 (2005) 852–871

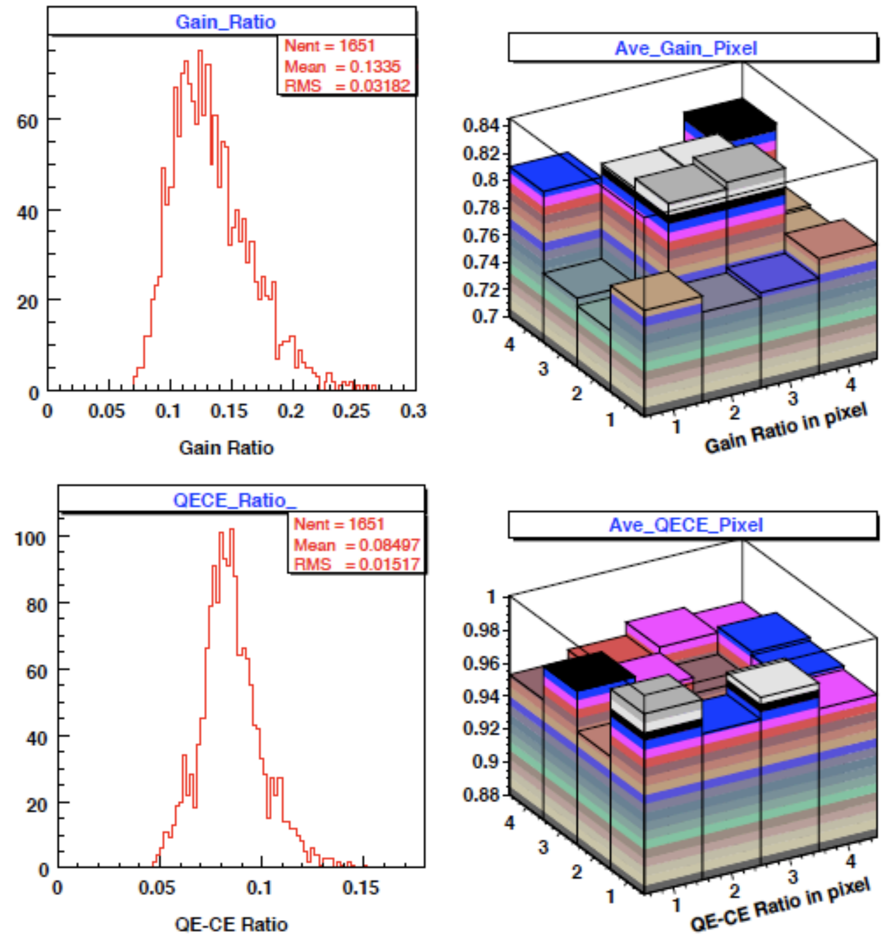

Fig. 6. The uniformity of gain and effective collection efficiency (understood as collection efficiency × quantum efficiency, or CE × QE) of all tested tubes. Top left shows the gain RMS/mean taken over all 128 fiber positions on a tube. Bottom left shows RMS/mean of NPE, normalized and corrected by a monitor tube, The right two plots show the corresponding averages for all tubes as a function of the pixel position in a tube.

Linearity and Cross talk of M16

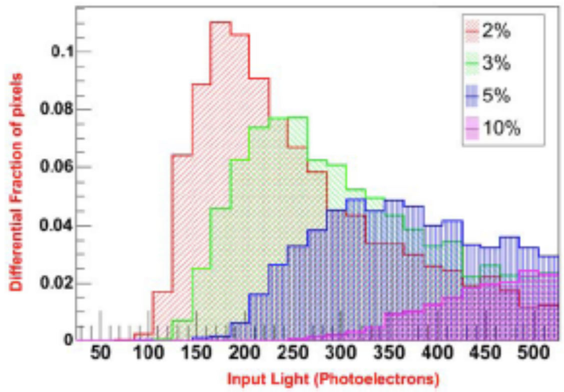

Fig. 8. Linearity range of pixels as a function of observed photoelectrons. The ordinate shows the fraction of all tested pixels which deviate from linearity at the level of 2%, 3%, 5%, and 10% for a given flux of photoelectrons.

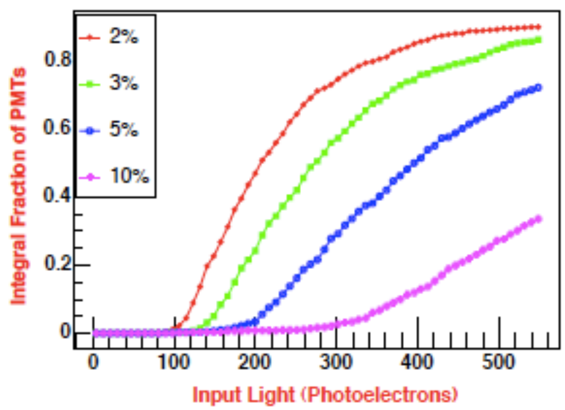

Fig. 9. Linearity range of PMTs as a function of observed photoelectrons. The ordinate shows the integrated fraction of all tested PMTs in which at least one pixel deviates from linearity at the level of 2%, 3%, 5%, and 10% for a given flux of photoelectrons.

K. Lang et al. / Nuclear Instruments and Methods in Physics Research A 545 (2005) 852–871 865

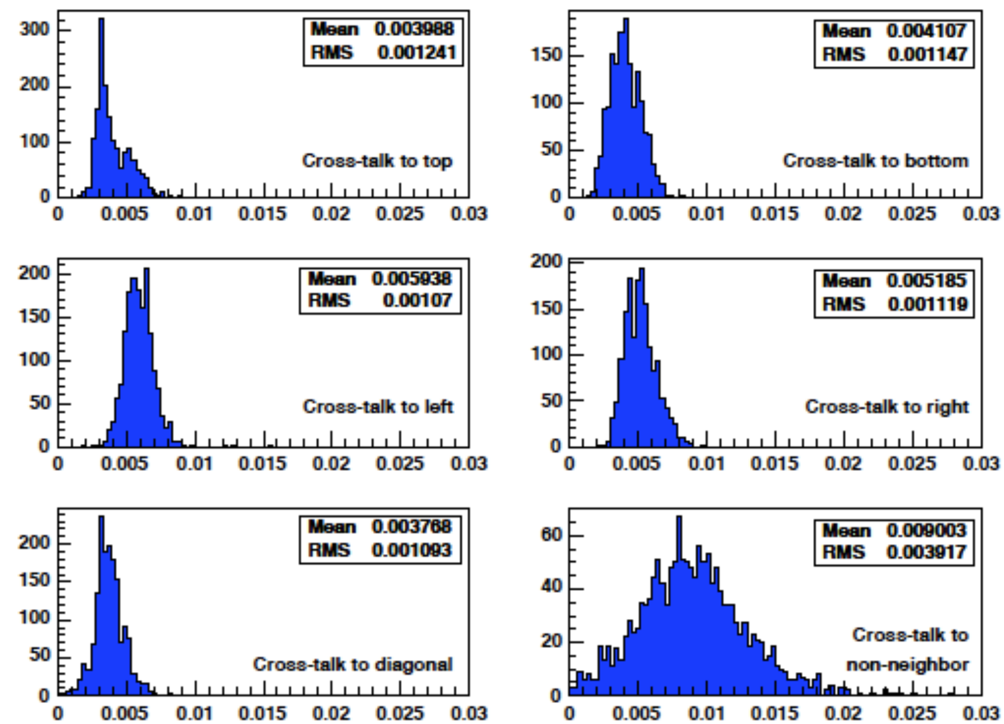

Fig. 10. The distributions of the magnitude of the cross-talk averaged over eight fiber positions in each pixel. The plots show the ratios of charges in a cross-talk pixel to the illuminated pixel. The figures represent the main six distinct categories of cross-talk from the illuminated pixel to: (1) the top pixel, (2) the bottom pixel, (3) the left pixel, (4) the right pixel, (5) the sum of all diagonal pixels, and (6) sum of all non-neighboring pixels, respectively.

ELSEVIER

Available online at www.sciencedirect.com

SCIENCE DIRECT

Nuclear Instruments and Methods in Physics Research A 539 (2005) 668–678

NUCLEAR INSTRUMENTS & METHODS IN PHYSICS RESEARCH Section A

www.elsevier.com/locate/nima

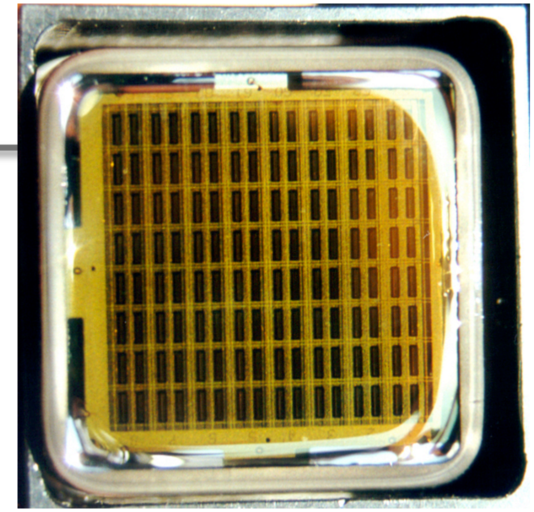

Performance of Hamamatsu 64-anode photomultipliers for use with wavelength—shifting optical fibres

N. Tagg[a,*], A. De Santo[a,1], A. Weber[a], A. Cabrera[a], P.S. Miyagawa[a], M.A. Barker[a,2], K. Lang[b], D. Michael[c], R. Saakyan[d], J. Thomas[d]

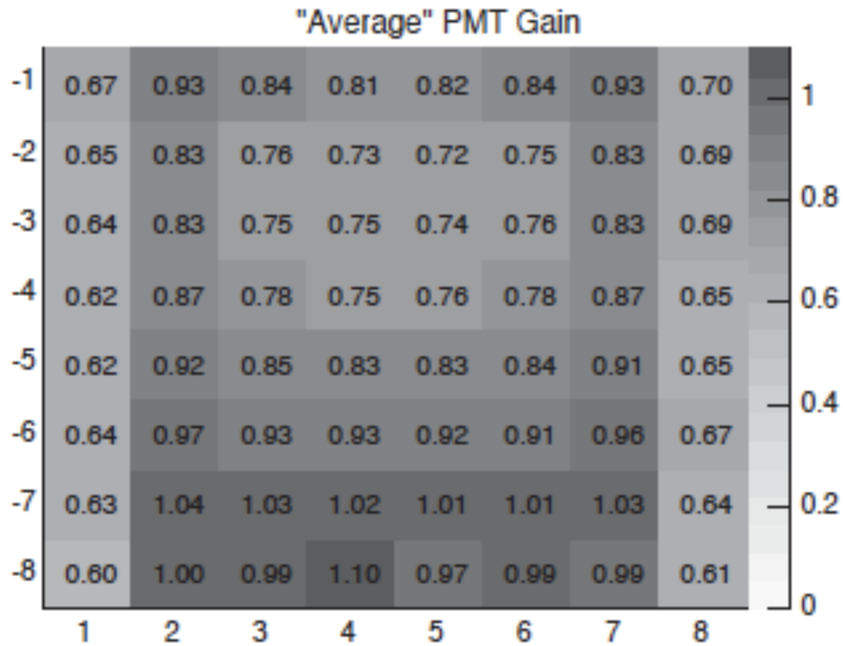

Fig. 9. Pixel gain pattern.The average gain for each pixel position is shown, averaged over 219 PMTs. Units are gain, to be multiplied by 10^6. Dynode slats run left to right.

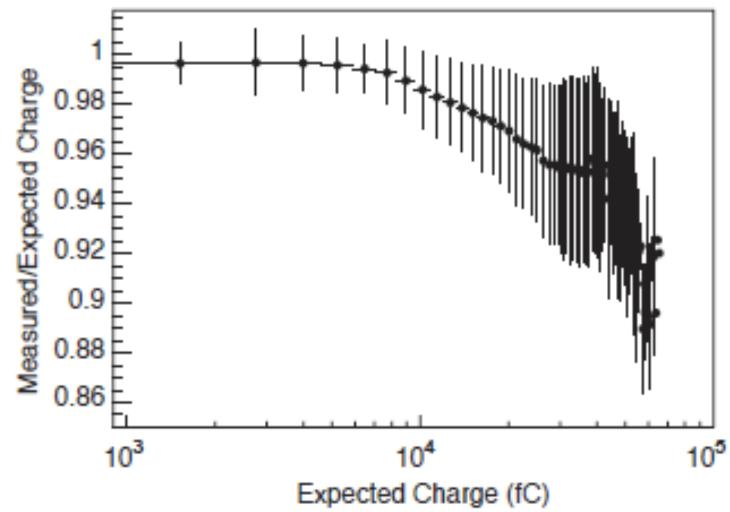

Fig. 11. Nonlinearity curve. The abscissa shows the expected charge response for pulses at different light levels. (The center of the plot is 10^4 fC $\simeq$ 80p.e.). The ordinate scale shows the fractional deviation of the measured PMT charge from linearity. Vertical bars represent the RMS variation amongst all the pixels in the sample. The round markers show the average trend. Data is shown for all pixels with light injected at seven different intensities between ~10 and ~300 p.e.

The third detector - CalDet

•MINOS calibration challenge:
- •Near/Far relative calibration to 2%
- •absolute calibration of 5%

•Main ingredients:
- •cosmic ray muons
  - •energy scale calibration
  - •strip-to-strip response
  - •muon energy unit (MEU)
- •light injection system
  - •PMT gain drifts
  - •PMT/electronics linearity
- •calibration detector (CalDet)
  - •define MEU
  - •topology and pattern recognition

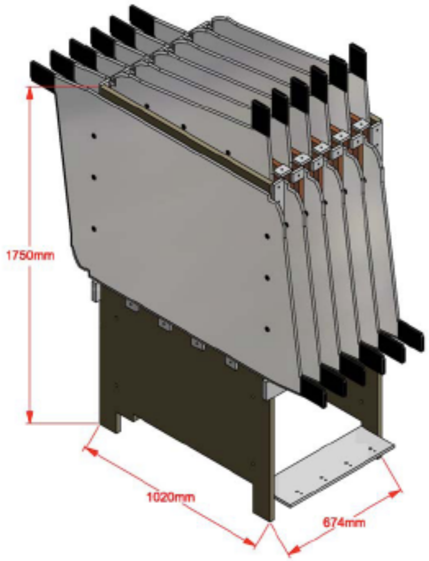

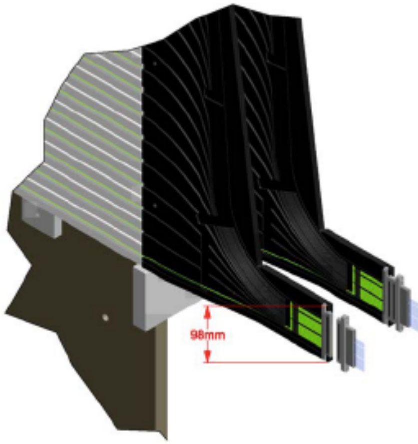

CalDet – it's an experiment

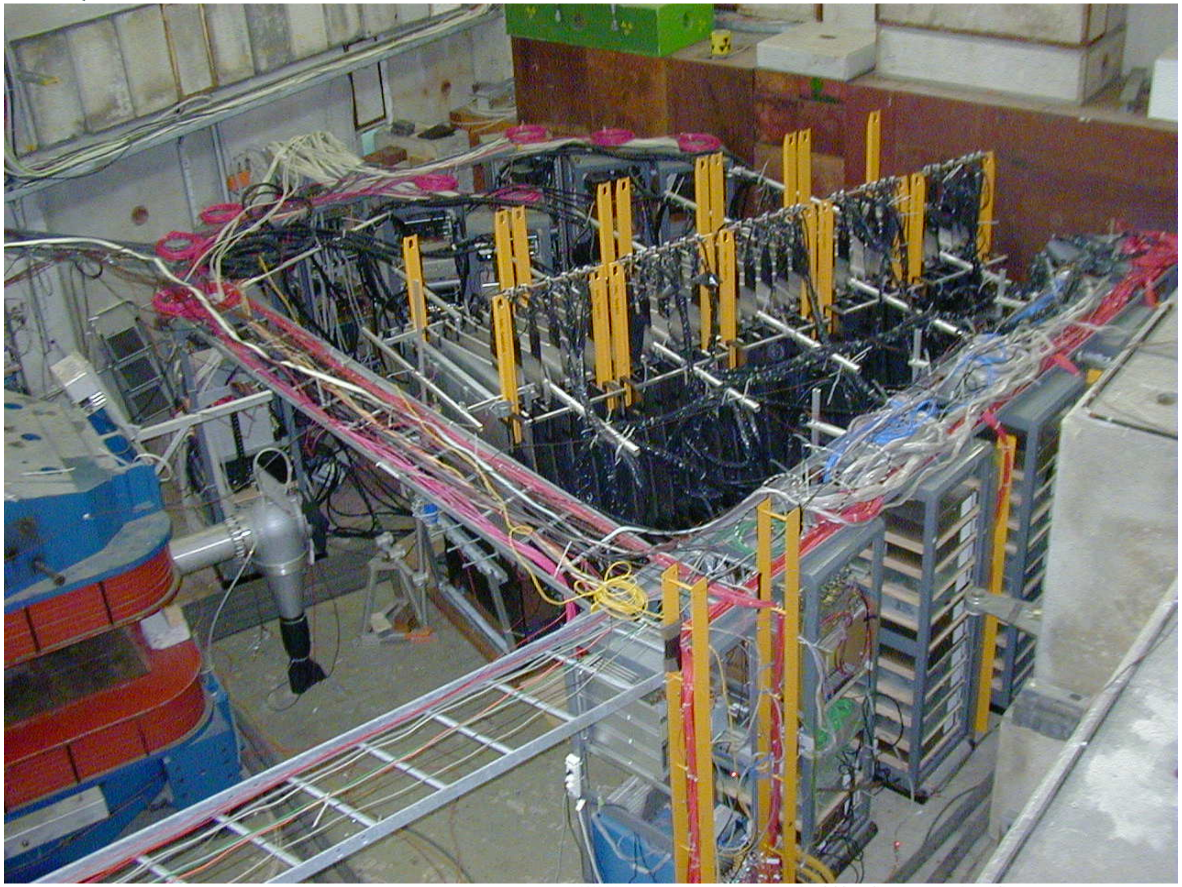

- ◆5 tons
- ◆1 m x 1 m x 3.7 m
- ◆60 MINOS planes
- ◆5 modules (for moving)
- ◆24 strips/plane
  (a total of 1440 strips)
- ◆Consecutive scintillator
  planes rotated 90°
- ◆FarDet and/or NearDet readout
- ◆Full MINOS calibration scheme
- ◆Clear and green (to simulate size of far detector) ribbon cable transports light to PMTs
- ◆No B field
- ◆ Took data 2001-2003

ELSEVIER

Available online at www.sciencedirect.com

SCIENCE DIRECT•

Nuclear Instruments and Methods in Physics Research A 556 (2006) 119–133

NUCLEAR INSTRUMENTS & METHODS IN PHYSICS RESEARCH Section A

www.elsevier.com/locate/nima

The MINOS calibration detector

P. Adamson[a], G. Crone[a], L. Jenner[a], R. Nichol[a], R. Saakyan[a], C. Smith[a], J. Thomas[a], M. Kordosky[b,*], K. Lang[b], P. Vahle[b], A. Belias[c], T. Nicholls[c], G. Pearce[c], D. Petyt[c], M. Barker[d], A. Cabrera[d], J. Hartnell[d], P.S. Miyagawa[d], N. Tagg[d], A. Weber[d], E. Falk Harris[e], P.G. Harris[e], R. Morse[e], P. Symes[e], D. Michael[f], P.J. Litchfield[g], R. Lee[h], S. Boyd[i]

MINOS Calibration Detector Response

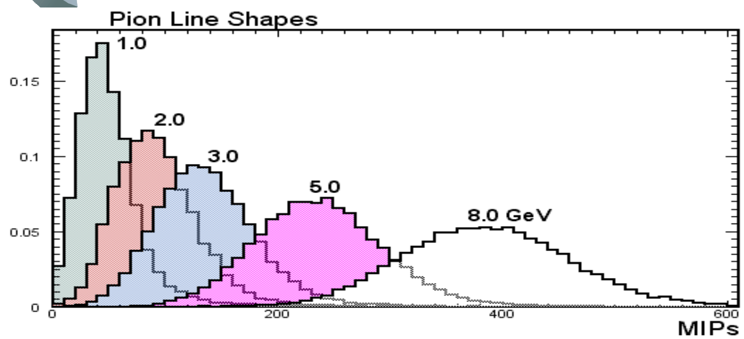

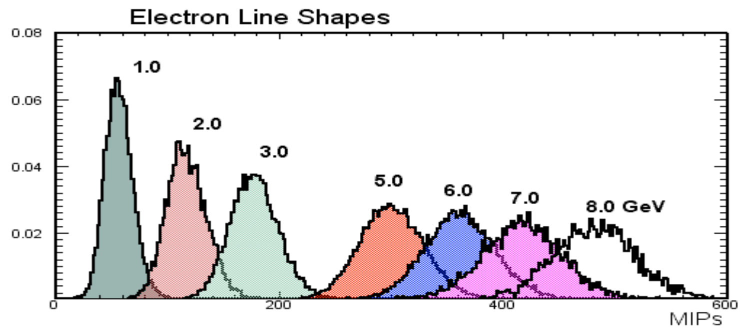

Energy resolution

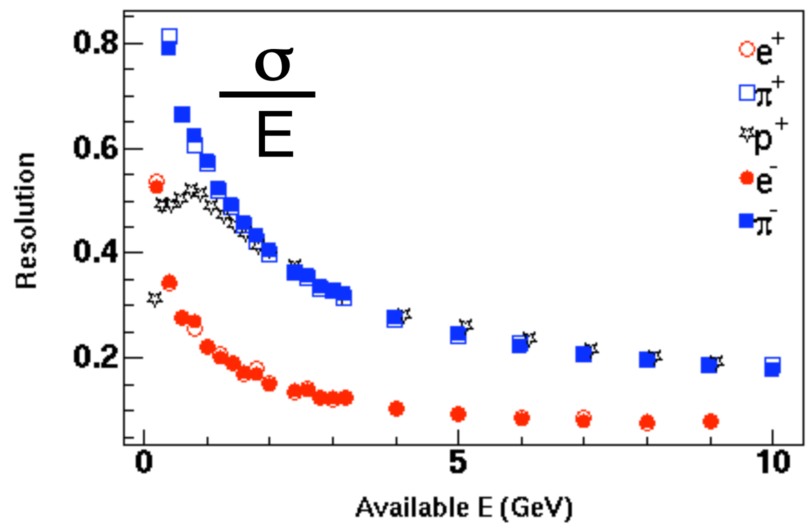

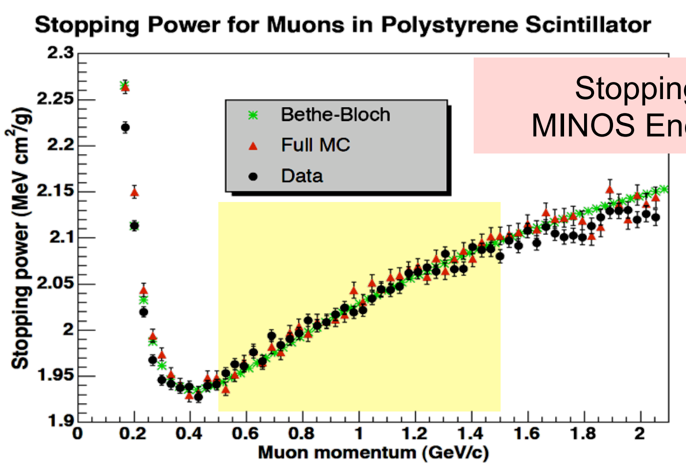

Stopping CR muons:
MINOS Energy Unit (MEU)

Had: $\frac{56\%}{\sqrt{E}} \oplus 2\%$

EM: $\frac{21.4\%}{\sqrt{E}} \oplus \frac{4.1\%}{E}$

MINOS Calibration Detector – 2 GeV events

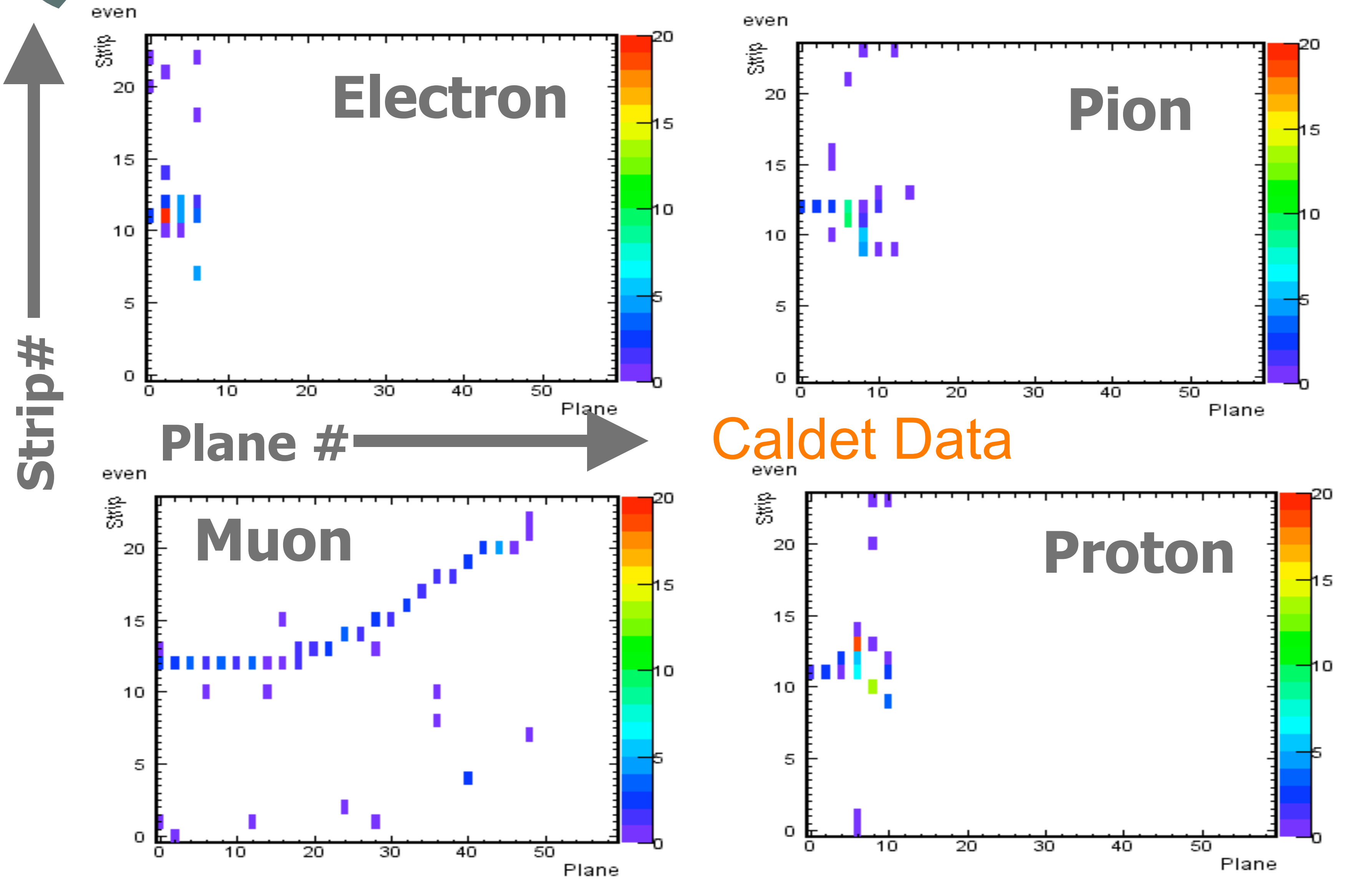

In print… (Far vs Near in Caldet)

Comparisons of the MINOS Near and Far Detector Readout Systems at a Test Beam

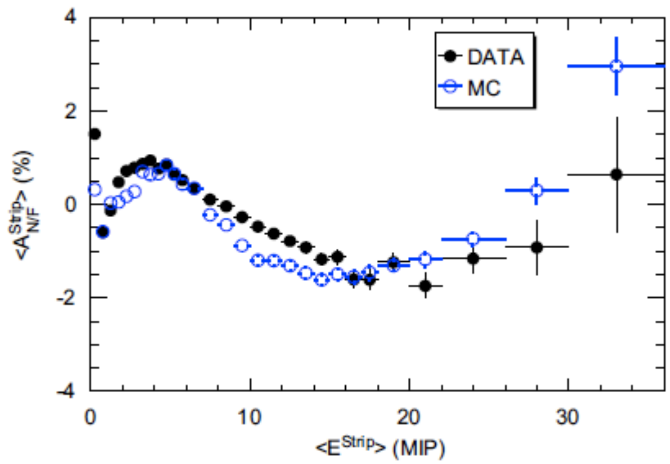

Fig. 40. Near-to-far asymmetry, Eq. (5), in the relative energy response as a function of the deposited energy, before linearity correction.

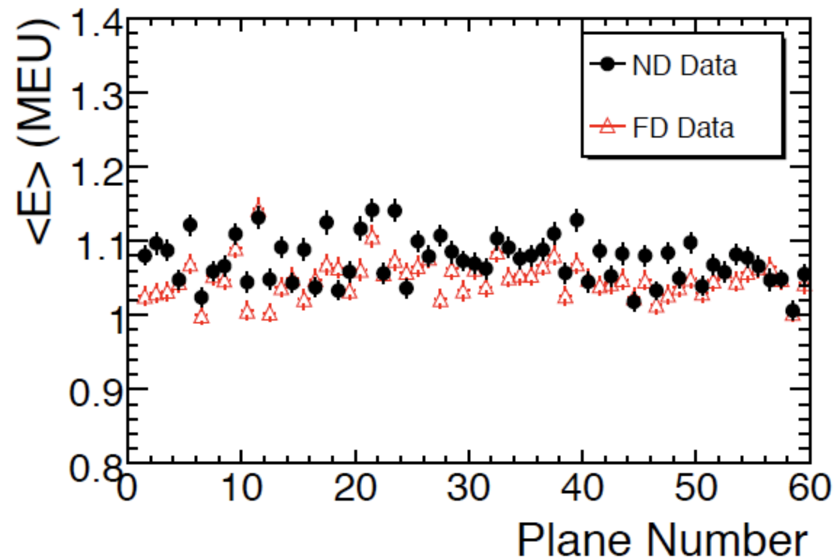

Fig. 2. Average calibrated energy deposited versus plane by >2 GeV/c test beam muons. The error bars show the statistical error, thus the jitter from point to point is indicative of systematic error in the uniformity calibration. The observed response spread of the points is 2.4% and 3.0% for the FD and ND readout systems respectively.

Available online at www.sciencedirect.com
SCIENCE DIRECT®
ELSEVIER
Nuclear Instruments and Methods in Physics Research A 545 (2005) 145–155
NUCLEAR INSTRUMENTS & METHODS IN PHYSICS RESEARCH
Section A
www.elsevier.com/locate/nima

Spontaneous light emission from fibers in MINOS

S. Avvakumov[a], W.L. Barrett[b], T. Belias[c], C. Bower[d], A. Erwin[e], M. Kordosky[f], K. Lang[f,*], R. Lee[g], J. Liu[f], W. Miller[h], L. Mualem[h], R. Nichol[i], J. Nelson[j], G. Pearce[c], M. Proga[f], B. Rebel[d], K. Ruddick[h], C. Smith[k], J. Thomas[i], P. Vahle[f], R. Webb[l]

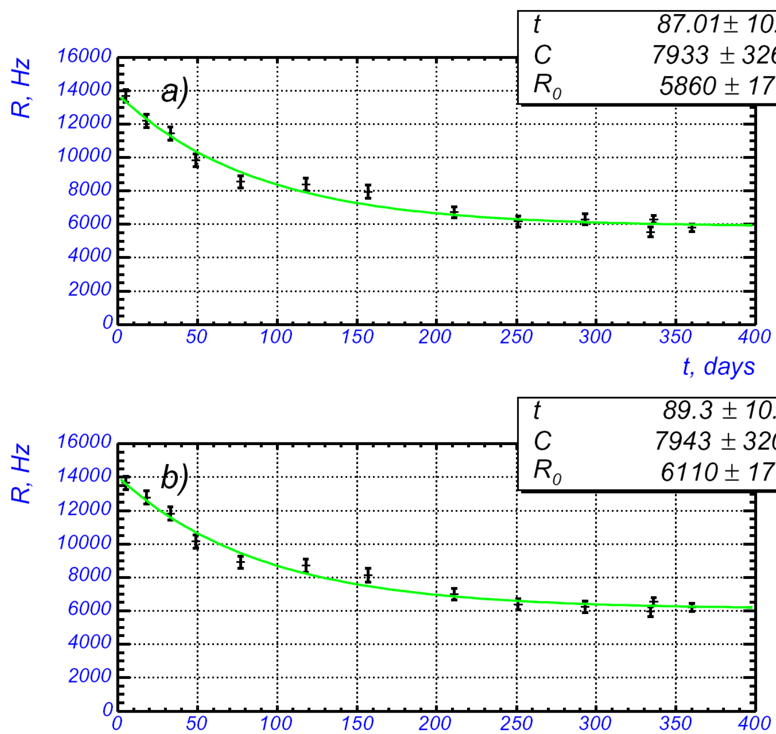

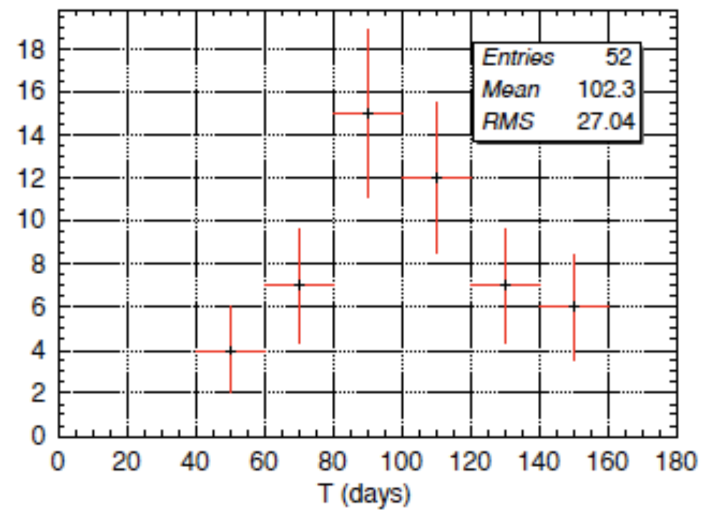

Fig. 2. A distribution of decay time constants determined from fits to the data from 51 fully commissioned planes (between detector plane 61 to 120). We used a simple exponential function of the form $R = C + R_0 e^{-t/T}$. Examples of such fits are shown in Fig. 1.

Special tests of spontaneous light emission by WLS fibers

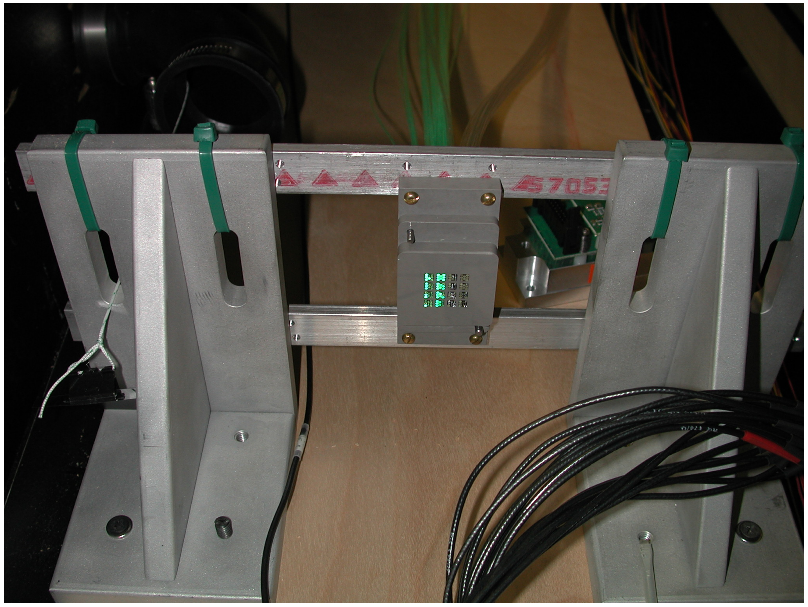

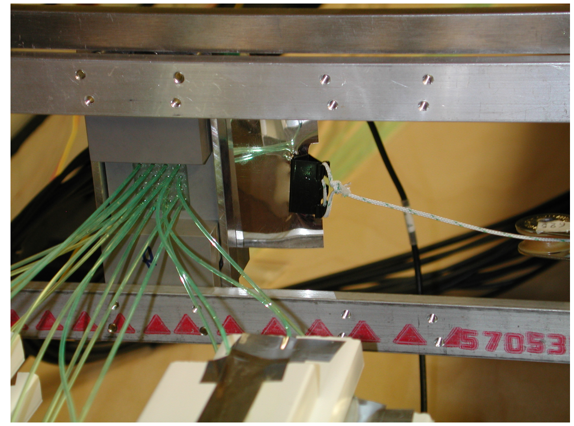

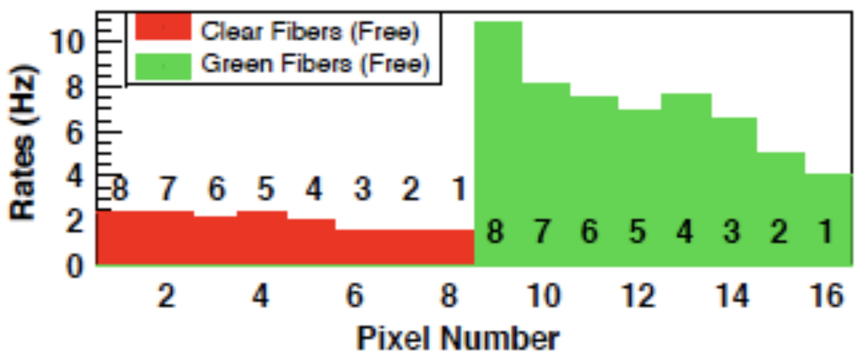

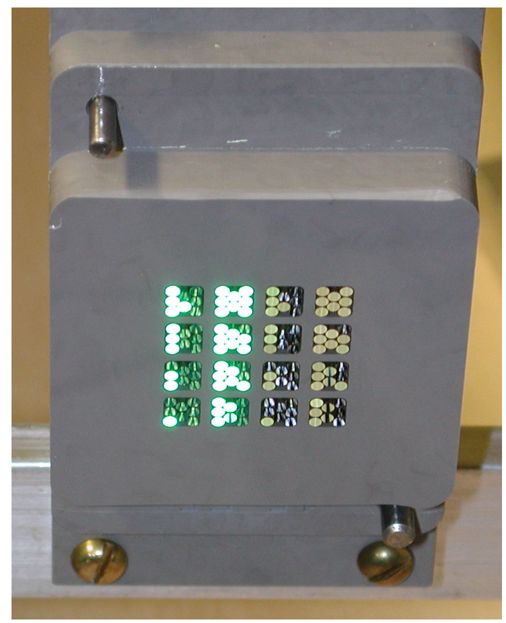

Special tests of spontaneous light emission by WLS fibers

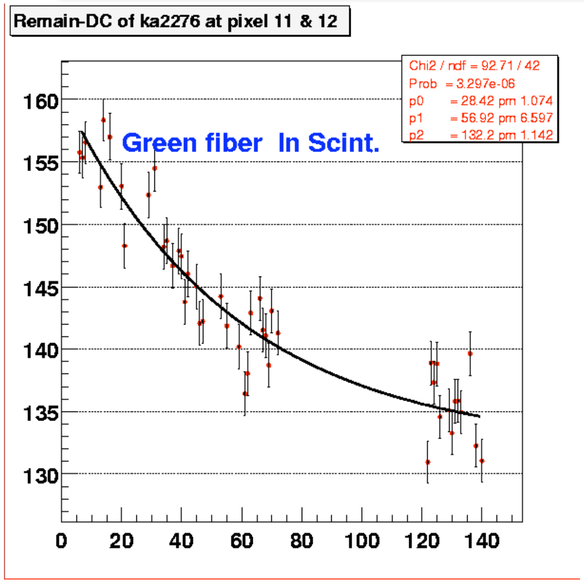

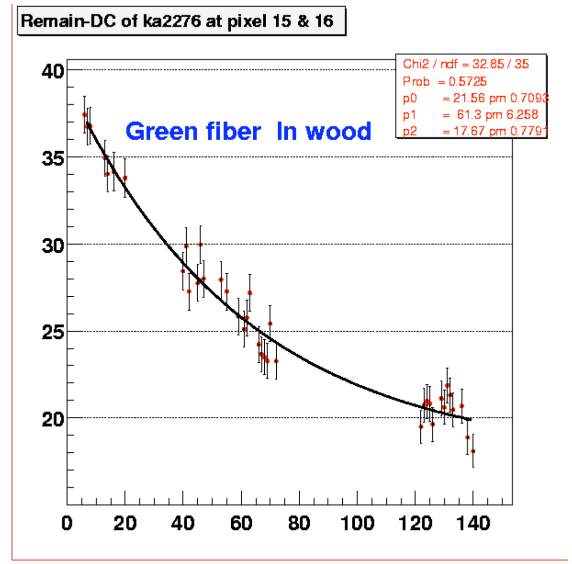

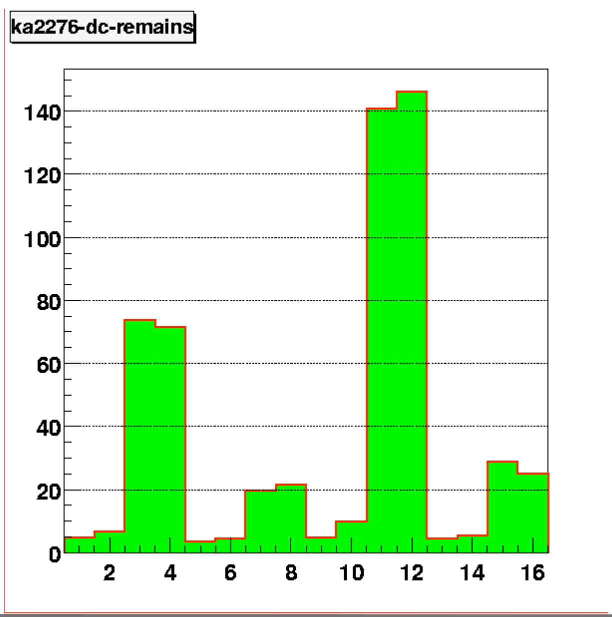

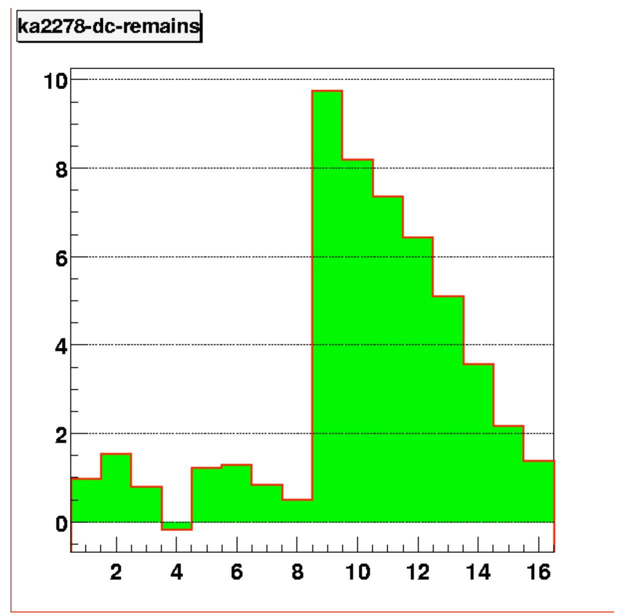

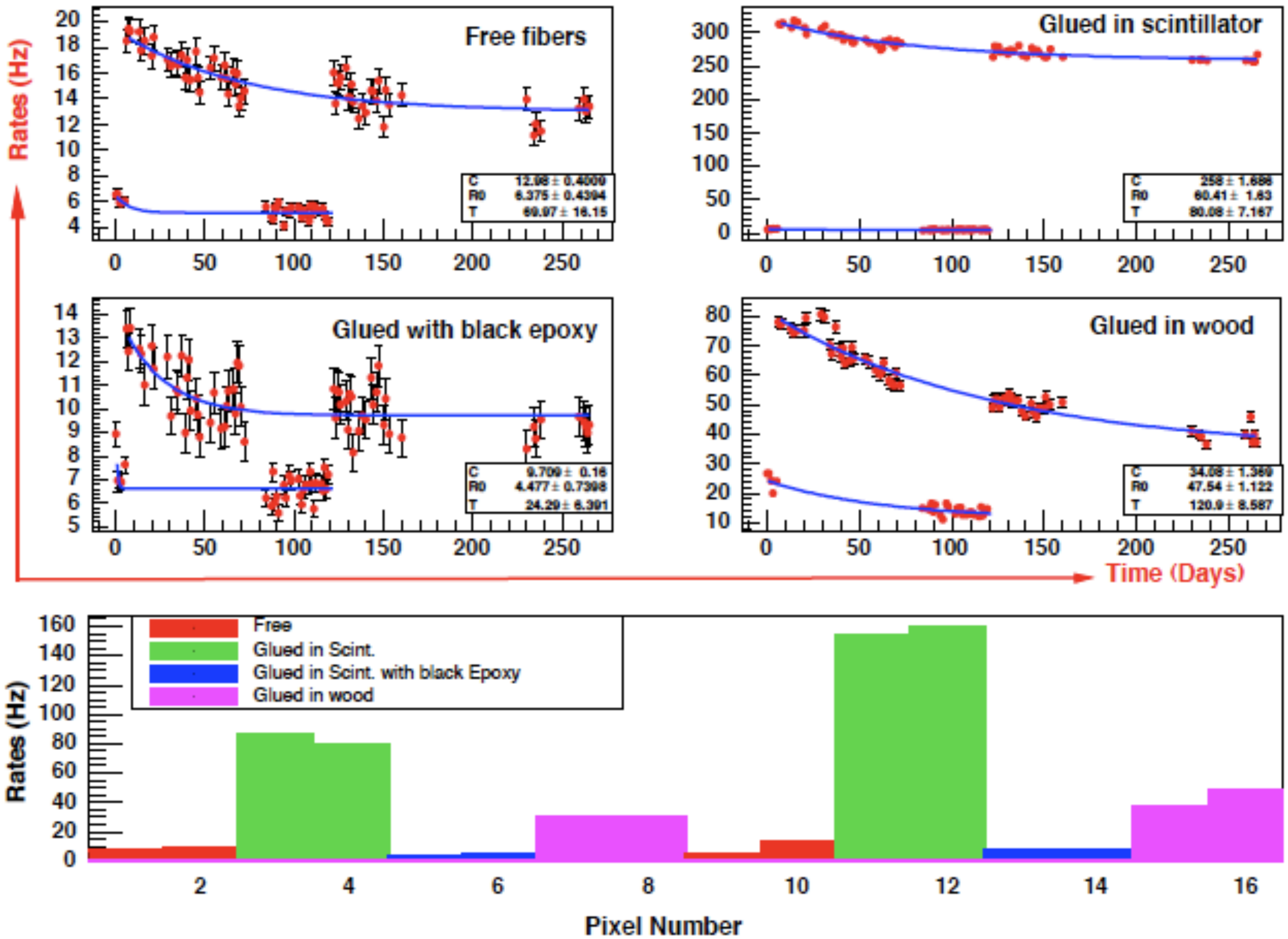

Fig. 3. Net background rates (i.e., total rates minus the intrinsic PMT dark noise) (in Hz) of the first PMT. The tube had 16 fibers connected to it. Pairs of fibers were mounted in four different ways. They were (1) left free, (2) glued in scintillator strips, (3) glued in scintillator strips with blackened Epon 815C epoxy, and (4) glued in wooden strips. Fiber lengths were 75 cm in pixels 1–8 and 150 cm in pixels 9–16. The rates at the end of our experiment (i.e., 260 days after the start of these tests) for all 16 pixels are shown in the bottom panel. Top four panels show total rates in 150 cm fibers as a function of elapsed time (in days). Solid lines represent the fit to an exponential function discussed in the text. The lower sets of data points in each plot show rates measured with the shutter in (i.e., the intrinsic dark noise of pixels). The solid line through these points shows the interpolated values used for background subtraction.

Spontaneous rate / length

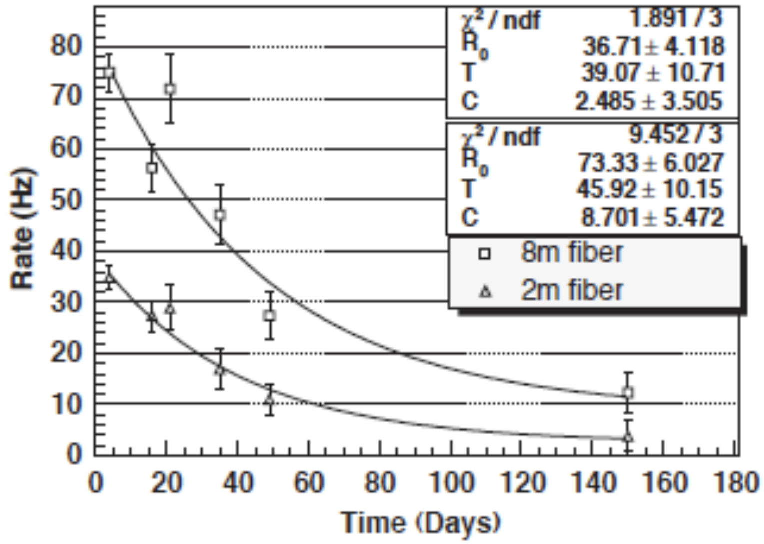

Fig. 8. Rates measured for 2- and 8-m-long free fibers as a function of time.

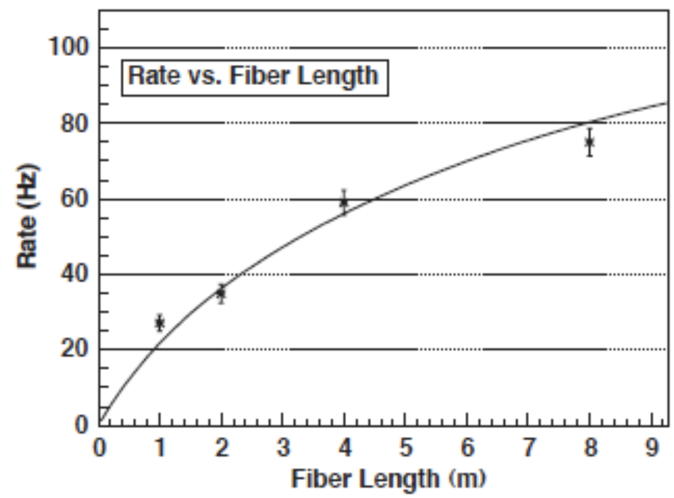

Fig. 7. Measured rates for groups of free wavelength-shifting fibers of different lengths installed in grooves in wooden strips. The line is a fit to the data using equation 1 with a, the overall normalization, as the only free parameter. The fit yields $a = (27 \pm 1)$ Hz/m.

Table 2
Attenuation corrected emission rates for exponential and asymptotic components of WLS fiber emission for fibers glued with Epon [9], free Bicron fibers [16], and clear fibers

Test condition	Initial rate (Hz/m)	Asymptotic rate (Hz/m)
Kuraray WLS fiber in Epon 815C	75 ± 4	9 ± 1
Bicron WLS fiber free	35 ± 4	−3 ± 3
Kuraray clear fiber free	8 ± 2	0 ± 2

Table 1
Attenuation corrected emission rates for exponential and asymptotic components of WLS fiber emission

Fiber length (m)	Initial rate		Asymptotic rate	
	R (Hz)	a (Hz/m)	R (Hz)	a (Hz/m)
1	29 ± 2	35 ± 7	2 ± 1	3 ± 1
2	38 ± 2	28 ± 2	2 ± 2	2 ± 2
4	77 ± 5	33 ± 2	10 ± 4	5 ± 2
8	81 ± 3	25 ± 1	9 ± 3	3 ± 1

New experimental challenges in neutrino physics - intensity

Near Detector spill

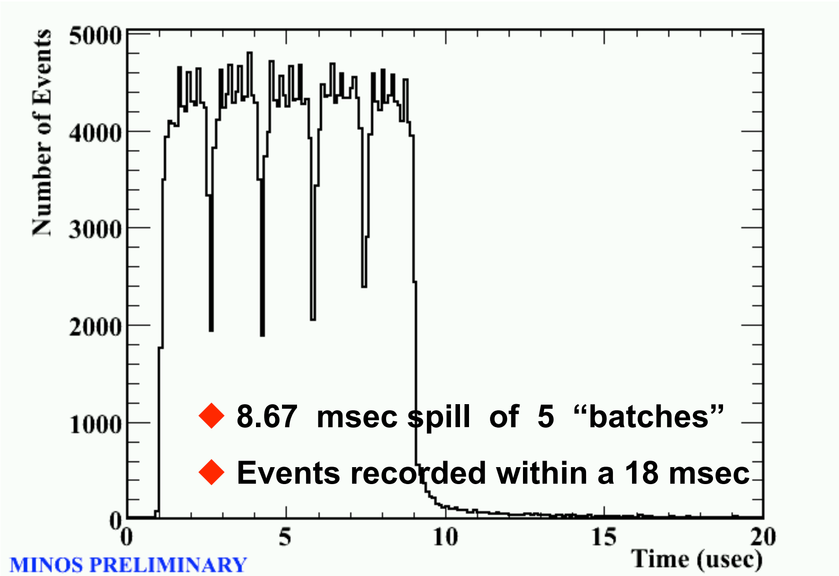

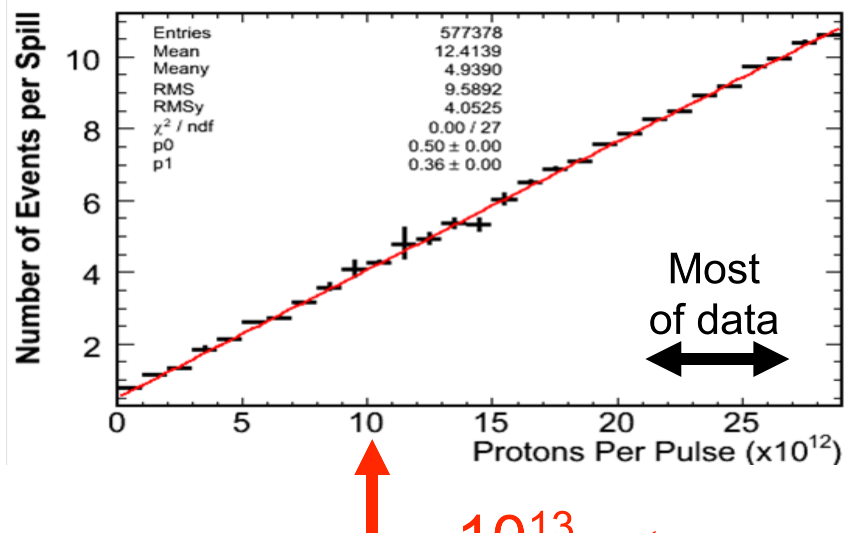

10^{13} protons per pulse

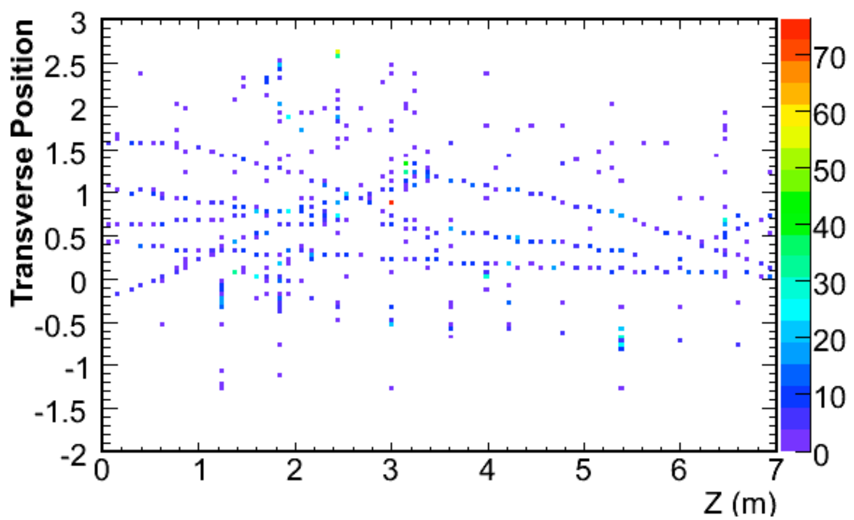

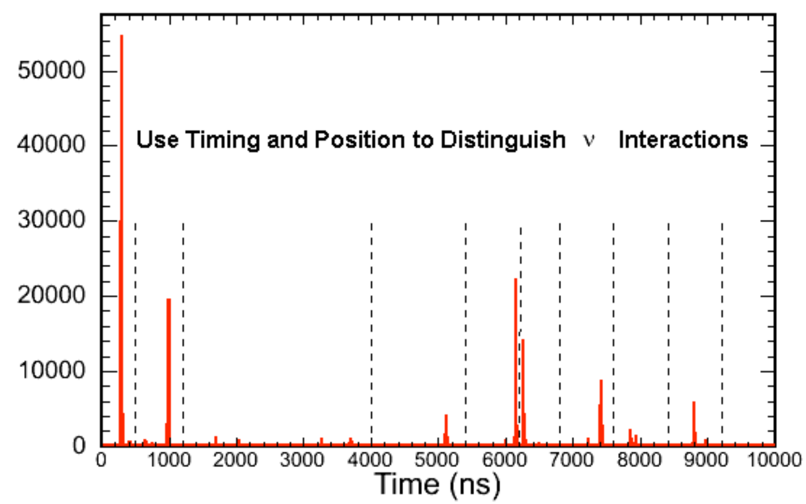

New experimental challenges in neutrino physics - intensity

Near Detector spill

1 spill lasts ~10 μs

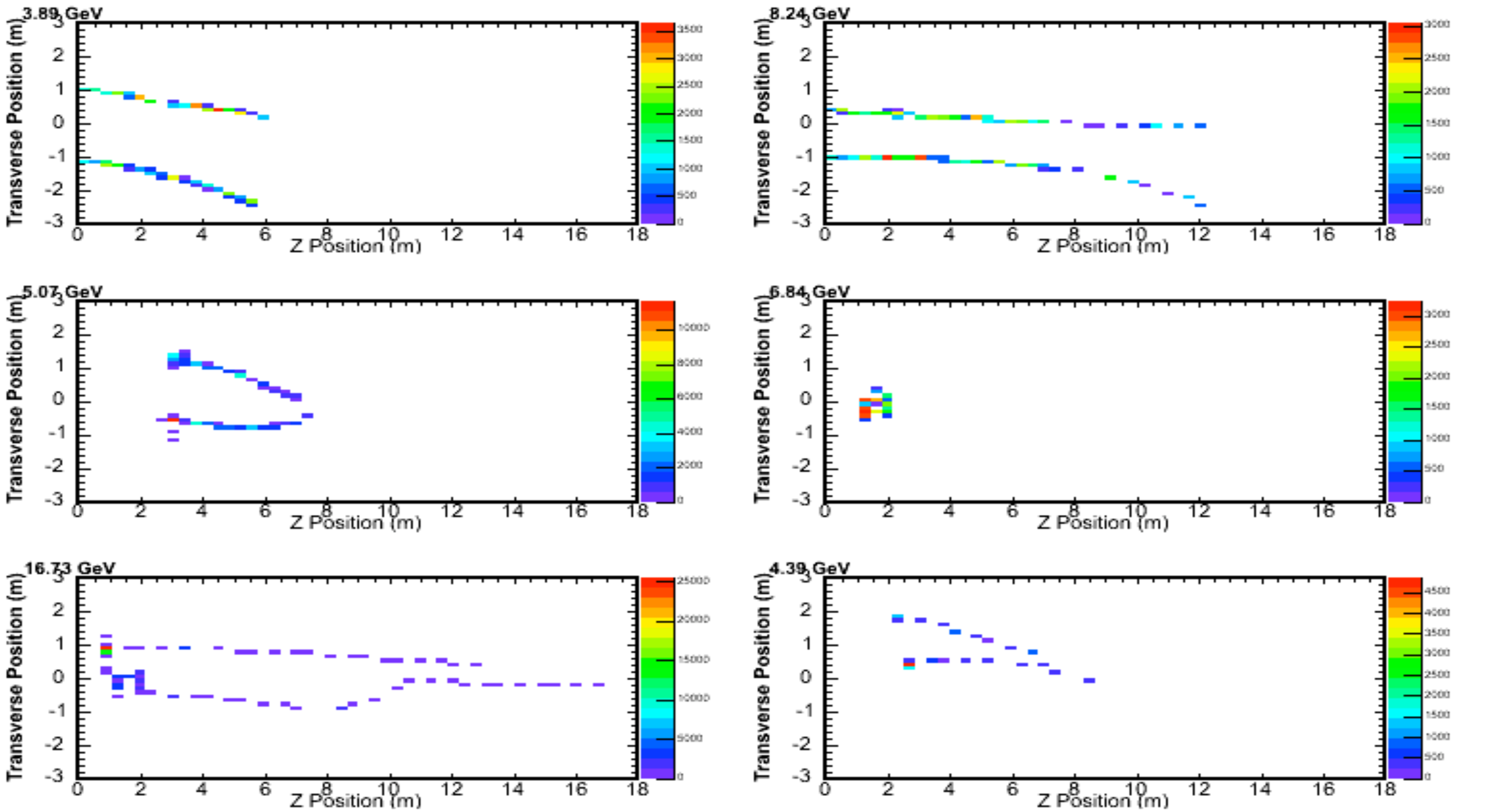

Calibration – stopping muons (MEU)

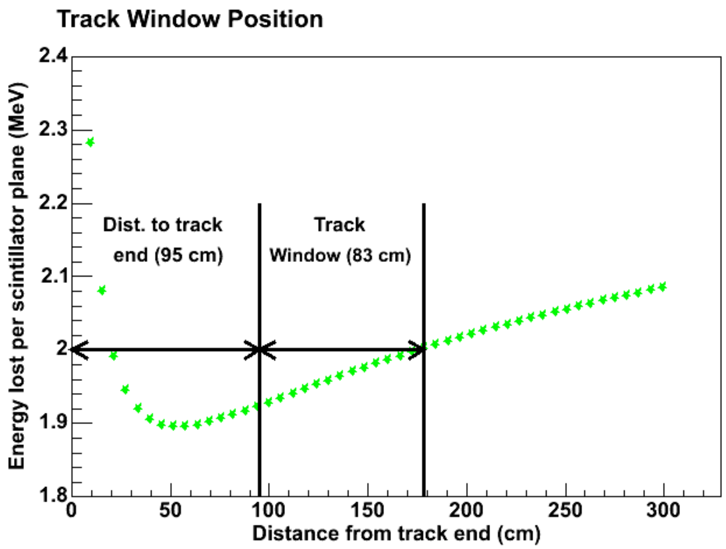

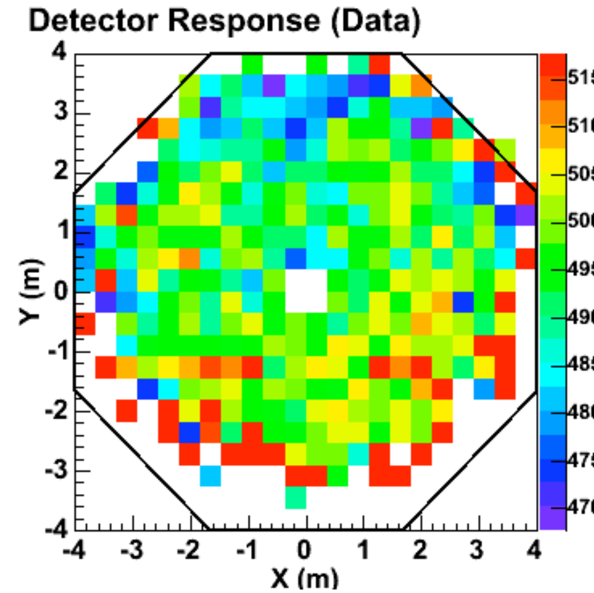

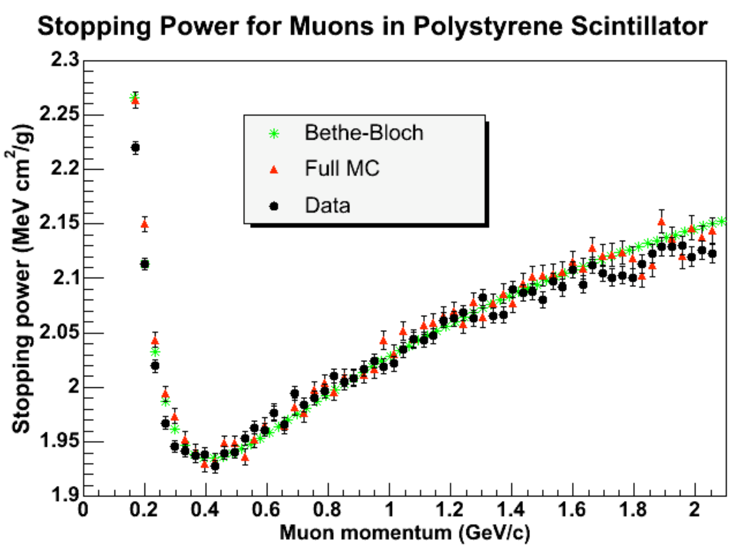

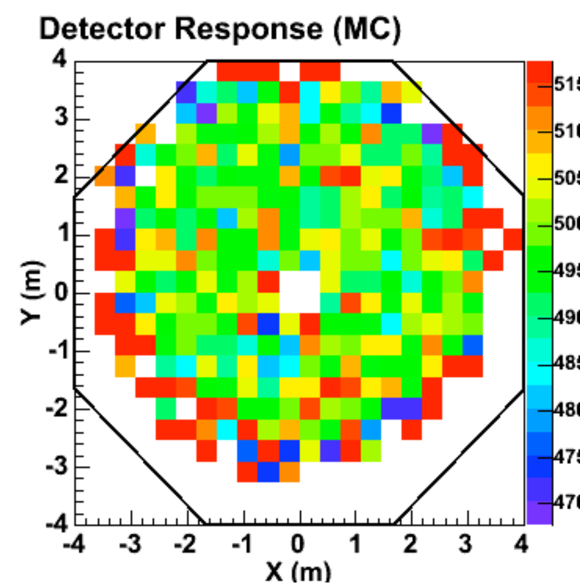

MEU – MINOS Energy Unit

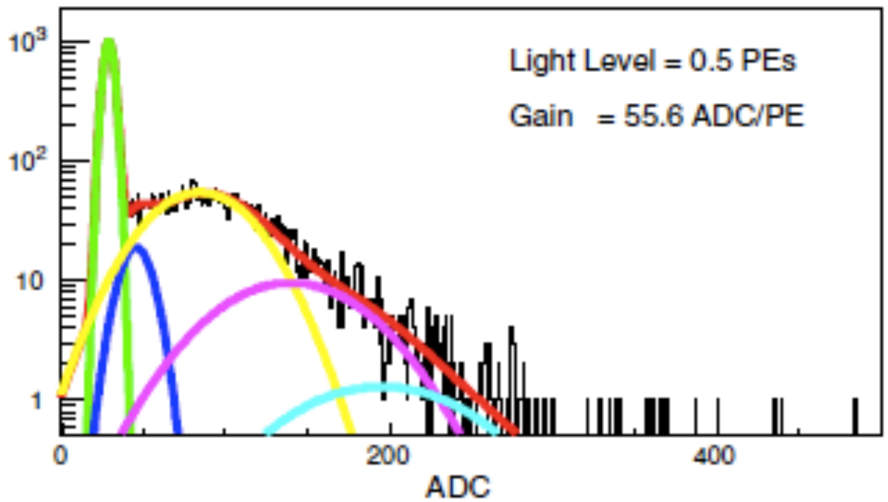

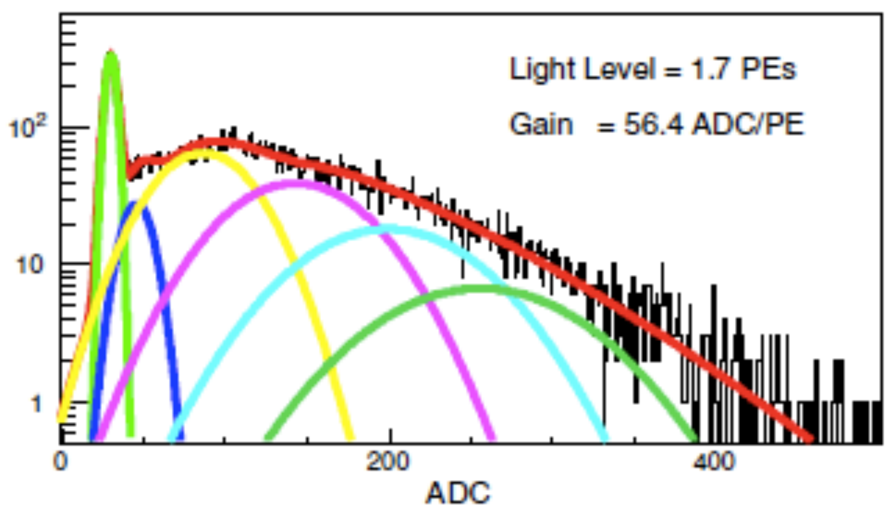

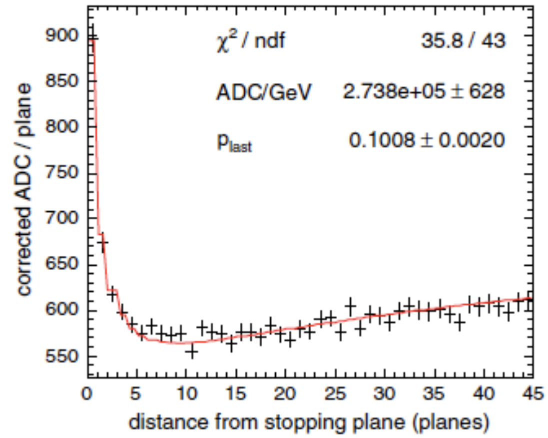

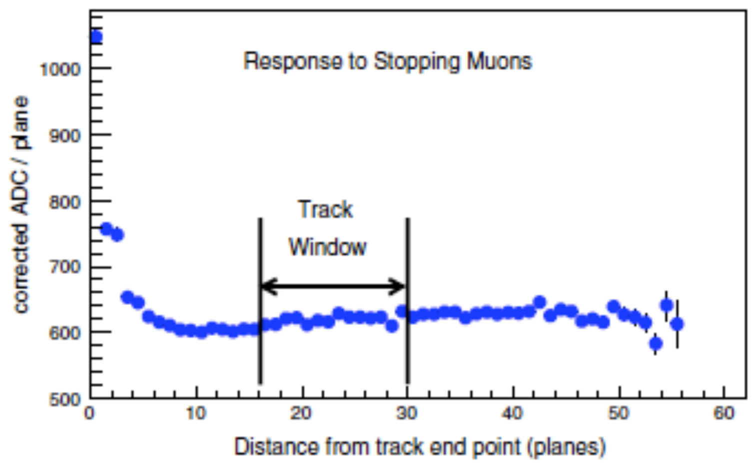

Fig. 13. The average response to stopping muons as a function of the distance from the end of the track along with the window used in the signal-scale calibration. The signals were corrected for gain drift, non-linearity, strip light-output non-uniformity and temperature fluctuations.

The MINOS Collaboration

28 institutions
140 scientists

Argonne • Athens • Benedictine • Brookhaven • Caltech • Cambridge • Campinas • Fermilab Harvard • Holy Cross • IIT • Indiana • Minnesota-Twin Cities • Minnesota-Duluth • Otterbein Oxford • Pittsburgh • Rutherford • Sao Paulo • South Carolina • Stanford • Sussex • Texas A&M Texas-Austin • Tufts • UCL • Warsaw • William & Mary

Lessons learned (hopefully)

- Avoid “building a ship in a bottle”
- Better horizontal than vertical access (tunnel vs mine)
- Share responsibilities among as many institutions as possible in all stages of the experiment (collaboration integration)
- Larger detector with PMTs impossible (spectral attenuation)
- Spontaneous light emission in WLS fibers

"I wish to thank my parents for making it all possible...and I wish to thank my children for making it necessary."

Victor Borge

Backup slides

ν_e appearance

- Expect: 27 ± 5(stat) ± 2(syst)
- Observed: 35 events
- Observed is 1.5σ higher than background expectation
- We do observe a similar sized excess of events in a (independent, signal-less) sideband region

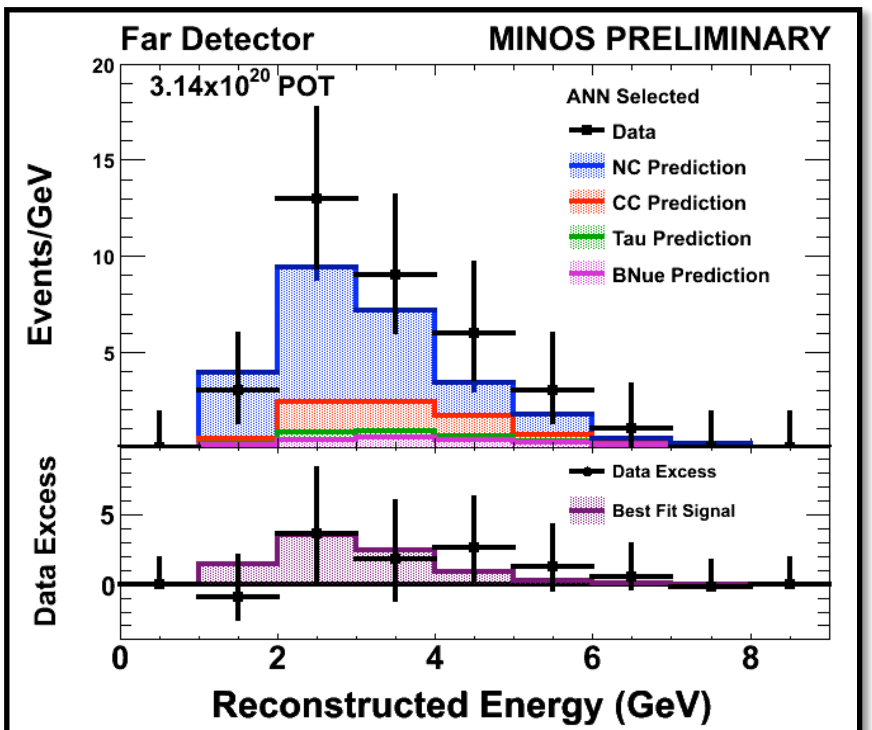

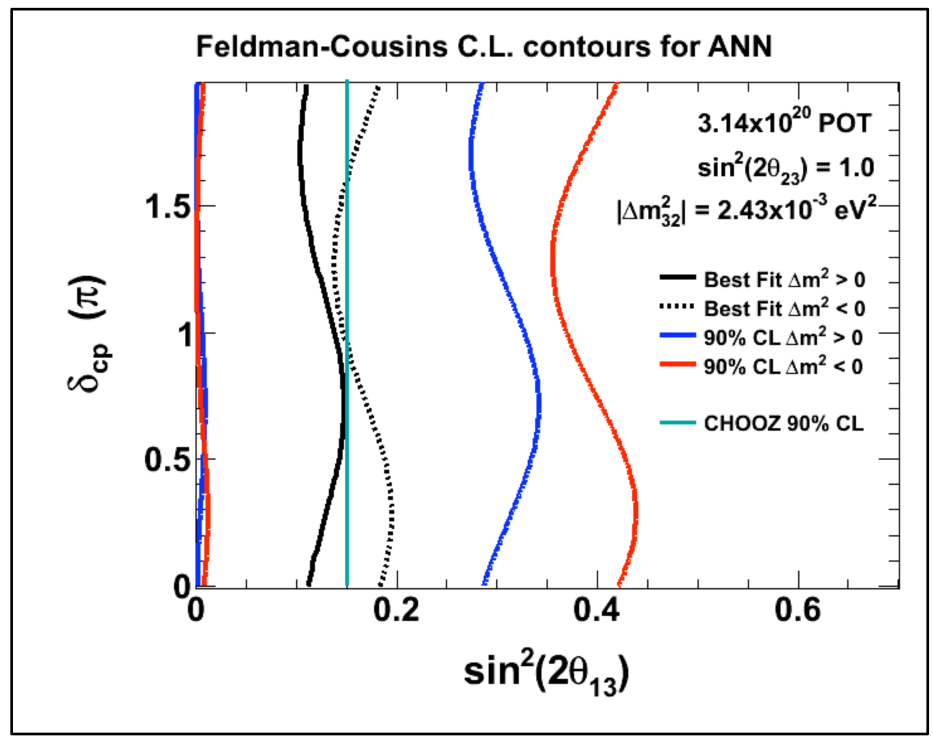

A search for $\nu_\mu \rightarrow \nu_{sterile}$

For E_{vis} < 3 GeV:
f < 0.35, 90% C.L.

For E_{vis} < 120 GeV:
f < 0.17, 90% C.L.

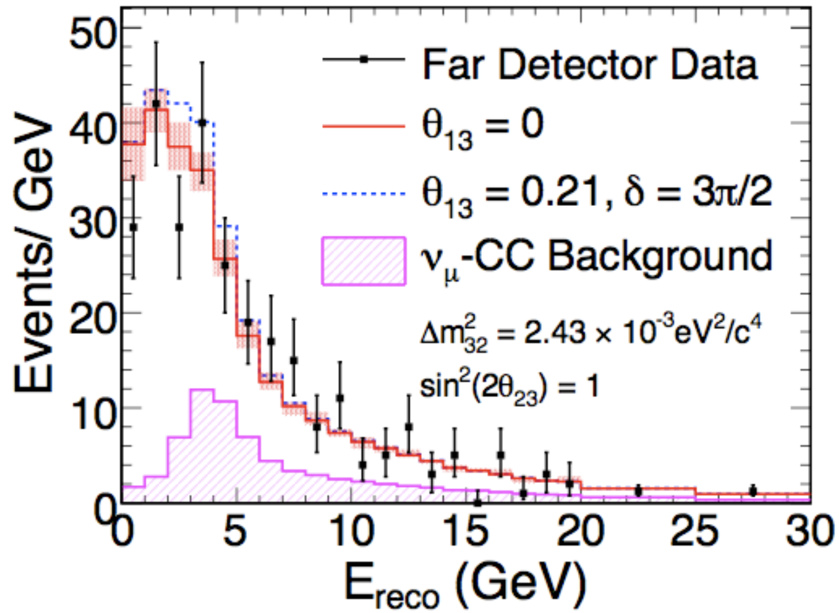

$$P_{\nu_\mu \rightarrow \nu_\mu} = 1 - \alpha_\mu \sin^2(1.27 \Delta m^2 L/E)$$

$$P_{\nu_\mu \rightarrow \nu_e} = \alpha_e \sin^2(1.27 \Delta m^2 L/E)$$

$$P_{\nu_\mu \rightarrow \nu_s} = \alpha_s \sin^2(1.27 \Delta m^2 L/E)$$

$$P_{\nu_\mu \rightarrow \nu_\tau} = 1 - P_{\nu_\mu \rightarrow \nu_\mu} - P_{\nu_\mu \rightarrow \nu_e} - P_{\nu_\mu \rightarrow \nu_s}$$

$$f_s \equiv \frac{P_{\nu_\mu \rightarrow \nu_s}}{1 - P_{\nu_\mu \rightarrow \nu_\mu}}$$

Energy Range (GeV)	Data	MC	Significance (σ)
0-3	100	115.16 ± 7.67	1.15
0-5	165	175.92 ± 10.42	0.65
0-120	291	292.63 ± 15.02	0.10

Anti-neutrino disappearance (NEW !!!)

- Observe **42 events** in the Far detector
- Predicted events with CPT conserving oscillations:
  - ⇨ **58.3 ± 7.6 (stat.) ± 3.6 (syst.)**
- Predicted events with null oscillations:
  - ⇨ **64.6 ± 8.0 (stat.) ± 3.9 (syst.)**
- CPT conserving point from the MINOS neutrino analysis is within the 90% contour

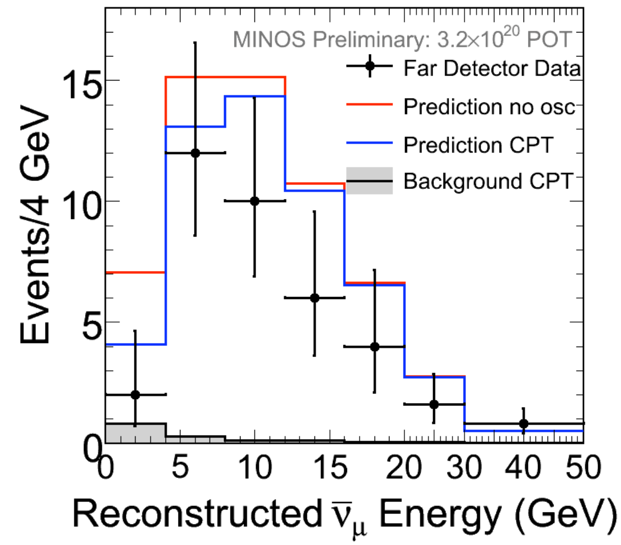

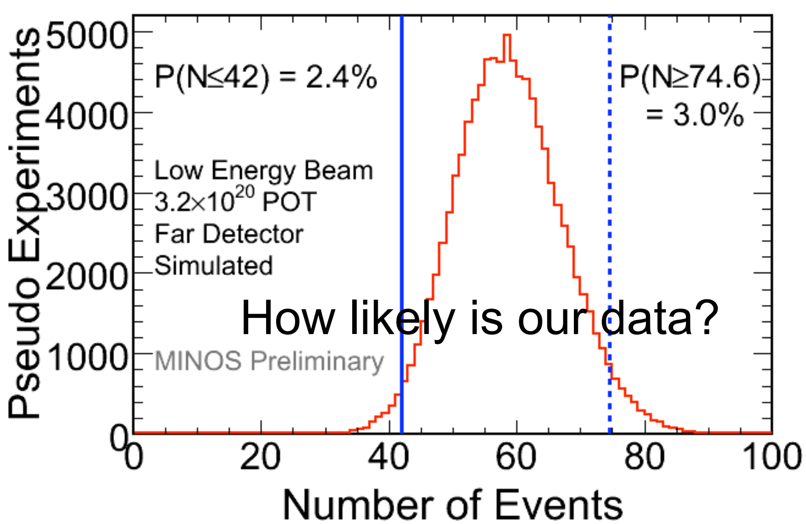

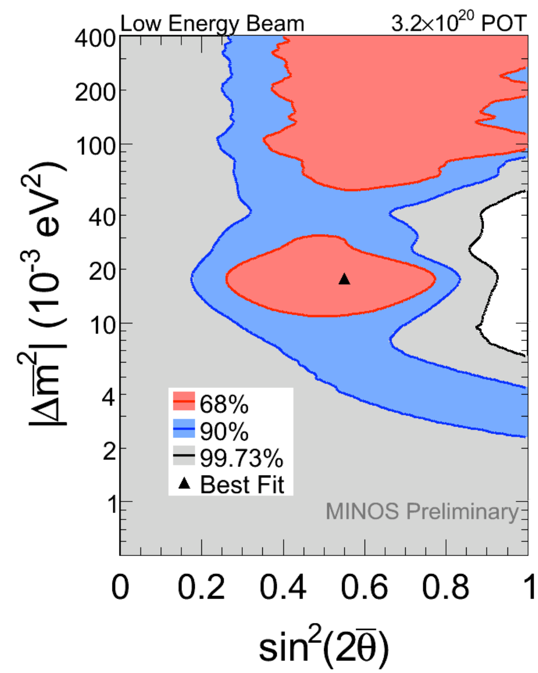

PERIODIC TABLE OF THE ELEMENTS

1 IA	2 IIA	3 IIIB	4 IVB	5 VB	6 VIB	7 VIIB	8 VIII	9 VIII	10 VIII	11 IB	12 IIB	13 IIIA	14 IVA	15 VA	16 VIA	17 VIIA	18 VIIIA
1 H Hydrogen 1.00794																	2 He Helium 4.002602
3 Li Lithium 6.941	4 Be Beryllium 9.012182											5 B Boron 10.811	6 C Carbon 12.0107	7 N Nitrogen 14.00674	8 O Oxygen 15.9994	9 F Fluorine 18.9984032	10 Ne Neon 20.1797
11 Na Sodium 22.989770	12 Mg Magnesium 24.3050											13 Al Aluminum 26.981538	14 Si Silicon 28.0855	15 P Phosph. 30.973761	16 S Sulfur 32.066	17 Cl Chlorine 35.4527	18 Ar Argon 39.948
19 K Potassium 39.0983	20 Ca Calcium 40.078	21 Sc Scandium 44.955910	22 Ti Titanium 47.867	23 V Vanadium 50.9415	24 Cr Chromium 51.9961	25 Mn Manganese 54.938049	26 Fe Iron 55.845	27 Co Cobalt 58.933200	28 Ni Nickel 58.6934	29 Cu Copper 63.546	30 Zn Zinc 65.39	31 Ga Gallium 69.723	32 Ge German. 72.61	33 As Arsenic 74.92160	34 Se Selenium 78.96	35 Br Bromine 79.904	36 Kr Krypton 83.80
37 Rb Rubidium 85.4678	38 Sr Strontium 87.62	39 Y Yttrium 88.90585	40 Zr Zirconium 91.224	41 Nb Niobium 92.90638	42 Mo Molybd. 95.94	43 Tc Technet. (97.907215)	44 Ru Ruthen. 101.07	45 Rh Rhodium 102.90550	46 Pd Palladium 106.42	47 Ag Silver 107.8682	48 Cd Cadmium 112.411	49 In Indium 114.818	50 Sn Tin 118.710	51 Sb Antimony 121.760	52 Te Tellurium 127.60	53 I Iodine 126.90447	54 Xe Xenon 131.29
55 Cs Cesium 132.90545	56 Ba Barium 137.327	57–71 Lantha-nides	72 Hf Hafnium 178.49	73 Ta Tantalum 180.9479	74 W Tungsten 183.84	75 Re Rhenium 186.207	76 Os Osmium 190.23	77 Ir Iridium 192.217	78 Pt Platinum 195.078	79 Au Gold 196.96655	80 Hg Mercury 200.59	81 Tl Thallium 204.3833	82 Pb Lead 207.2	83 Bi Bismuth 208.98038	84 Po Polonium (208.982415)	85 At Astatine (209.987131)	86 Rn Radon (222.017570)
87 Fr Francium (223.019731)	88 Ra Radium (226.025402)	89–103 Actinides	104 Rf Rutherford (261.1089)	105 Db Dubnium (262.1144)	106 Sg Seaborg. (263.1186)	107 Bh Bohrium (262.1231)	108 Hs Hassium (265.1306)	109 Mt Meitner. (266.1378)	110 (269, 273)	111 (272)	112 (277)		114 (289)		116 (289)		118 (293)

Series															
Lanthanide series	57 La Lanthan. 138.9055	58 Ce Cerium 140.116	59 Pr Praseodym. 140.90765	60 Nd Neodym. 144.24	61 Pm Prometh. (144.912745)	62 Sm Samarium 150.36	63 Eu Europium 151.964	64 Gd Gadolin. 157.25	65 Tb Terbium 158.92534	66 Dy Dyspros. 162.50	67 Ho Holmium 164.93032	68 Er Erbium 167.26	69 Tm Thulium 168.93421	70 Yb Ytterbium 173.04	71 Lu Lutetium 174.967
Actinide series	89 Ac Actinium (227.027747)	90 Th Thorium 232.0381	91 Pa Protactin. 231.03588	92 U Uranium 238.0289	93 Np Neptunium (237.048166)	94 Pu Plutonium (244.064197)	95 Am Americ. (243.061372)	96 Cm Curium (247.070346)	97 Bk Berkelium (247.070298)	98 Cf Californ. (251.079579)	99 Es Einstein. (252.08297)	100 Fm Fermium (257.095096)	101 Md Mendelev. (258.098427)	102 No Nobelium (259.1011)	103 Lr Lawrenc. (262.1098)

EXTRUSION AT ITASCA PLASTICS

EXTRUSION AT ITASCA PLASTICS

EXTRUSION AT ITASCA PLASTICS

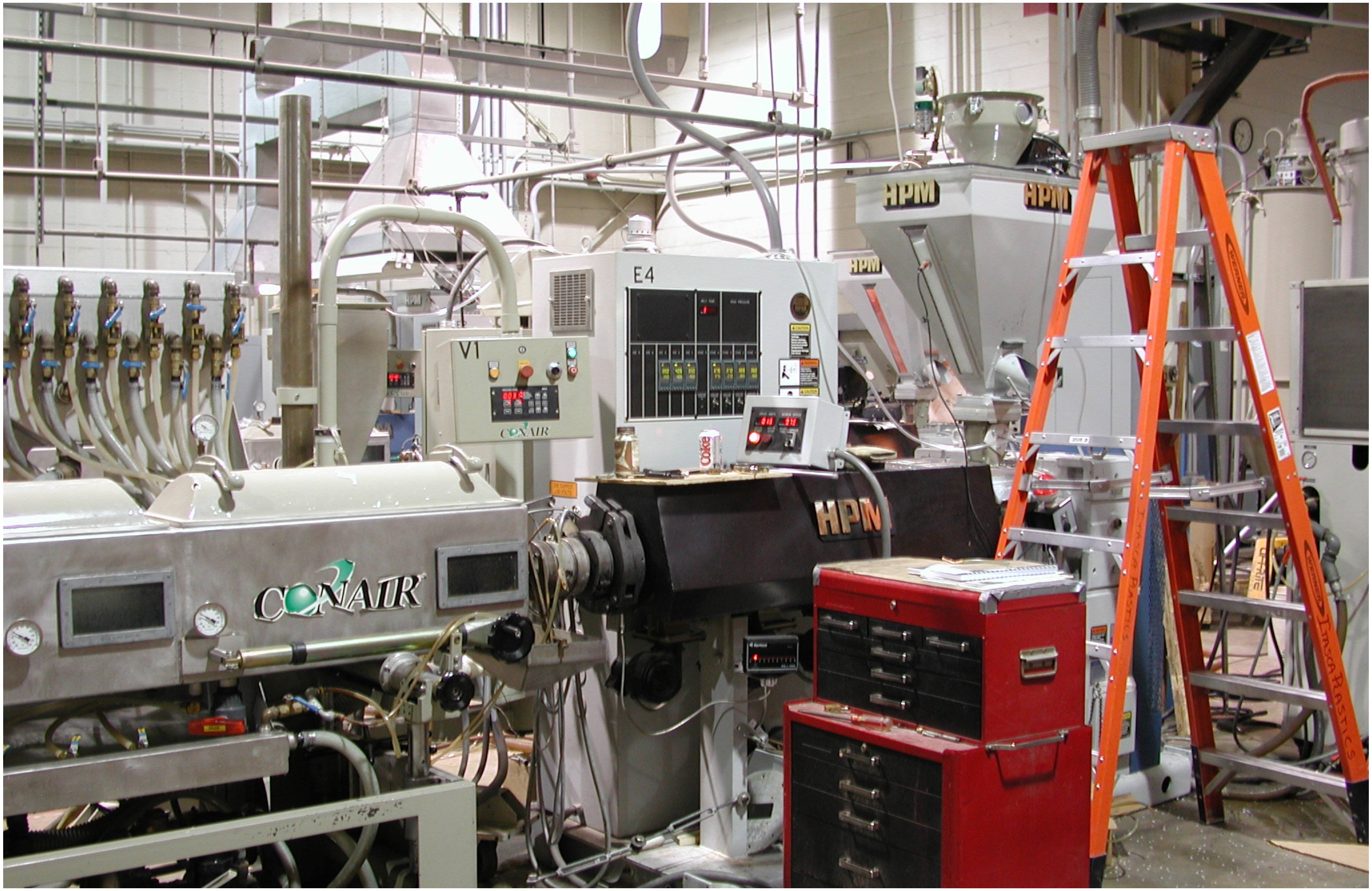

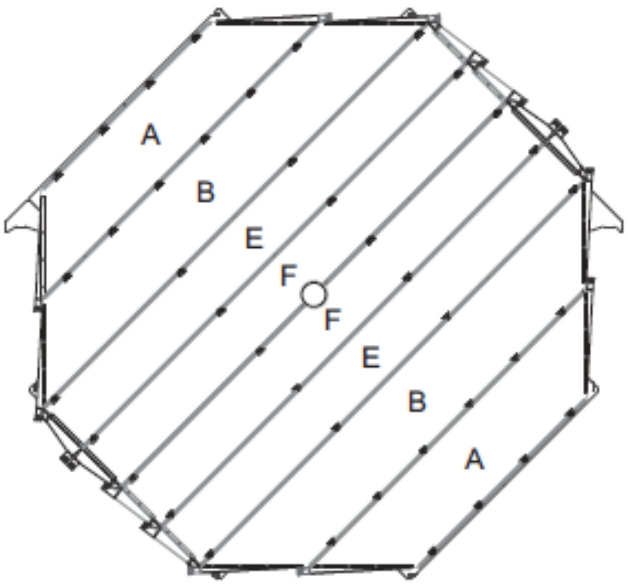
A
B
E
F
F
E
B
A

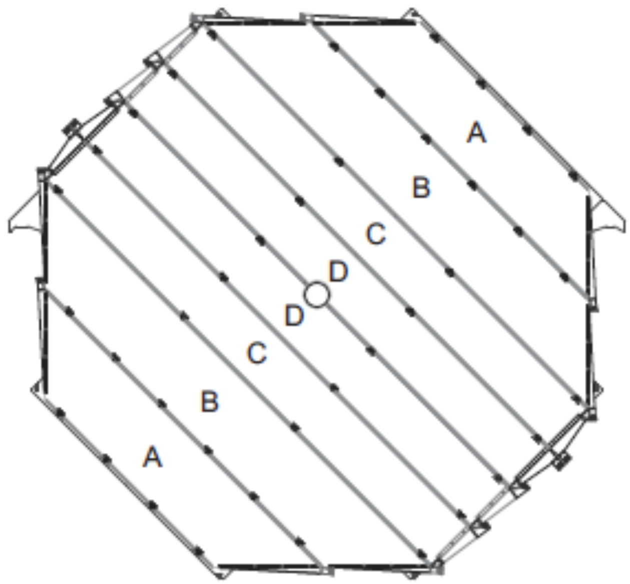
A
B
C
D
D
C
B
A

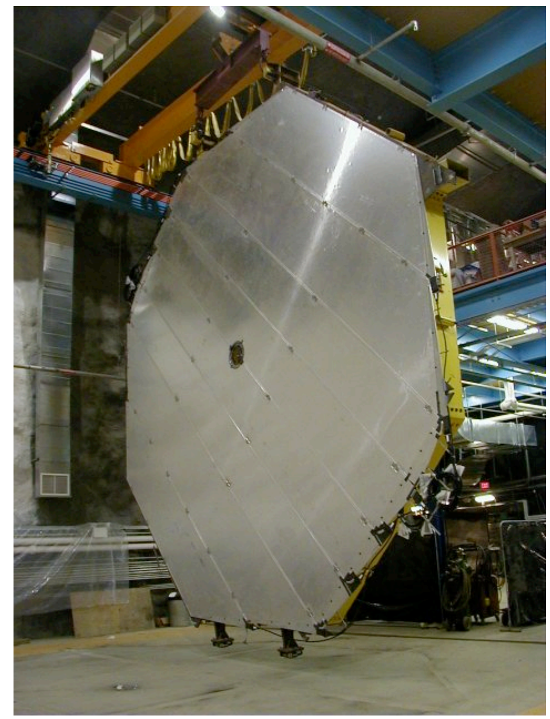

Far Detector Light Output

- The design critereon for the far detector was the light output.
  - → 4.7 pe's/muon (2 GeV muons) for the average sum of two strip ends.
- The measured light output is almost a factor of two higher than the design requirement.

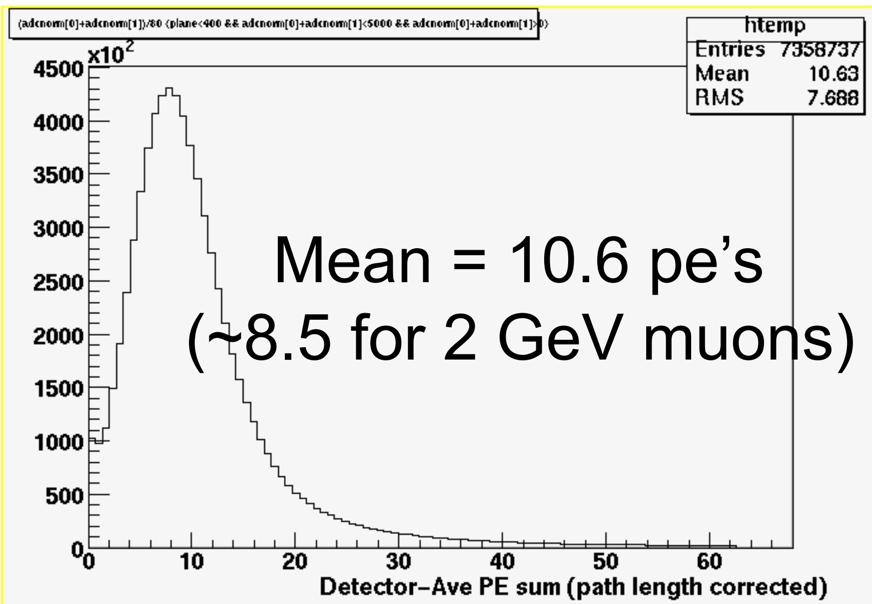

Light output measured for all strips for muons in the far detector. The light output is corrected to 1 cm pathlength per plane but is not corrected for PMT gain variations.

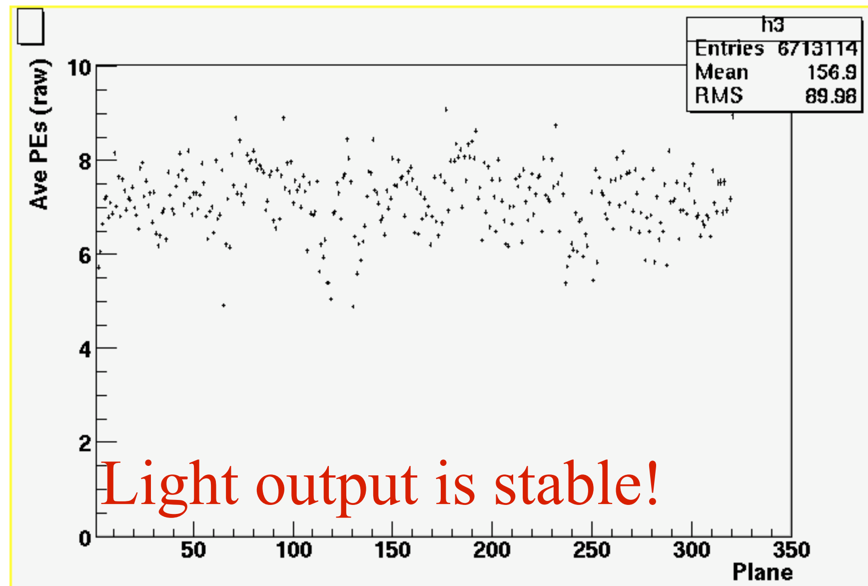

Average light output for one-side of readout vs plane number in the detector. (Not corrected for pathlength or gain variations). This shows the uniformity in the hardware and raw response.

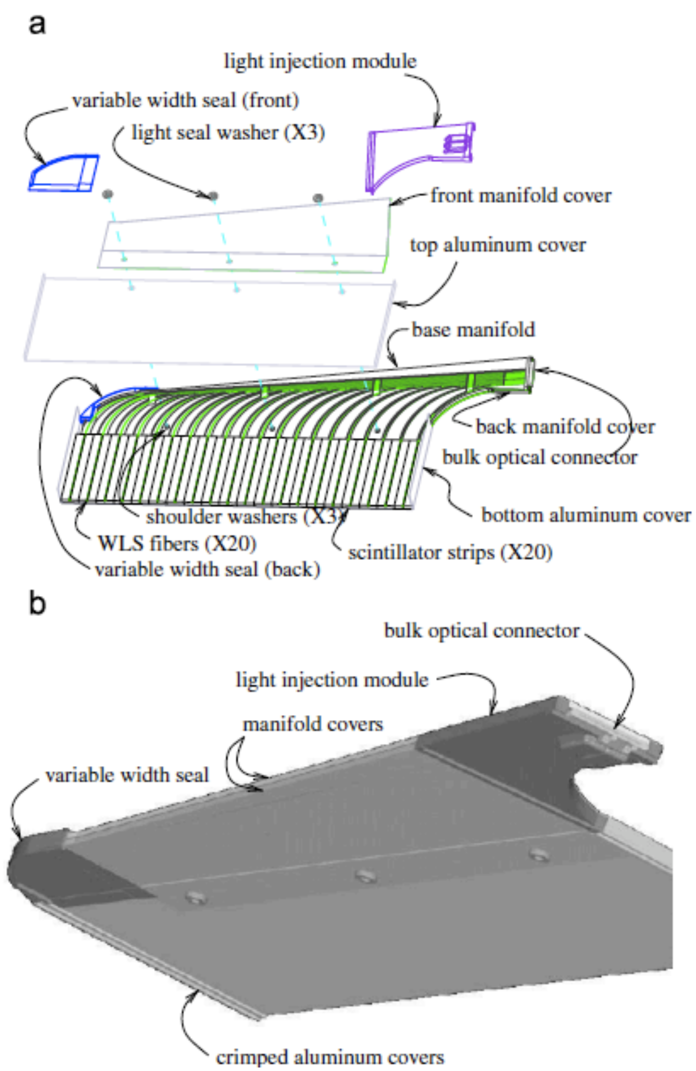
a
light injection module
variable width seal (front)
light seal washer (X3)
front manifold cover
top aluminum cover
base manifold
back manifold cover
bulk optical connector
bottom aluminum cover
shoulder washers (X3)
WLS fibers (X20)
scintillator strips (X20)
variable width seal (back)
b
bulk optical connector
light injection module
manifold covers
variable width seal
crimped aluminum covers

M16 and M64 for MINOS

FAR Detector

- Hamamatsu's R-5900-M16

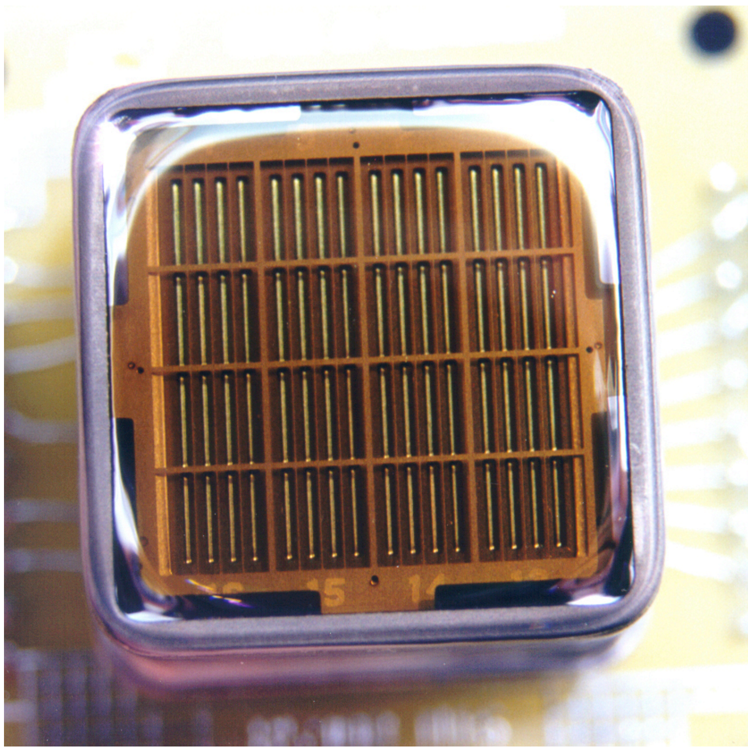

NEAR Detector

- Hamamatsu's R-5900-M64

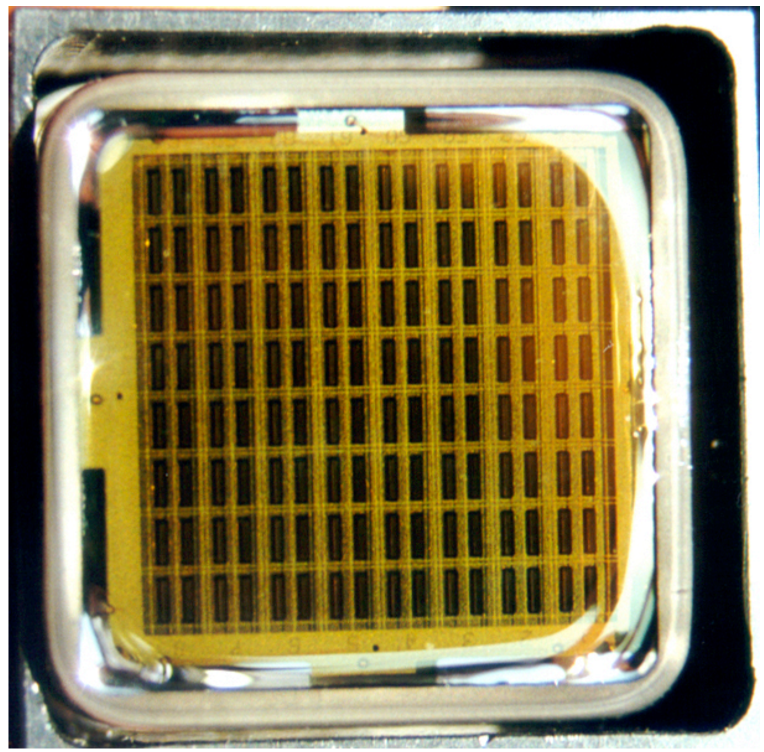

Alignment
optical and dynamic

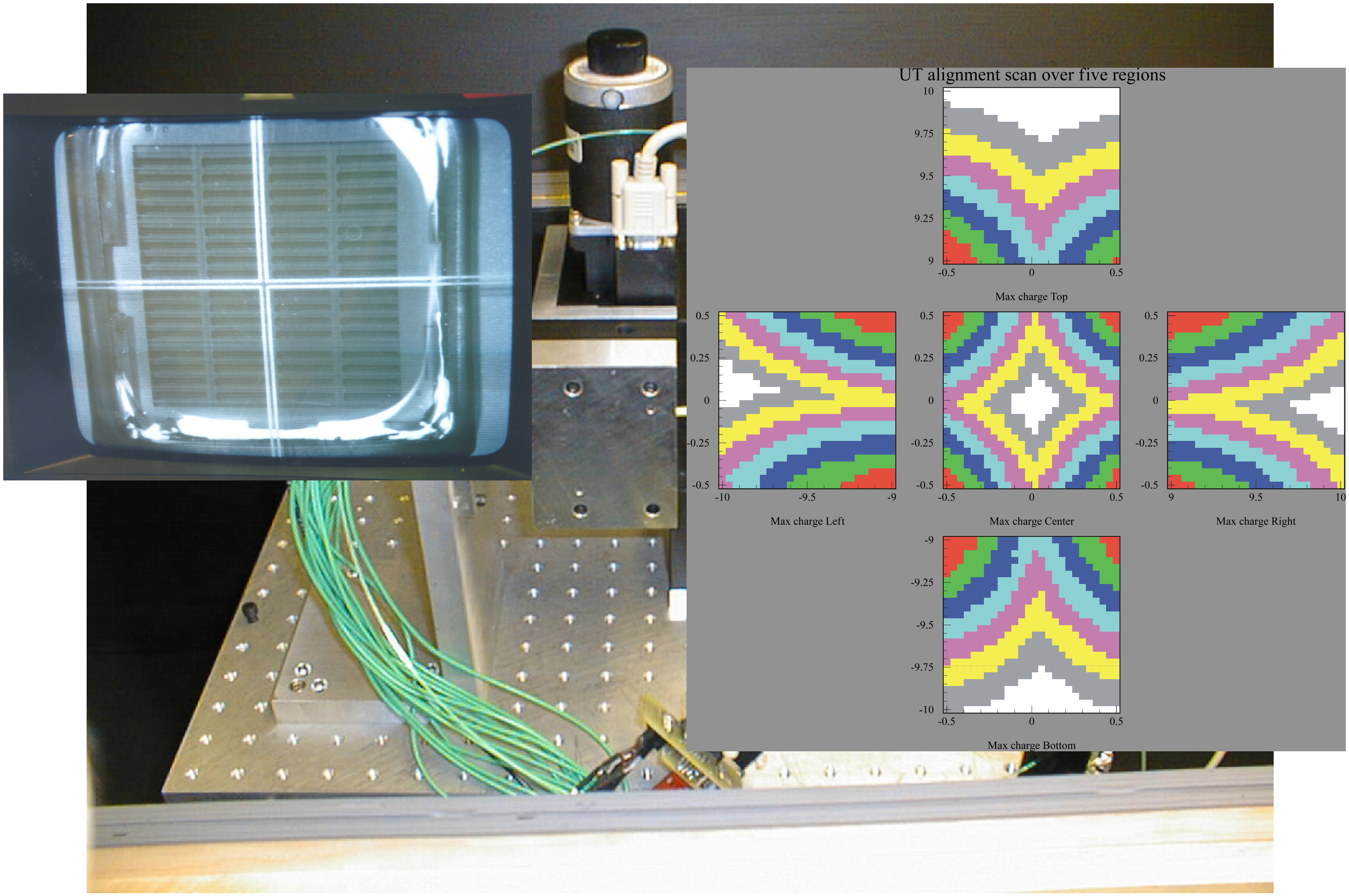

Tube 9c16a1

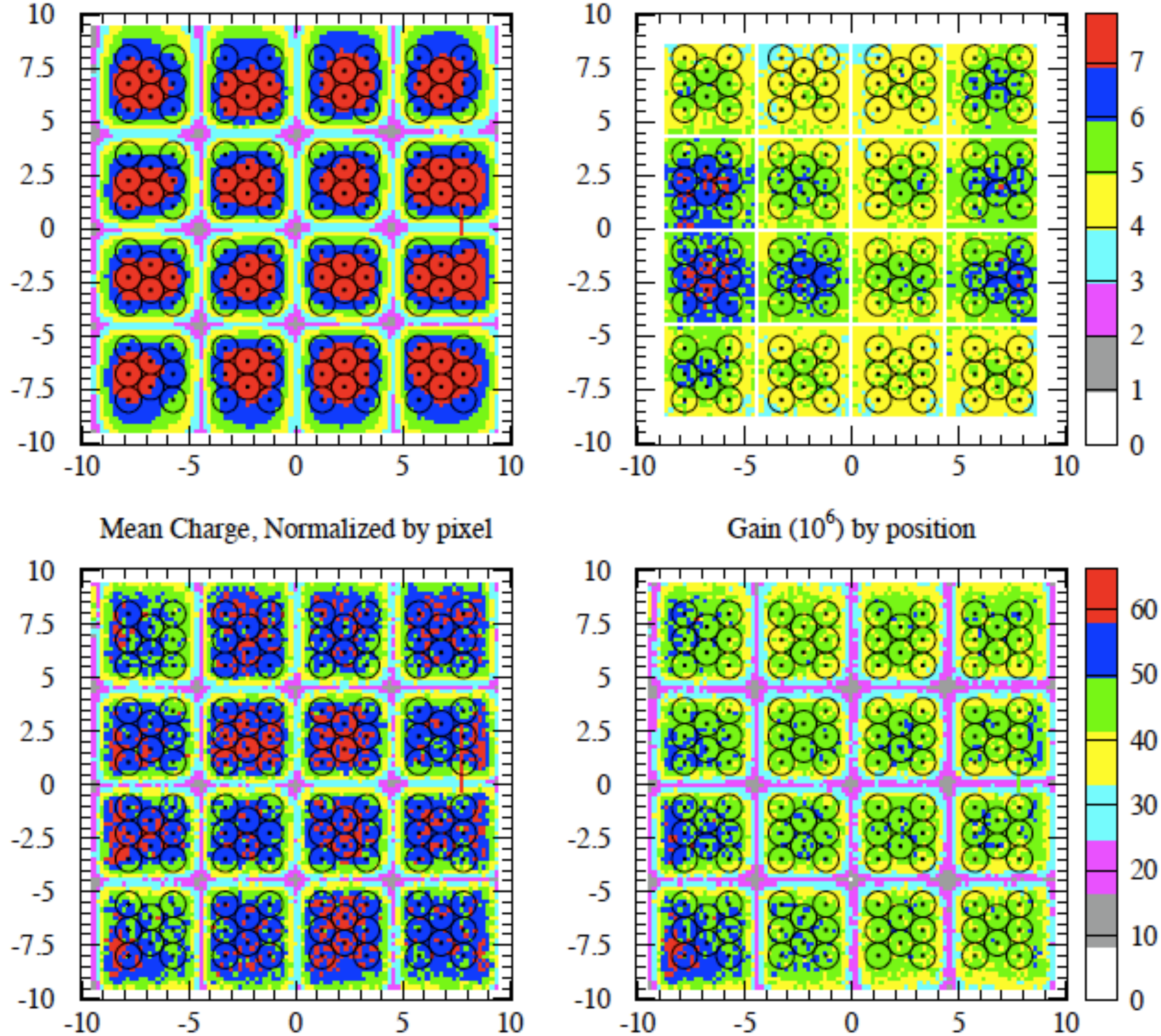

Mean Charge, Normalized by pixel

Gain (10^6) by position

Photoelectrons, Normalized by pixel

Photoelectrons by position

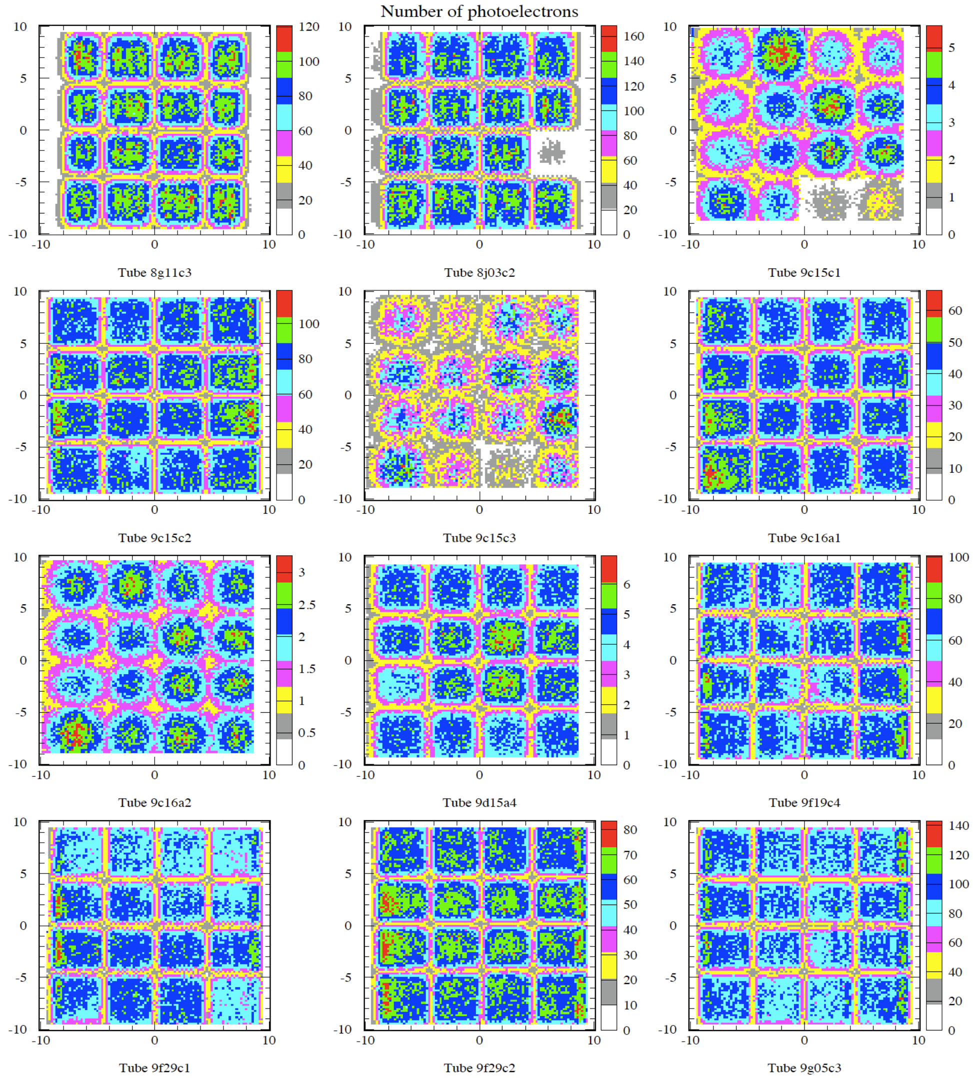

Figure 15: Number of photoelectrons contour plots for twelve PMT scans. Blank areas for 9C15C1 and 9C15C3 were due to bad cables, while the blank pixel #9 in 8J03C2 appears to be a damaged pixel. Note the relatively small sizes of the outer pixel columns in 8G11C3, compared to the 9* serial numbers, which shows the improvement in the effective pixel size. The fact that some tubes were scanned at very low light levels was due to a mistake which has since been corrected.

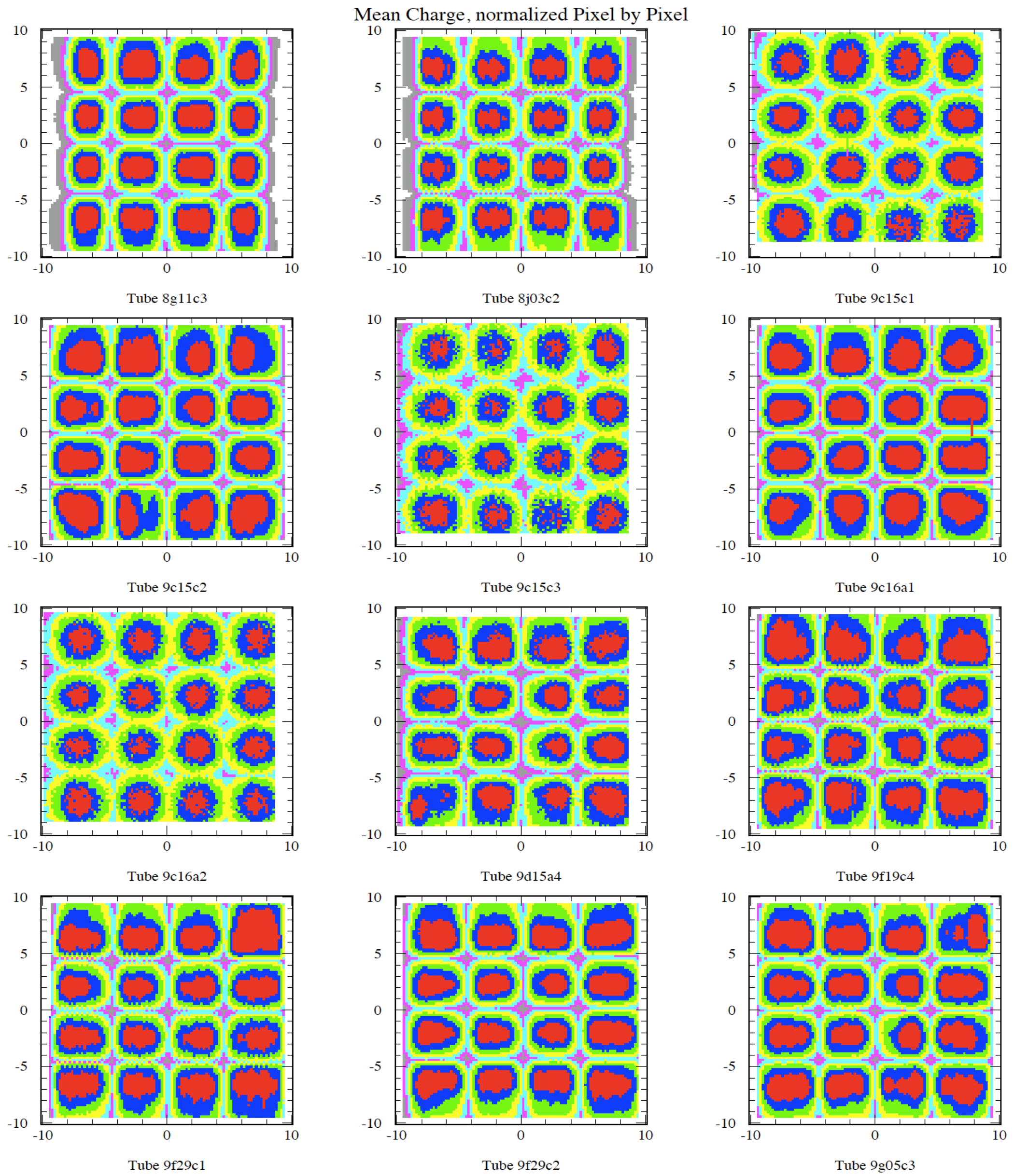

Figure 14: Charge contours, normalized pixel by pixel, for twelve PMT s-cans. These plots are the pulsed equivalent to the DC scans conducted by Hamamatsu.

MINOS Calibration Detector
– an experiment 2001-2003 at CERN PS

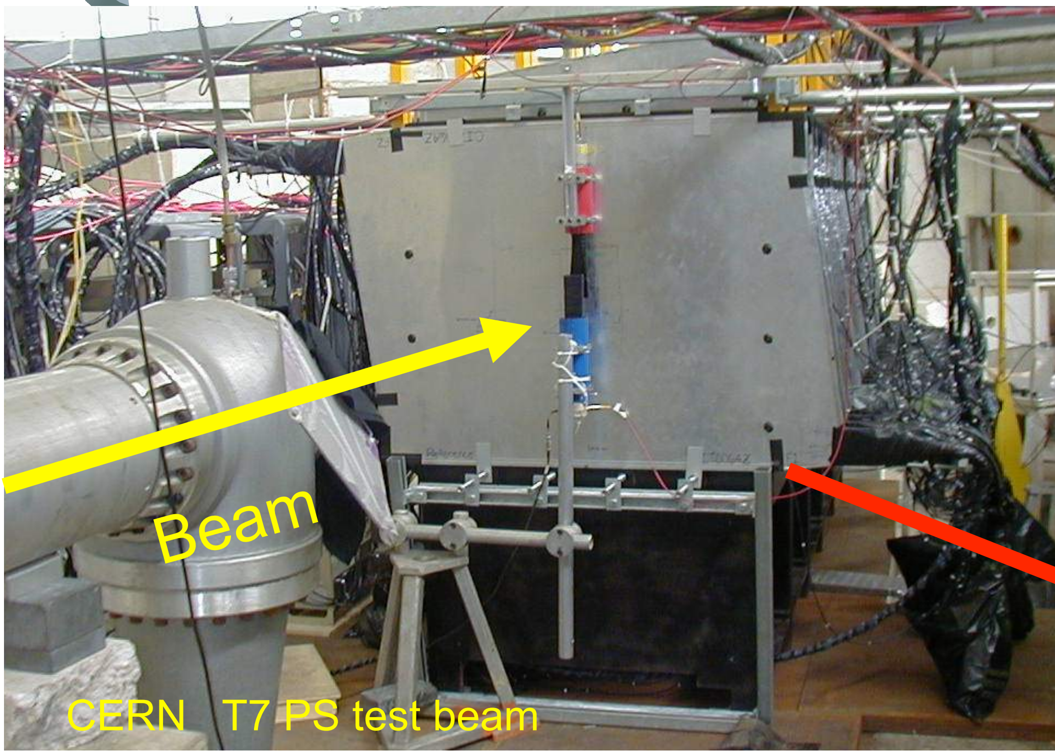

MINOS is a 3-detector Experiment!

- 5 tons (5 modules for moving)
- 1 m x 1 m x 3.7 m
- 60 MINOS planes
- Long WLS andClear fiber cables
- No B field
- 24 strips/plane (a total of 1440 strips)
- X-Y views
- FarDet and/or NearDet readout

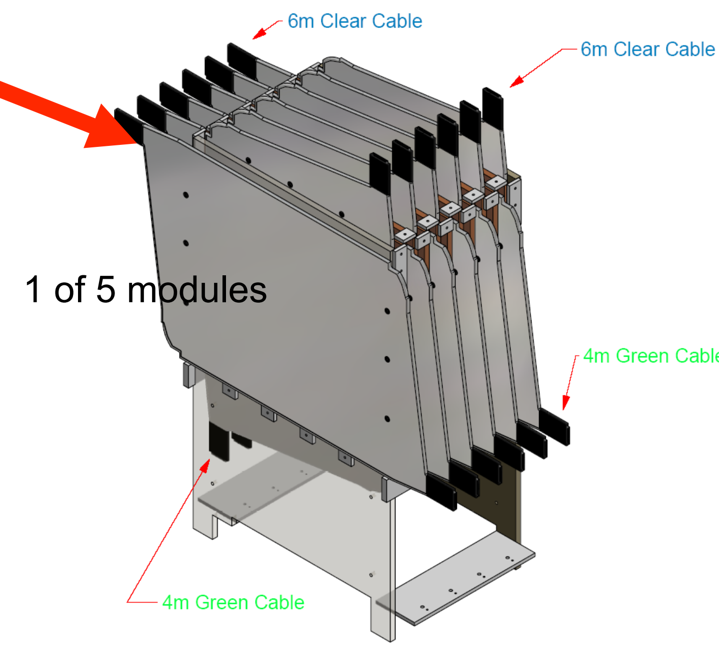

- ◆Exercise a full MINOS calibration scheme
- ◆Determine the absolute energy scale to <5%
- ◆Establish relative energy scale <2%
- ◆Energy and topology response
- ◆Monte Carlo tuning
- ◆Beam p,π,e,μ 05-10 GeV/c
- ◆Cosmic ray muons (stopping)

M16 base (voltage divider)

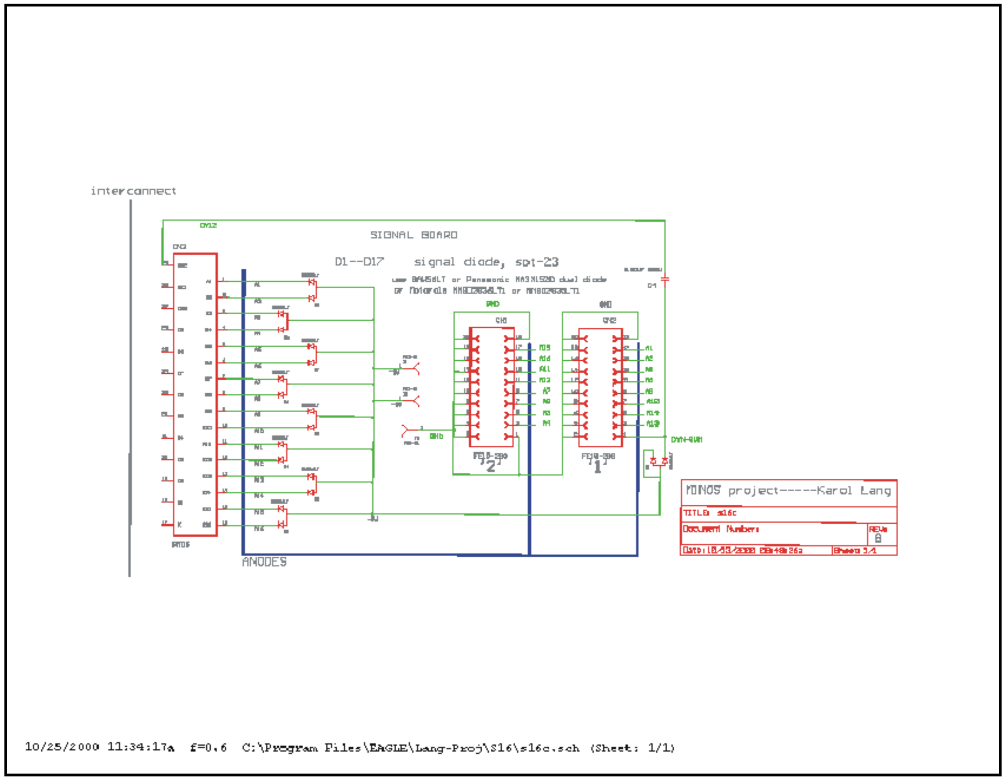

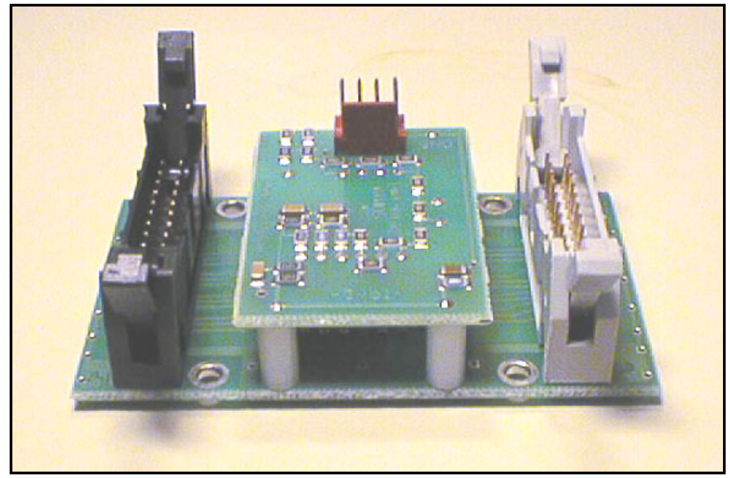

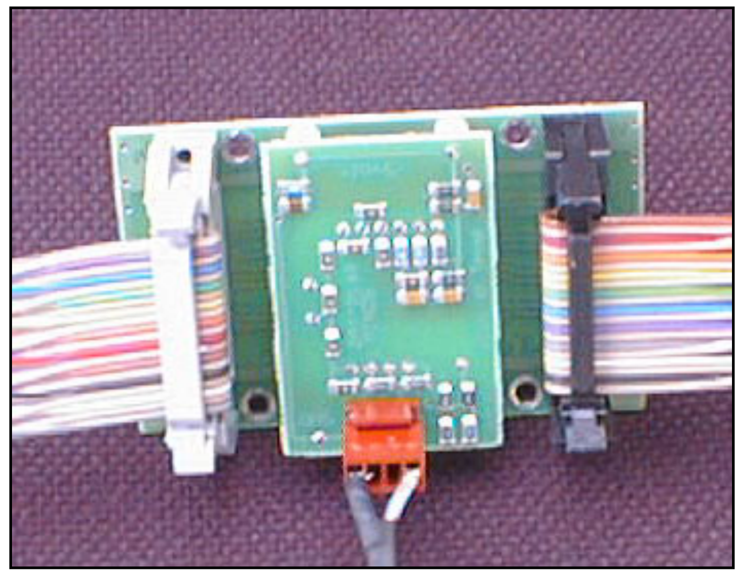

- ~1500 made (400 more next week)
- No conformal coating
  (leakeage current < 10 nA
  see detailes later)